



National Library
of Canada

Bibliothèque nationale
du Canada

Canadian Theses Service

Service des thèses canadiennes

Ottawa, Canada
K1A 0N4

NOTICE

The quality of this microform is heavily dependent upon the quality of the original thesis submitted for microfilming. Every effort has been made to ensure the highest quality of reproduction possible.

If pages are missing, contact the university which granted the degree.

Some pages may have indistinct print especially if the original pages were typed with a poor typewriter ribbon or if the university sent us an inferior photocopy.

Reproduction in full or in part of this microform is governed by the Canadian Copyright Act, R.S.C. 1970, c. C-30, and subsequent amendments.

AVIS

La qualité de cette microforme dépend grandement de la qualité de la thèse soumise au microfilmage. Nous avons tout fait pour assurer une qualité supérieure de reproduction.

S'il manque des pages, veuillez communiquer avec l'université qui a conféré le grade.

La qualité d'impression de certaines pages peut laisser à désirer, surtout si les pages originales ont été dactylographiées à l'aide d'un ruban usé ou si l'université nous a fait parvenir une photocopie de qualité inférieure.

La reproduction, même partielle, de cette microforme est soumise à la Loi canadienne sur le droit d'auteur, SRC 1970, c. C-30, et ses amendements subséquents.

THE UNIVERSITY OF ALBERTA

PHOTODIODE ARRAY SPECTROMETER SYSTEMS FOR INDUCTIVELY
COUPLED PLASMA ATOMIC EMISSION SPECTROMETRY

BY

KEITH LEPLA



A THESIS

SUBMITTED TO THE FACULTY OF GRADUATE STUDIES AND RESEARCH
IN PARTIAL FULFILMENT OF THE REQUIREMENT FOR THE DEGREE
OF DOCTOR OF PHILOSOPHY

DEPARTMENT OF CHEMISTRY

EDMONTON, ALBERTA

SPRING 1989



National Library
of Canada

Bibliothèque nationale
du Canada

Canadian Theses Service Service des thèses canadiennes

Ottawa, Canada
K1A 0N4

The author has granted an irrevocable non-exclusive licence allowing the National Library of Canada to reproduce, loan, distribute or sell copies of his/her thesis by any means and in any form or format, making this thesis available to interested persons.

The author retains ownership of the copyright in his/her thesis. Neither the thesis nor substantial extracts from it may be printed or otherwise reproduced without his/her permission.

L'auteur a accordé une licence irrévocable et non exclusive permettant à la Bibliothèque nationale du Canada de reproduire, prêter, distribuer ou vendre des copies de sa thèse de quelque manière et sous quelque forme que ce soit pour mettre des exemplaires de cette thèse à la disposition des personnes intéressées.

L'auteur conserve la propriété du droit d'auteur qui protège sa thèse. Ni la thèse ni des extraits substantiels de celle-ci ne doivent être imprimés ou autrement reproduits sans son autorisation.

ISBN 0-315-52943-1

Canada

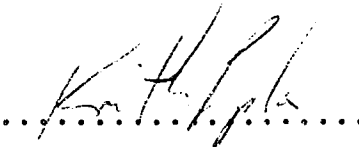
THE UNIVERSITY OF ALBERTA

RELEASE FORM

NAME OF AUTHOR: KEITH LEPLA
TITLE OF THESIS: PHOTODIODE ARRAY SPECTROMETER SYSTEMS FOR
INDUCTIVELY COUPLED PLASMA EMISSION
SPECTROMETRY.
DEGREE FOR WHICH THESIS WAS PRESENTED: Ph.D.
YEAR THIS DEGREE WAS GRANTED: 1989

Permission is hereby granted to THE UNIVERSITY OF ALBERTA LIBRARY to reproduce single copies of this thesis and to lend or sell such copies for private, scholarly or scientific research purposes only.

The author reserves other publication rights, and neither the thesis nor extensive extracts from it may be printed or otherwise reproduced without the author's written permission.


.....

(Students signature)

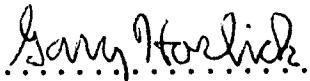
Permanent address:
204 10416 86 Ave.
Edmonton, Alberta
T6E 2M5

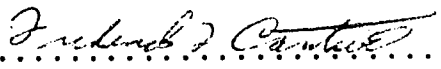
Date: January 24, 1989

THE UNIVERSITY OF ALBERTA

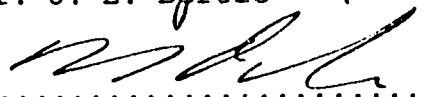
FACULTY OF GRADUATE STUDIES AND RESEARCH


The undersigned certify that they have read, and recommend to the Faculty of Graduate Studies and Research for acceptance, a thesis entitled PHOTODIODE ARRAY SPECTROMETER SYSTEMS FOR INDUCTIVELY COUPLED PLASMA ATOMIC EMISSION SPECTROMETRY submitted by Keith Lepa in partial fulfilment of the requirements for the degree of Doctor of Philosophy.


.....
Dr. G. Horlick (Supervisor)


.....
Dr. F. F. Cantwell


.....
Dr. J. E. Bertie


.....
Dr. N. Dovichi


.....
Dr. D. W. Smith


.....
Dr. J. W. Olesik

Date: January 24, 1989

To my parents

ABSTRACT

The development of a microcomputer controlled photodiode array (PDA) spectrometer is described. The system consists of a microcomputer (IBM-pc), commercial analog-digital I/O board (Data Translation DT2801-A), commercial software (ASYST Scientific Software), and a simple in-lab designed clock/timer interface. The system is simpler in design and operation than previous PDA spectrometers designed around minicomputers.

Three data processing techniques have been implemented as routine procedures for the PDA spectrometer. Fourier domain interpolation is used to interpolate peak shapes and thus enable accurate determination of relative peak heights. A procedure for automated wavelength calibration has been developed. Also, a method has been developed to select integration times for the PDA so that the optimum integration times will be used regardless of signal intensity. When combined, the data processing procedures improve the accuracy, speed, and dynamic range, and decrease the operator skill required for the operation of the PDA spectrometer. Overall, an improvement in spectrometer performance of three to four times can be realized, without changing the PDA or the spectrometer configuration. Using these procedures, a method for the measurement of excitation temperatures in the

ICP, based on the relative intensities of Fe emission lines, was developed.

A fiber optic cable was installed in the PDA spectrometer and was used to optically couple the ICP source and the spectrometer. The fiber optic cable can be positioned virtually in any location and can be easily repositioned to view a different region of the source. The PDA spectrometer with the fiber optic cable has the capability to perform a number of unique measurements and has been used to study the optical properties of the ICP-mass spectrometer (ICP-MS). In addition to increasing the analytical capabilities of the ICP-MS, an optical channel has been used to study the effects of central gas flow rate, RF power, and spatial position on signal intensity and signal noise.

ACKNOWLEDGEMENT

I would like to thank my supervisor, Gary Horlick for his advice and direction throughout this work. I would also like to thank all members of the research group, especially George Gillson for getting me started, Margaret-Anne Vaughan for her help with the ICP-MS, Greg King and Mike Stewart for programming hints, Joe Lam and V. K. for knowing where everything was, and Bruce Todd for many interesting discussions.

My thanks also goes to the staff of the Chemistry Department Electronics, Machine, and Glass shops for their expertise and patience.

Lastly, I would like to acknowledge the three years of funding from the Natural Sciences and Engineering Research Council.

TABLE OF CONTENTS

Chapter	Page
1. Photodiode Arrays in ICP Spectroscopy	
1.1 Introduction.....	1
1.2 PDA Spectrometers for ICP Spectrochemical Analysis.....	6
1.3 Plasma Diagnostics with PDA Spectrometers....	10
1.4 Spectrometer Configurations for PDAs.....	14
1.5 PDA Developments.....	16
References	20
2. Photodiode Array Systems for ICP-AES	
2.1 Introduction	25
2.2 Hamamatsu S2304Q-1024 PDA	27
2.3 Reticon 1024S with RC1000 and RC1001 Boards.....	35
2.4 Reticon 1024S with RC1024S Board	39
2.5 IBM-pc Data Acquisition System	41
2.6 PDA Performance	43
2.7 Conclusions	50
References	55
3. Data Processing for a Photodiode Array Spectrometer	
3.1 Spectral Line-Diode Registry Effects with a PDA.....	56
3.1.1 Introduction.....	56
3.1.2 PDA Sampling Process.....	57

3.1.3	Recovery of Spectral Information.....	60
3.2	Wavelength Calibration.....	70
3.2.1	Introduction.....	70
3.2.2	Primary Wavelength Calibration.....	71
3.2.3	Secondary Wavelength Calibration.....	76
3.3	Dynamic Range.....	80
3.4	Conclusions	94
	References	96
4.	Excitation Temperature Measurements with a PDA Spectrometer	
4.1	Introduction.....	98
4.2	Results and Discussion.....	102
	References	113
5.	Fiber Optic Entrance Slit for a PDA Spectrometer	
5.1	Introduction.....	115
5.2	Instrumentation.....	117
5.3	Spatial Profiling.....	117
5.4	Spectral Resolution.....	122
5.5	Spectral Throughput.....	126
5.6	Conclusion.....	128
	References	129
6.	Simultaneous Optical and Mass Measurements for the ICP	
6.1	Introduction.....	130
6.2	Instrumentation.....	135
6.3	Effect of Plasma Operating Parameters on Optical and Mass Spectrochemical Signals.....	137

6.4	Effect of Plasma Parameters on Oxides	
	Species.....	149
6.5	Matrix Effects.....	154
6.6	Drift.....	161
6.7	Conclusion.....	163
	References	166
7.	Simultaneous Optical and Mass Noise Studies for the ICP	
7.1	Introduction.....	168
7.2	Instrumentation for Noise Amplitude Studies.....	170
7.3	Results and Discussion.....	178
	7.3.1 Noise Amplitude Spectra.....	178
	7.3.2 Noise Feature in the ICP.....	181
	7.3.3 1/f Noise.....	197
7.4	Conclusion	201
	References	203
8.	Future Developments	
8.1	Advances in Image Sensor Technology.....	204
8.2	Other Advances Affecting PDAs.....	207

LIST OF TABLES

Table		Page
2.1	PDA sensitivity, measured from slopes of analytical calibration curves.....	45
2.2	PDA detection limits measured with a 10 second integration time.....	51
3.1	Error in peak maximum location for Fe I lines using peak search routine.....	75
3.2	Error in peak maximum location for Fourier domain zero filled Fe I spectrum.....	77
3.3	Error in peak maximum location using secondary calibration procedure for Fe I spectrum.....	81
4.1	Iron lines, excitation energies, and transition probabilities used for calculation of excitation temperature.....	103
5.1	Attenuation of light throughput by fiber optic cable.....	127
7.1	Standard plasma operating conditions.....	179

LIST OF FIGURES

Figure	Page
1.1 Schematic diagram of Czerny-Turner type monochromator with photodiode array (PDA) detector.....	3
1.2 Schematic diagram of PDA sensor electronics.....	4
1.3 Schematic diagram of monochromator in the spatial configuration with PDA mounted vertically.....	11
2.1 Block diagram of ICP-PDA spectrometer.....	26
2.2 Schematic of Hamamatsu C2325 (Low Noise) driver/amplifier board.....	28
2.3 Schematic diagram of Data Translation DT2801-A I/O and Intel 8253 clock/timer interface.....	30
2.4 Hamamatsu C2325 driver/amplifier evaluation board with Peltier effect cooler and warm and cold side copper bus.....	33
2.5 Photograph of a) Hamamatsu C2325 board and b) Peltier effect cooler with copper bus.....	34
2.6 Side view of Reticon 1024S PDA with RC1000, RC1001, and 8253 clock/timer boards and Peltier effect cooling system.....	36
2.7 Schematic diagram of Reticon RC1000 and RC1001 driver/amplifier boards.....	37

2.8	Schematic diagram of Czerny-Turner type monochromator with Reticon PDA and RC1024S evaluation board.....	40
2.9	Schematic diagram of Reticon 1024S PDA and RC1024S evaluation board with Peltier effect cooling system.....	42
2.10	ICP-PDA spectra of a) 1 $\mu\text{g/mL}$ Ca, b) 1 $\mu\text{g/mL}$ Mg and c) 10 $\mu\text{g/mL}$ Zn measured with a 1 second integration time.....	47
2.11	ICP-PDA spectrum of 100 ng/mL Cd and Zn measured with a 25 second integration time.....	48
3.1	Illustration of the sampling of a spectral image by a PDA detector.....	58
3.2	a) 32 pixels of Mn PDA spectrum, b) as in a) with small shift in grating position, c) Fourier domain zero filled spectrum of a), d) Fourier domain zero filled spectrum of b).....	61
3.3	Fourier domain zero filling procedure.....	64
3.4	Peak height of Mn 279.4 nm line in PDA spectra as a function of grating position, lower curve, raw PDA spectra, upper curve, zero filled PDA spectra.....	66
3.5	Fourier transform of HeNe laser line with a) 100 μm entrance slit width and b) 10 μm entrance slit width.....	68

3.6	a) 32 pixels of Mg spectrum acquired with 30 μm entrance slit width, b) zero filled spectrum of a), c) zero filled spectrum of a) with apodization with Gaussian peak shape.....	69
3.7	Fe I ICP-PDA spectrum, centered at 374 nm.....	72
3.8	Wavelength calibration plot, peak position as wavelength versus peak position as diode number.....	73
3.9	a) Fe I spectrum with primary calibration of wavelength axis, b) Fe I spectrum as in a) with small grating shift, c) cross correlation of a) and b).....	79
3.10	Dynamic range for Reticon PDA with 5 second integration time.....	83
3.11	Peak height of 422 nm line of a Ca hollow cathode lamp, as a function of PDA integration time.....	86
3.12	PDA dark current as a function of PDA integration time.....	88
3.13	ICP-PDA spectrum of 10 $\mu\text{g/mL}$ Mg and 0.1 $\mu\text{g/mL}$ Mn with a) a single integration time and b) multiple integration times.....	90
3.14	ICP-PDA spectra as in Figure 3.13 with vertical scale expanded 10 times.....	91
3.15	ICP-PDA spectra as in Figure 3.13 with vertical scale expanded 100 times.....	92

3.16	ICP-PDA multiple integration time spectrum in Figure 3.13 with vertical scale expanded 1000 times.....	93
4.1	Fe I spectrum centered at 370 nm, used in calculation of excitation temperature.....	104
4.2	Fe II spectrum centered at 260 nm, used in calculation of excitation temperature.....	105
4.3	Zero filled spectra for Fe I spectrum from Figure 4.1.....	107
4.4	Zero filled spectra for Fe II spectrum from Figure 4.2.....	108
4.5	Boltzmann plot for a) Fe I lines and b) Fe II lines.....	109
4.6	Excitation temperature as function of RF power and central (nebulizer) gas flow rate for a) Fe I lines and b) Fe II lines.....	111
5.1	Schematic diagram of Czerny-Turner type monochromator with PDA detector and fiber optic cable input.....	118
5.2	Schematic diagram of apparatus to test the spatial profiling accuracy of the fiber optic cable.....	119
5.3	Spatial profile of light pattern from Teflon block.....	121
5.4	Spatial emission profile of the ICP for a) Sr II and b) Sr I.....	123

5.5	ICP-PDA spectrum of Mn triplet measured with a) convention entrance slit PDA spectrometer (100 μm slit width) and b) PDA spectrometer with fiber optic input.....	124
6.1	Schematic diagram of experimental system for simultaneous optical and mass spectrochemical measurements.....	136
6.2	Vertical spatial emission profile (lateral across the ICP) for Sr II and Sr I.....	138
6.3	ICP-PDA spectrum of 1 $\mu\text{g/mL}$ Sr and Sc, with spectrometer centered at approximately 440 nm.....	139
6.4	Sr ⁺ mass signal as a function of central gas flow rate at 1.1 kW RF power.....	140
6.5	Sr ⁺ mass signal as a function of central gas flow rate at 1.1, 1.3, and 1.5 kW RF powers.....	142
6.6	Sr II emission signal as function of central gas flow rate at 1.1 kW RF power.....	143
6.7	Sr II emission signal as function of central gas flow rate at 1.1, 1.3, and 1.5 kW RF powers.....	144
6.8	Sr II emission and Sr ⁺ mass signals as function of central gas flow rate at a) 1.5, b) 1.3, c) 1.1 kW RF power.....	145
6.9	Ba II emission as a function of central gas flow rate at observation zones 1, 2, 3, and 4 mm from the sampling cone.....	147

6.10	Sr II emission, Sr I emission, and Sr ⁺ mass signals as function of central gas flow rate at a) 1.5, b) 1.3, c) 1.1 kW RF power.....	148
6.11	ICP-PDA La II emission spectrum, 0.7 Lpm central gas flow rate and 1.1 kW RF power.....	151
6.12	ICP-PDA LaO emission spectrum, 1.1 Lpm central gas flow rate and 1.1 kW RF power.....	152
6.13	a) La II and LaO emission and b) La ⁺ and LaO ⁺ mass signals as a function of central gas flow rate.....	153
6.14	Ti II emission measured with the PDA spectrometer versus TiO ⁺ signal measured with the mass spectrometer.....	155
6.15	Effect of Na concentration on Sc II emission and Sc ⁺ ion signals.....	157
6.16	Effect of central gas flow rate on a) Sr II emission and b) Sr ⁺ ion signals with and without 1000 µg/mL Na.....	158
6.17	Effect of central gas flow rate on a) Sr II emission and b) Sr ⁺ ion signals with and without 1000 µg/mL Tl.....	160
6.18	Drift of Sr II emission, Sr I emission, and Sr ⁺ ion signals as a function of time.....	162
7.1	Schematic diagram of Czerny-Turner type monochromator with fiber optic input and PMT detector.....	171

7.2	Schematic diagram of simultaneous optical and mass noise amplitude measurement system.....	173
7.3	Diagram of portion of Elan signal processing board electronics.....	174
7.4	Diagram of Analog Devices AD650 configured in the frequency to voltage conversion mode.....	175
7.5	Analytical calibration curve for analog measurement of Sr ⁺ mass signal.....	177
7.6	Noise amplitude spectra of a) Sr II emission and b) Sr ⁺ mass signal.....	180
7.7	Noise amplitude spectra of Sr II emission signal measured at RF powers of a) 0.8, b) 0.9, c) 1.0, d) 1.1, e) 1.2, f) 1.3, and g) 1.4 kW.....	183
7.8	Noise amplitude spectra of Sr ⁺ mass signal measured at RF powers of a) 0.8, b) 0.9, c) 1.0, d) 1.1, e) 1.2, f) 1.3, and g) 1.4 kW.....	184
7.9	Frequency of noise feature in optical and mass signal as a function of RF power.....	185
7.10	Noise amplitude spectra of Sr II emission measured at outer gas flow rates of a) 9, b) 10, c) 11, d) 12, e) 13, f) 14, and g) 15 Lpm.....	186
7.11	Noise amplitude spectra of Sr ⁺ mass signal measured at outer gas flow rates of a) 9, b) 10, c) 11, d) 12, e) 13, f) 14, and g) 15 Lpm.....	187

7.12	Frequency of noise feature in optical and mass signal as a function of outer gas flow rate.....	188
7.13	Noise amplitude spectra of Sr II emission measured at spatial positions of a) 9, b) 11, c) 13, d) 15, e) 17, f) 19, g) 21, and h) 23 mm from the load coil.....	190
7.14	Noise amplitude spectra of Sr ⁺ mass signal measured at spatial positions of a) 9, b) 11, c) 13, d) 15, e) 17, f) 19, g) 21, and h) 23 mm from the load coil.....	191
7.15	Frequency of noise feature in optical and mass signal as a function of sampling cone to load coil distance.....	192
7.16	Noise amplitude spectra of Sr II emission measured at optical observation zones of a) 1, b) 2, c) 3, d) 4, e) 5, f) 6, g) 7, and h) 8 mm from the sampling cone.....	193
7.17	Noise amplitude spectrum of Sr II emission viewed end on from above the plasma.....	195
7.18	Noise amplitude spectrum of Sr II emission using a long torch with optical observation zones a) 15, b) 17, c) 19, d) 21, e) 23, and f) 25 mm above the load coil.....	196
7.19	Noise amplitude spectra of Sr II emission measured at concentrations of a) 0.004, b) 0.01, c) 0.02, d) 0.04, e) 0.1, f) 0.2, g) 0.4, and h) 1.00 µg/mL.....	199

7.20 Noise amplitude spectra of Sr⁺ mass signal
measured at concentrations of a) 0.004, b)
0.01, c) 0.02, d) 0.04, e) 0.1, f) 0.2, g)
0.4, and h) 1.00 μg/mL..... 200

Chapter 1

Photodiode Arrays in ICP Spectroscopy

1.1 Introduction

Conventional spectrometers used for inductively coupled plasma-atomic emission spectroscopy (ICP-AES) are one of two basic types, the direct reading polychromator or the scanning monochromator [1]. The direct reading polychromator consists of an entrance slit, a concave grating to disperse the light, and a series of exit slits in the exit focal plane. Each slit is positioned to monitor a single spectral line and behind each slit is a photomultiplier tube (PMT) detector. This configuration makes it possible to detect up to 60 lines simultaneously, resulting in a high sample throughput. However, flexibility in spectral line selection is limited, as the position of the slits can not be changed. This makes it difficult to obtain off-peak background corrections.

The scanning monochromator is a more flexible arrangement than the direct reader. Light from the entrance slit is collimated on a plane grating and the dispersed light is focused on an exit slit. Virtually any spectral line or

background feature can be detected by a PMT behind the exit slit by rotating the grating to select the wavelength at the exit slit. The sequential line by line detection decreases the sample throughput and precludes the use of internal standards.

The ideal spectrometer for ICP-AES would be one that combines the multichannel capabilities of the direct reader with the flexibility of the scanning monochromator. One approach is to replace the exit slit assembly with a linear photodiode array (PDA) (Figure 1.1). A PDA mounted in the exit focal plane of a monochromator is able to record a continuous spectral region, simultaneously detecting analyte emission and spectral background.

The PDA is a linear image sensor consisting of a series of individual photodiodes, all formed on a single silicon wafer and packaged as an integrated circuit. Diodes are formed on the silicon wafer by diffusing p-type regions into an n-type silicon substrate. All diodes are reverse biased to operate in a charge storage mode and can be schematically represented by a diode and a capacitor in parallel (Figure 1.2). Photons striking a diode create electron-hole pairs, reducing the charge across the p-n junction. To initiate readout of the PDA, a digital pulse is applied to the input of a shift register on the chip. This start pulse opens the FET switch to the first diode, allowing the diode to recharge to its full reverse bias. The current required to restore the charge is proportional to the light intensity at that diode

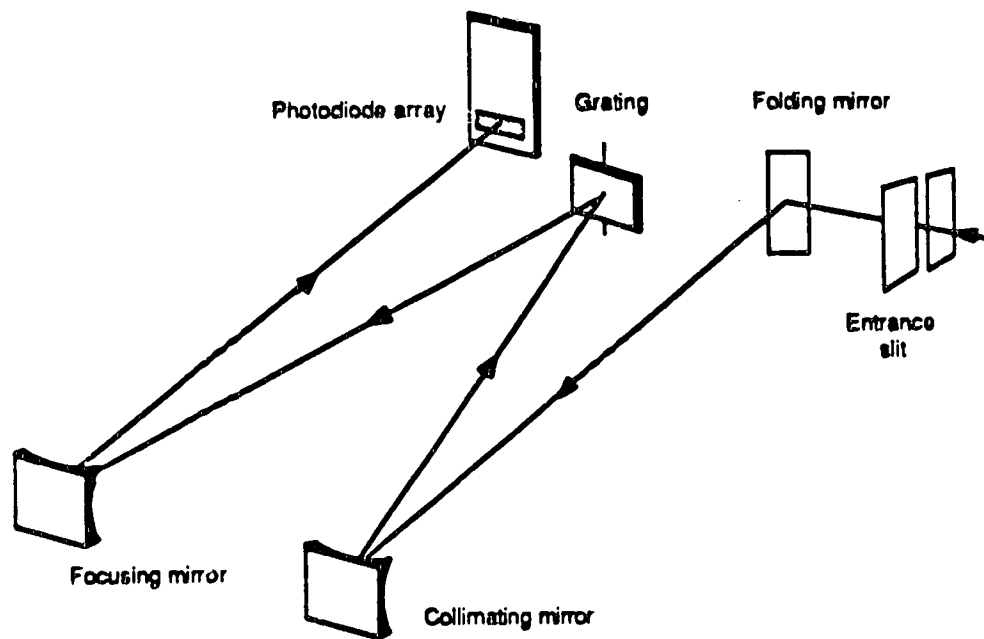


Figure 1.1 Schematic diagram of Czerny-Turner type monochromator with photodiode array (PDA) detector.

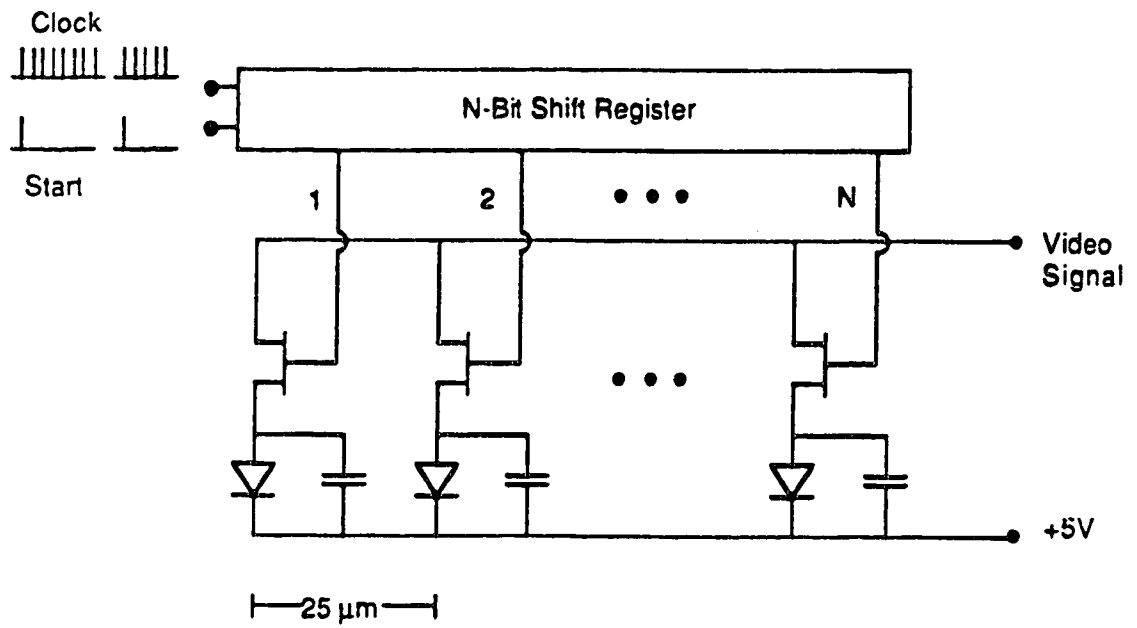


Figure 1.2 Schematic diagram of PDA sensor electronics.

and is measured at the video output. A digital clock signal is applied to the shift register, opening the next FET switch, recharging the next diode. In this manner the diodes (pixels) are read out sequentially. The rate of readout is controlled by the clock frequency, and is typically 10 to 100 kHz. The time between start pulses determines the time between PDA readouts, the integration time. Integration times can be selected according to incident light levels. Low light levels require longer integration times to allow significant charge to be depleted at the p-n junctions, while high photon fluxes require short integration times to prevent complete charge depletion on a diode.

Although an electronic image sensor is the only method to record electronically a continuous spectral region truly simultaneously, the PDA has not achieved a wide degree of acceptance as a detector for atomic spectroscopy. First, the optimum sensitivity of the PDA is in the spectral range of 600 to 800 nm [2]. Most atomic spectroscopic measurements take place in the 200 to 400 nm region, where the PDA response is significantly less sensitive. In trace analysis, where sensitivity is at a premium, the PMT has been the detector of choice because of its good UV response.

The second reason involves resolution and wavelength coverage. Atomic emission lines are on the order of 10 pm in width and would, ideally require a pixel spacing of 1 pm to ensure sufficient resolution and peak definition. In such a case a 1024 element PDA would cover a wavelength region of

only 1 nm. When the PDA is configured in a spectrometer to cover say, 50 nm, then the per pixel resolution increases to 50 pm.

Despite these problems, PDAs have been developed for ICP spectrochemical analysis. PDA spectrometers are widely used in the area of plasma diagnostics and recently a number of unique spectrometer configurations have been designed to alleviate the resolution-wavelength coverage dilemma inherent to the PDA.

1.2 PDA Spectrometers for ICP Spectrochemical Analysis

The status of PDAs in spectrochemical analysis prior to 1977 has been reviewed by Horlick and Coddling [3]. In this review the operation and performance of PDAs were described in detail and the application of a PDA spectrometer to flame emission, atomic absorption, dc arc emission, laser plume emission, and UV-visible molecular absorption was illustrated.

In 1978 a new PDA (Reticon 1024S) was introduced [4]. The new PDA was designed specifically for spectroscopic applications. It was operationally identical to previous PDAs, but had a new pixel size. Previously the largest pixel size available was 25 μm by 0.609 mm, the new PDA had dimensions of 25 μm by 2.5 mm. By increasing the height of a pixel, the charge that could be stored on a p-n junction was increased, thus increasing the sensitivity. This pixel format

also better matched the exit slit formats of most spectrometers.

This PDA was later incorporated in a 1 meter monochromator for ICP-AES [5]. The PDA spectrometer was evaluated for linearity, dynamic range, detection limits, signal to noise ratios, and spectral resolution and was directly compared to a scanning PMT monochromator and other image sensor based spectrometers. The PDA was found to have detection limits comparable to the PMT, if longer measurement times were used. For example, the PDA detection limit for Zn 213.8 nm was 0.03 ng/mL with a 164 second measurement time and the PMT detection limit was 0.026 ng/mL with a 10 second integration time. For emission lines at longer wavelengths, comparable detection limits could be obtained at similar measurement times, for example, Sr 338.0 nm had a PDA detection limit of 0.6 ng/mL at 16.4 seconds and a PMT detection limit of 1 ng/mL at 10 seconds.

McGeorge and Salin [6] described a PDA spectrometer for ICP-AES. A 1024 element PDA (Reticon 1024S) was mounted in the exit focal plane of a 1 meter monochromator. The interface between the PDA and a single board computer was described in detail. The analytical performance of this spectrometer was studied from both a practical and theoretical point of view. Measurement times, photon flux, spectral response [7], signal to noise ratios [8], and data acquisition [9] were considered. It was found that for analytical lines above 230 nm and at concentrations above the

detection limit, the PDA performed, on the basis of signal to noise ratios, as well as a PMT based spectrometer. At concentrations near the detection limit and for lines below 230 nm, measurement times one order of magnitude longer were required for the PDA to approach performance of a PMT.

McGeorge and Salin [10] also addressed some of the resolution problems associated with a PDA spectrometer. A polynomial peak fitting routine was developed to locate peak maxima with sub-diode accuracy. Also, with a stepper-motor controlled scanning spectrometer, a method to interpolate peak shapes with sub-diode accuracy was developed [11].

Van der Plas et al. [12] have described a continuum correction procedure for quantitative peak detection for high resolution PDA spectra. The method was adapted from a program used with a sequential scanning monochromator. Although much of the continuum can be removed with spectral blank subtraction, the method does have potential for the quantitative measurement of slightly overlapping spectral peaks.

Edlson et al. [13] have described an ICP-PDA spectrometer for the isotopic analysis of Pu. The spectrometer utilizes a 1024 element PDA and is capable of high resolution, 6 pm per pixel and has a total wavelength coverage of 6 nm. The simultaneous, multi-wavelength nature of the PDA enabled a rapid analysis, thus minimizing the amount of Pu that had to be handled.

Recently, this same PDA spectrometer [14] has been used for cataloguing the ICP emission spectra of elements. The goal of the research was to develop a standard reference library of ICP spectral lines over the range 192 nm to 293 nm. The PDA is able to detect several hundred lines simultaneously, greatly reducing the time required to record the reference spectra.

The multichannel nature of the PDA makes it well suited to the measurement of transient signals. A series of sequentially acquired PDA spectra can show how several spectral lines and background change as a function of time. Carr and Horlick [15] used a PDA spectrometer to measure the transient signal from an ICP coupled to a laser vaporization sample introduction system. A series of PDA spectra were acquired to follow the time behaviour of several emission lines as the laser vaporized sample plume passed through the ICP.

ICP-PDA spectrometers have also been developed for analysis of organic matrices. Hughes et al. [16] described a method for the determination of C, H, N, and O in organic compounds. The method was later improved to include lines of C, H, N, and O all in a single, relatively large spectral window, from 650 to 950 nm [17]. The emission spectra of the non-metals are somewhat less complex than the spectra of most metals. As a result, resolution is not a critical factor. With proper line selection, clearly resolved lines for all the elements can be located in the single spectral window.

Keane and Fry [18] went on to expand the method to include F, Cl, Br, I, and S. These elements could be detected simultaneously, along with C, H, N, and O.

The determination of sulfur in xylene [19] and oxygen in organic matrices [20] has also been reported using an ICP-PDA spectrometer.

1.3 Plasma Diagnostics with PDA Spectrometers

PDA spectrometers have been used in two basic configurations, spectral and spatial, for obtaining fundamental plasma data. In the spectral configuration the PDA is mounted horizontally in the exit focal plane of a spectrometer as shown in Figure 1.1. The PDA is oriented along the spectral axis, so that multi-wavelength data is obtained.

In the spatial configuration the PDA is mounted vertically in the exit focal plane as in Figure 1.3. In a stigmatic monochromator, with a spectrochemical source imaged on the entrance slit, the PDA, in this configuration, can be used to measure emission as a function of vertical height in the source. If this entire spectrometer is now rotated by 90 degrees, relative to the source, emission as a function of lateral distance across the source can be measured. With this configuration only a single wavelength can be monitored at a time.

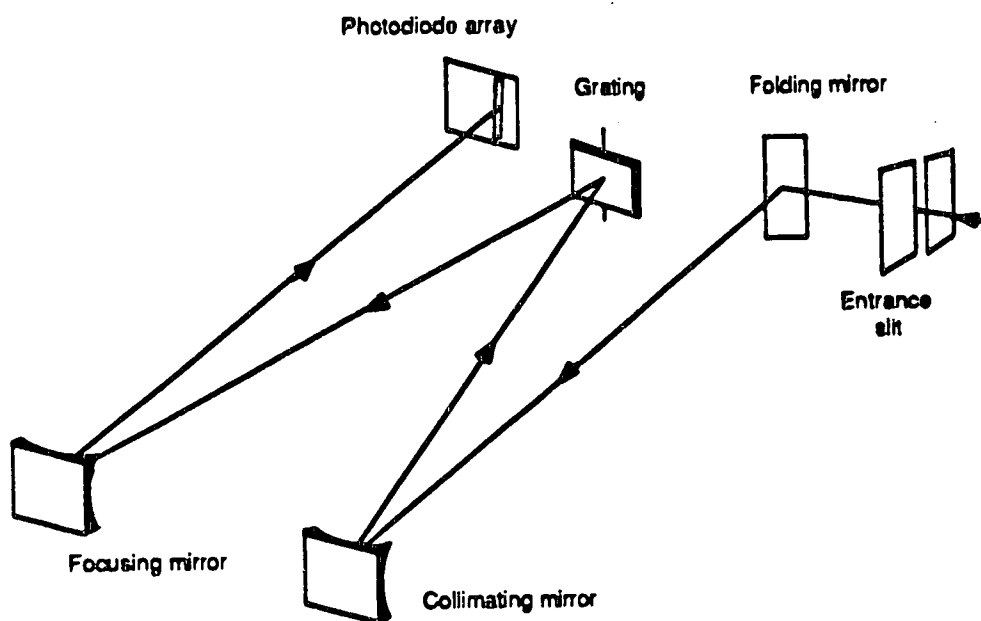


Figure 1.3 Schematic diagram of monochromator in the spatial configuration with PDA mounted vertically.

Edmonds and Horlick [21] described a 256 element PDA spectrometer for spatially resolved measurements. The PDA was mounted vertically in the exit focal plane and was used to measure vertical emission profiles of an ICP source. With the PDA in this configuration the entire emission profile could be acquired in a single scan.

Blades and Horlick [22] used a spectrometer in this configuration to study the effects of RF power and aerosol gas flow rate on the emission intensity as a function of observation height. The effect of easily ionizable element matrices on the vertical emission profile was also investigated [23]. Choot and Horlick [24] used this spectrometer to measure the vertical spatial profiles of an Ar-N₂ mixed gas ICP.

As mentioned above lateral spatial profiles can be measured with such a PDA spectrometer if it is rotated 90 degrees relative to the ICP [25]. The lateral profile can be Abel inverted to provide radially resolved emission data. The method was later developed to account for asymmetries in the ICP discharge [26]. Furuta and Horlick [27] used both vertical and lateral spatial profiles to study analyte emission and to measure spatially resolved excitation temperatures in the ICP.

PDA spectrometers have also been used extensively in the spectral configuration, to make multi-wavelength measurements for fundamental plasma studies. Choot and Horlick used a 1024

element PDA spectrometer to measure analyte and background spectra [28], signal to noise ratios [29], and peak width to calculate electron density [30] in Ar-N₂ mixed gas plasmas.

Caughlin and Blades [31] described a 1024 element PDA spectrometer for spectral measurements. With this spectrometer Blades et al. have investigated excitation temperatures [32], spatially resolved electron densities [33], analyte ionization [34], and excitation conditions in low flow torches [35] for the ICP.

Walker and Blades [36] developed a spectrometer with a 4096 element PDA. Pixels in this PDA are on 15 μm centers and are 0.5 mm high. The total light sensitive area is 61 mm long. Resolution is 37 pm, full width at half maximum (FWHM) and the wavelength coverage is approximately 48 nm. The 4096 element PDA allows higher resolution and better peak shape definition than previous PDA spectrometers and yet maintains a comparable wavelength coverage. Blades et al. have used this spectrometer for excitation temperature measurements [37], in computer modelling of emission spectra [38], to study the effect of nebulizer gas flow rate on electron density [39], and to study the effect of RF power on excited state level populations [40].

Many of these plasma studies would not have been possible, if not for the multichannel capabilities of the PDA. In a diagnostic study a single parameter may require several thousand individual intensity measurements. In the study by Choot and Horlick [30], electron density maps were

measured at 90 spatial positions in the ICP. The PDA spectrometer was used to acquire a multi-wavelength spectrum at each position with a single scan. Without the PDA, a single electron density map would have required 5760 individual intensity measurements. In the case of the PDA spectrometer in the spatial configuration, Blades and Horlick [25] stated that the PDA not only increased the speed and ease of acquiring Abel inverted data, but also improved the spatial accuracy with which the lateral profiles can be acquired.

Without simultaneous multi-wavelength or spatially resolved data and computer controlled acquisition, experiment times would have been prohibitive and many of these fundamental studies would not have been attempted.

1.4 Spectrometer Configurations for PDAs

All PDA spectrometers described to this point, have had a relatively simple optical configuration. The PDA has been mounted in the exit focal plane of a "monochromator" as shown in Figure 1.1. Simultaneous wavelength coverage is limited to a single spectral window ranging from 1 nm to 50 nm, depending on the pixel spacing of the PDA and the reciprocal dispersion of the monochromator. Emission lines from an ICP range from 200 nm to 400 nm and if the wavelength range covered by the PDA spectrometer is not sufficient, the grating must be moved and another window is selected. Once a

second window is required the technique is no longer truly simultaneous. There have been a number of approaches to attempt to increase the wavelength coverage and maintain the simultaneous measurement capabilities.

The most straight forward solution is to use a separate PDA for every spectral window. A spectrometer for atomic emission analysis is currently being developed using nine 1024 element PDAs mounted in the exit focal plane of a spectrograph [41]. The PDAs are overlapped slightly to provide continuous wavelength coverage over the range 200 to 1000 nm. The PDAs effectively become an electronic photographic plate. The system is relatively expensive and the hardware required to control the PDAs is extensive.

Along similar lines another multiple PDA system has been designed for ICP-AES [42]. Six 128 element PDAs were used to replace the PMTs in a direct reading polychromator. Each PDA covers a 1.7 nm spectral window, with a 13 pm per pixel resolution and each was controlled with its own single board computer [43]. Several spectral lines and background could be detected within each window and with careful selection, the six PDAs could be positioned to detect a number of elements. Although the spectral coverage is not continuous, the PDAs can be moved in the focal plane relatively easily, making the spectrometer more flexible than the conventional PMT based direct reading polychromator.

A novel PDA spectrometer configuration has been recently introduced [44]. The total spectrometer consists of three

optical subsystems. Light entering the spectrometer is dispersed and optically filtered with a mask in the first optical system, recombined in the second stage, and then redispersed with a high resolution echelle grating and detected by a PDA in the third section. Details of the optical configuration and the operation of the spectrometer have been described [45]. The spectral characteristics of this instrument have been evaluated [46] and it was reported to have the multi-wavelength capabilities and wide wavelength coverage of a direct reader. Since masks can be interchanged, it also has the flexibility of a scanning monochromator. The analytical capabilities of this new spectrometer have been investigated for multi-elemental, trace analysis of metals in oils [47].

1.5 PDA Developments

Before a PDA spectrometer can fully match or exceed the analytical capabilities of PMT spectrometers, both the UV sensitivity and resolution-wavelength coverage of PDA spectrometers must be improved. To improve the PDA sensitivity, image intensifiers have been used. The intensifiers are expensive and degrade resolution by two or three times and therefore, have not found widespread use. Another approach has been to use low noise electronics for signal amplification. This approach does not improve

sensitivity but increases the signal to noise ratio, allowing detection of low light levels.

Wavelength coverage will be extended when larger PDAs, with more pixels are developed, but until improvements in integrated circuit fabrication technology is realized larger PDAs are not possible.

One area of technology that has developed sufficiently and can reduce the cost and improve the performance of a PDA spectrometer is microcomputer technology. Over the last five to ten years microcomputers have appeared in almost every laboratory application. Their wide spread use has resulted in the generation of a variety of hardware and software products for laboratory applications.

If the information in a PDA spectrum is to be utilized to the maximum, the spectrum must be digitized and stored in a digital computer. The microcomputer makes this procedure simpler and more affordable. In the following chapter the development of a microcomputer controlled PDA spectrometer is described in detail. The system consists of a microcomputer (IBM-pc), commercial analog-digital I/O board (Data Translation DT2801-A), commercial software (ASYST Scientific Software), and a simple in-lab designed clock/timer interface. The system is simpler in design and operation than previous PDA spectrometers designed around minicomputers.

The availability of software and the relative simplicity of programming a microcomputer make it possible to take full advantage of available computing power and data processing

techniques. Data processing maximizes the information that can be obtained from a PDA spectrum. Three data processing techniques have been effected as routine procedures for the PDA spectrometer and will be described in Chapter 2.

Zero filling or Fourier domain interpolation is described and is used to interpolate peak shapes and thus enables accurate determination of relative peak heights. A procedure for automated wavelength calibration has been developed. Once the wavelength axis is converted from diode numbers to wavelength it is possible to automate peak detection. Also, a method has been developed to select integration times for the PDA so that the optimum integration times will be used regardless of signal intensity.

When combined, the data processing procedures improve the accuracy, speed, and dynamic range, and decrease the operator skill required for the operation of the PDA spectrometer. Overall, an improvement in spectrometer performance of three to four times can be realized, without changing the PDA or the spectrometer configuration. With this increased performance, analytical and diagnostic applications, not previously possible, can now be developed.

Using all these procedures, a method for the measurement of excitation temperatures in the ICP, based on the relative intensities of Fe emission lines, was developed.

A goal in designing the PDA spectrometer was to develop an instrument that could be used to perform a variety of measurements with a variety of sources. To increase the

flexibility of our PDA spectrometer, a fiber optic cable was used to optically couple the source and the spectrometer. The conventional method of aligning emission source, lens, and spectrometer entrance slit can be restricted by the size of the components. The fiber optic cable can be positioned virtually in any location and can be easily repositioned to view a different region of the source. The characteristics of the fiber optic cable has been evaluated, based on throughput and spectral and spatial resolution.

The PDA spectrometer with fiber optic cable has the capability to perform a number of unique measurements. The final chapters describe a study of the optical properties of the ICP-mass spectrometer (ICP-MS). In addition to increasing the analytical capabilities of the ICP-MS, an optical channel can be used to study the effects of central gas flow rate, RF power, and spatial position on signal intensity and signal noise.

References

1. P. W. J. M. Boumans, "Inductively Coupled Plasma Emission Spectroscopy" Pt.2, Wiley-Interscience, New York, (1987)
2. Hamamatsu Technical Data Sheet, PCD Linear Image Sensors S2304 Series
3. G. Horlick and E. G. Coddling, "Contemporary Topics in Analytical and Clinical Chemistry" Vol.1, D.M. Hercules ed., Plenum Press, (1977)
4. Y. Talmi and R. W. Simpson, Appl. Optics, **19**, 1401, (1980)
5. F. Grabau and Y. Talmi, "Multichannel Image Detectors" Vol.2, p.75, American Chemical Society, ACS Symposium Series 236, Washington, (1983)
6. S. W. McGeorge and E. D. Salin, Spectrochim. Acta, **38B**, 633, (1983)
7. S. W. McGeorge and E. D. Salin, Spectrochim. Acta, **40B**, 435, (1985)
8. S. W. McGeorge and E. D. Salin, Spectrochim. Acta, **40B**, 447, (1985)
9. S. W. McGeorge and E. D. Salin, Spectrochim. Acta, **40B**, 1039, (1985)

10. S. W. McGeorge and E. D. Salin, *Anal. Chem.*, **57**, 2740, (1985)
11. S. W. McGeorge and E. D. Salin, *Spectrochim. Acta*, **41B**, 327, (1986)
12. F. S. C. van der Plas, E. Uitbeijerse, M. T. C. de Loos-Vollebregt, and L. de Galan, *Spectrochim. Acta*, **42B**, 1027, (1987)
13. M. C. Edlson, E. L. DeKalb, R. K. Winge, and V. A. Fassel, *Spectrochim. Acta*, **41B**, 475, (1986)
14. R. K. Winge, V. A. Fassel, and M. C. Edlson, *Spectrochim. Acta*, **43B**, 85, (1988)
15. J. W. Carr and G. Horlick, *Spectrochim. Acta*, **37B**, 1, (1982)
16. S. K. Hughes, R. M. Brown Jr. and R. C. Fry, *Appl. Spectrosc.*, **35**, 396, (1981)
17. J. M. Keane, D. C. Brown and R. C. Fry, *Anal. Chem.*, **57**, 2526, (1985)
18. J. M. Keane and R. C. Fry, *Anal. Chem.*, **58**, 790, (1986)
19. M. W. Blades and P. Hauser, *Anal. Chem. Acta*, **157**, 163, (1984)
20. P. Ch. Hauser and M. W. Blades, *Appl. Spectrosc.*, **39**, 872, (1985)

21. T. E. Edmonds and G. Horlick, *Appl. Spectrosc.*, **31**, 536, (1977)
22. M. W. Blades and G. Horlick, *Spectrochim. Acta*, **36B**, 861, (1981)
23. M. W. Blades and G. Horlick, *Spectrochim. Acta*, **36B**, 881, (1981)
24. E. H. Choot and G. Horlick, *Spectrochim. Acta*, **41B**, 889, (1986)
25. M. W. Blades and G. Horlick, *Appl. Spectrosc.*, **34**, 696, (1980)
26. M. W. Blades, *Appl. Spectrosc.*, **37**, 371, 1983
27. N. Furuta and G. Horlick, *Spectrochim. Acta*, **37B**, 53, (1982)
28. E. H. Choot and G. Horlick, *Spectrochim. Acta*, **41B**, 907, (1986)
29. E. H. Choot and G. Horlick, *Spectrochim. Acta*, **41B**, 925, (1986)
30. E. H. Choot and G. Horlick, *Spectrochim. Acta*, **41B**, 935, (1986)
31. B. L. Caughlin and M. W. Blades, *Spectrochim. Acta*, **39B**, 1583, (1984)

32. B. L. Caughlin and M. W. Blades, *Spectrochim. Acta*, **40B**, 579, (1985)
33. B. L. Caughlin and M. W. Blades, *Spectrochim. Acta*, **40B**, 987, (1985)
34. B. L. Caughlin and M. W. Blades, *Spectrochim. Acta*, **40B**, 1539, (1985)
35. L. L. Burton and M. W. Blades, *Appl. Spectrosc.*, **40**, 256, (1986)
36. Z. Walker and M. W. Blades, *Spectrochim. Acta*, **41B**, 761, (1986)
37. M. W. Blades, B. L. Caughlin, Z. H. Walker, and L. L. Burton, *Prog. Anal. Atom. Spectrosc.*, **10**, 57, (1987)
38. L. L. Burton and M. W. Blades, *Spectrochim. Acta*, **41B**, 1063, (1986)
39. B. L. Caughlin and M. W. Blades, *Spectrochim. Acta*, **42B**, 353, (1987)
40. Z. Walker and M. W. Blades, *Spectrochim. Acta*, **42B**, 1077, (1987)
41. K.J. Timmons and D. W. Snow, XXV Colloquium Spectroscopicum Internationale, Toronto Ont. paper no, H4.2, (1987)

42. R. Evans, PhD. Thesis, Department of Chemistry,
University of Alberta, Edmonton, Alberta, (1983)
43. G. Horlick and T. McGowan, XXV Colloquium
Spectroscopicum Internationale, Toronto Ont. paper no,
H1.2, (1987)
44. G. M. Levy, A. Quaglia, and R. E. Lazure, Pittsburgh
Conference and Exposition on Analytical Chemistry and
Applied Spectroscopy, New Orleans, La., paper no. 749,
(1987)
45. G. M. Levy, A. Quaglia, R. E. Lazure, and S. W.
McGeorge, Spectrochim. Acta, **42B**, 341, (1987)
46. V. Karanossios and G. Horlick, Appl. Spectrosc., **40**,
413, (1986)
46. T. H. Huang, J. Chin. Chem. Soc., **34**, 199, (1987)

Chapter 2

Photodiode Array Systems for ICP-AES

2.1 Introduction

The basic PDA spectrometer is one in which a single PDA is mounted in the exit focal plane of a simple plane grating "monochromator". The schematic diagram of such a system was shown in Figure 1.1 in Chapter 1. A more complete block diagram of a PDA spectrometer system, with emphasis on the PDA system is shown in Figure 2.1.

The ICP is a model HFD-2500F Plasma-Therm system and the spectrometer is a Heath model EU-700. The spectrometer has a focal length of 350 mm and a reciprocal dispersion of about 2 nm/mm. Both of these systems are those used for most of our previous ICP-PDA spectrometer measurements, which were briefly reviewed in Chapter 1. The PDA used for many of those measurements was the E. G. & G. Reticon 1024S in conjunction with the RC1024S evaluation circuit board. In this chapter two new PDA systems will be described, the Hamamatsu S2304-1024Q PDA and a Reticon RC1024S system using the new RC1000 and RC1001 circuit boards. Details of mounting the arrays in

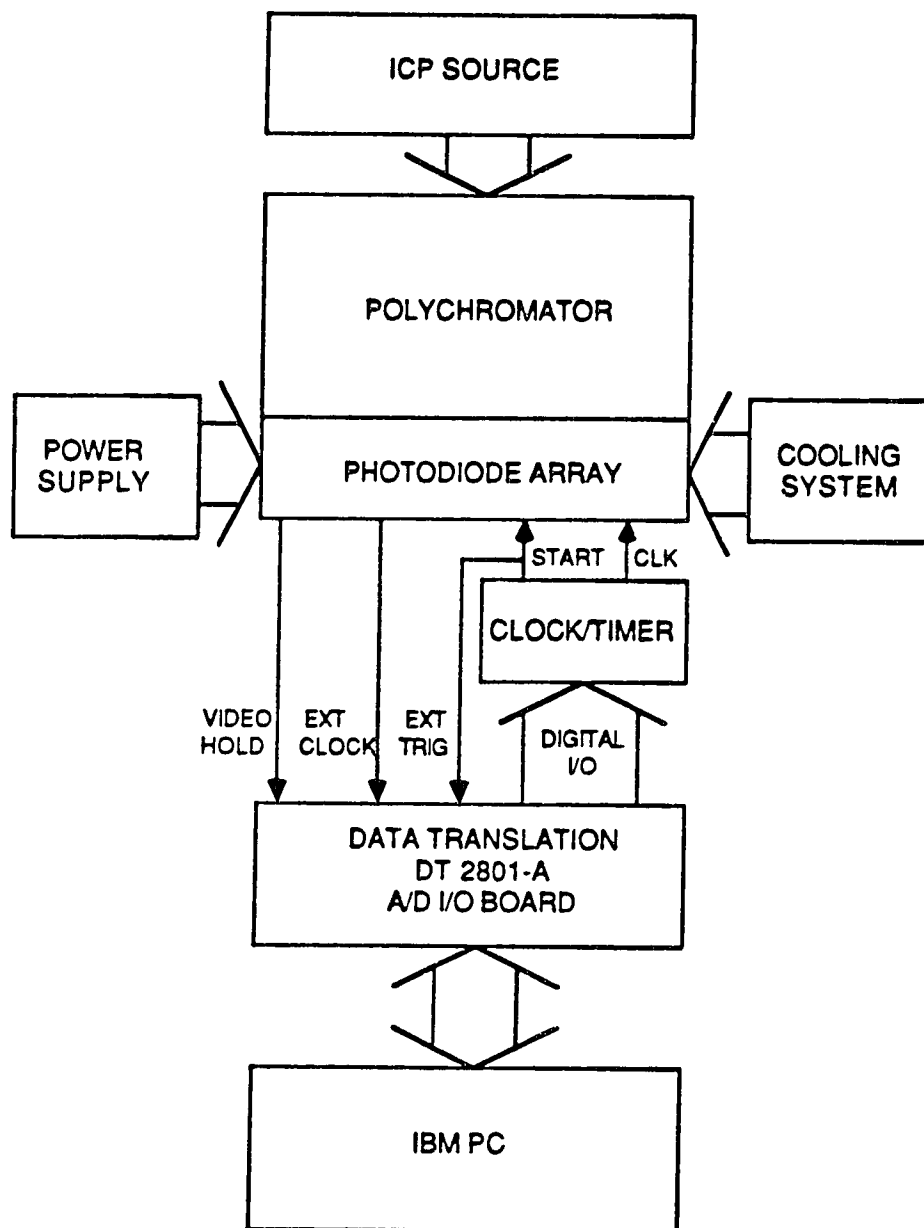


Figure 2.1 Block diagram of ICP-PDA spectrometer.

the spectrometer focal plane, Peltier based cooling sub-systems for the arrays, clocking systems, and interfacing the arrays to an IBM-pc are presented. Then, the operational and measurement characteristics of all arrays for ICP-AES will be briefly compared.

2.2 Hamamatsu S2304-1024Q PDA

The Hamamatsu S2304-1024Q PDA used for this study consists of 1024 elements with a center-to-center spacing of 25 μm (p islands 13 μm wide). The elements have a height of 2.5 mm. This basic geometry is essentially identical to that of an E. G. & G. Reticon 1024S device. The devices do differ with respect to the thickness of the silicon dioxide overcoat on the array. On the Hamamatsu device, this overcoat is only 0.4 μm thick, while it is 3 μm thick on the Reticon device.

A compact driver/amplifier board (Low Noise C2325) is available for the Hamamatsu array. The size of the board (~ 10 cm by 6.5 cm) is such that it can be readily mounted in the exit focal plane of the spectrometer. In addition, a slot is cut in the board allowing access to the back of the array which simplifies the design and mounting of a cooling system for the array. A schematic diagram of the Hamamatsu driver/amplifier board is shown in Figure 2.2. In order to run the array, in addition to power (+5V, +/-15V), one simply has to provide a start pulse (START) and a master clock signal (CLK). The start pulse initializes the PDA and the

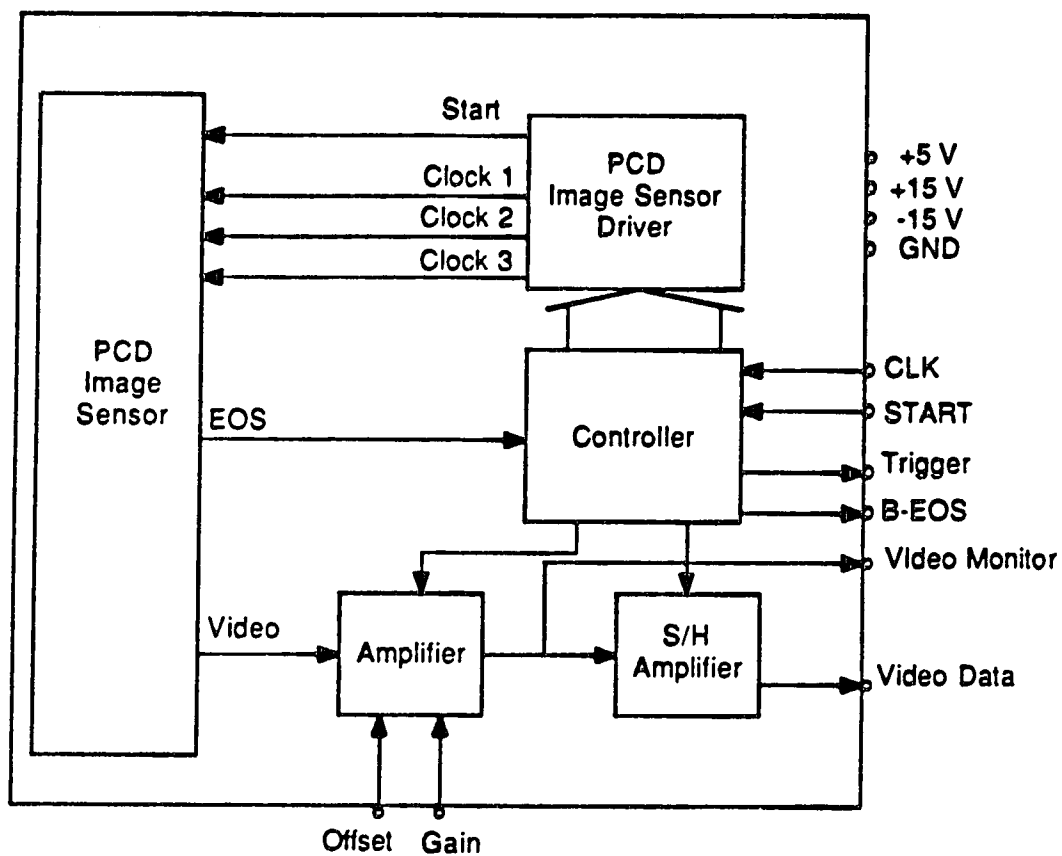


Figure 2.2 Schematic of Hamamatsu C2325 (Low Noise) driver/amplifier board.

driver/amplifier board and initiates readout of the array. The time between start pulses determines the integration time of an array measurement. The master clock (CLK) input drives the three phase clock on the driver/amplifier board. The three phase clock sequences the actual readout of the array. The maximum specified frequency for the CLK line is 250 kHz.

The two main outputs from this board are the Video Data line and the Trigger line. The Video Data line is simply the PDA output signal and the Trigger line is the output clock. It has a frequency that is 1/4 that of the input master clock and can be used to directly clock an ADC connected to the Video Data output line.

The Hamamatsu PDA system was interfaced to an IBM-pc using a Data Translation DT2801-A A/D I/O board and a custom built clock/timer (Figure 2.3). The DT2801-A is an interface board which plugs into a slot in the IBM-pc and it contains a 16 channel, 12 bit ADC, two 12 bit DAC's and two 8 bit digital I/O ports. The ADC can be external clocked and triggered, and the maximum conversion rate for the ADC is 27.5 kHz.

The clock/timer to provide the START and CLK signals to the array board was built using a 1 MHz crystal controlled oscillator and an Intel 8253 programmable interval timer. While the 8253 is designed to be run directly from a microcomputer bus, it can be completely controlled and operated from the digital I/O ports on the DT2801-A. The data

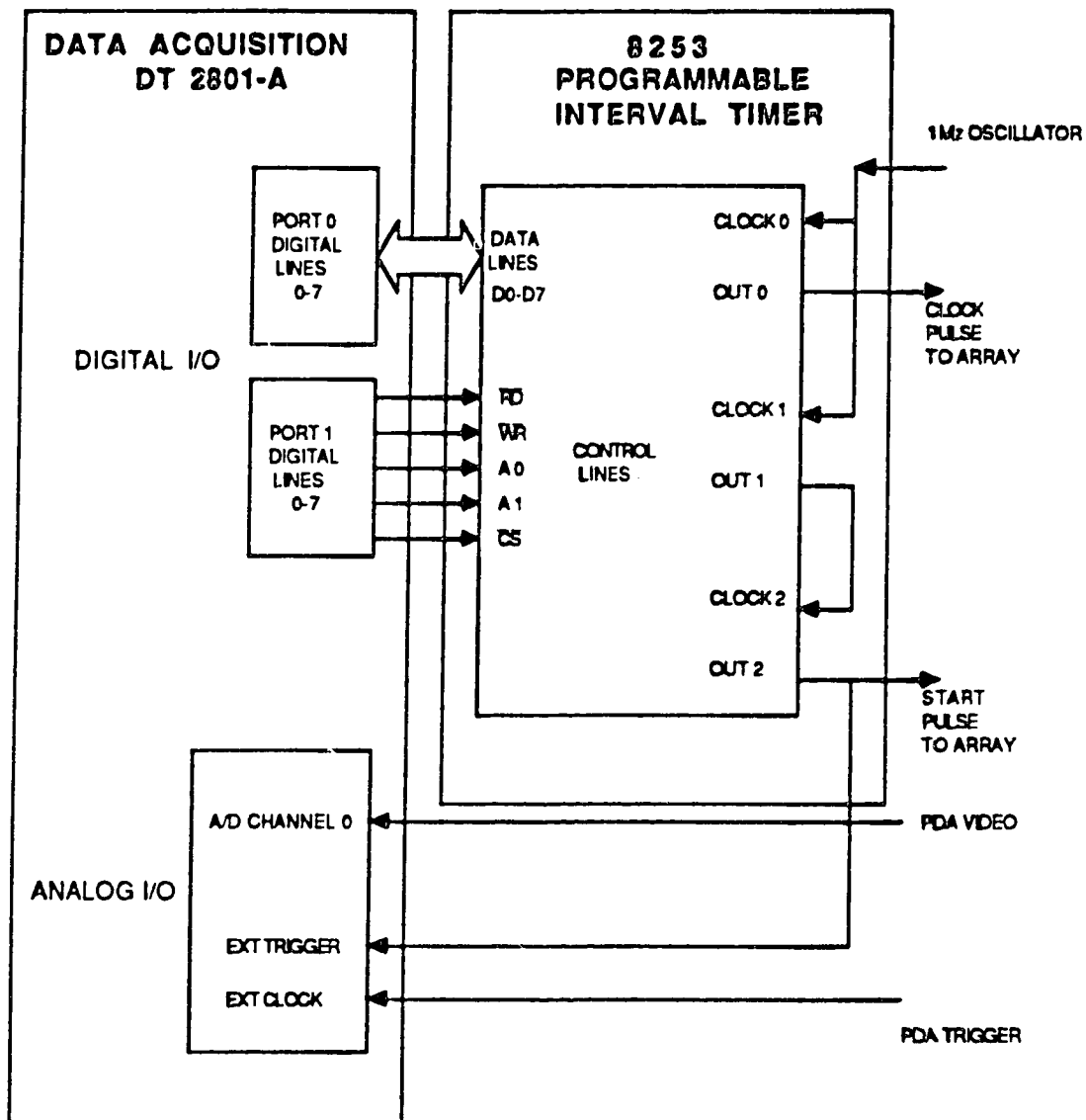


Figure 2.3 Schematic diagram of Data Translation DT2801-A I/O and Intel 8253 clock/timer interface.

lines of the 8253 were connected to Port 0 and the control lines were connected to Port 1 (Figure 2.3).

The 8253 contains three, independently programmable 16 bit counters. Counter 0 was used to provide the master clock signal. It was run as a divide by N counter (8253 Mode 2) [1]. With the 1 MHz input signal, software programmable clock rates from 1 MHz to 15 kHz could be generated. Since the maximum clocking rate for the ADC on the DT2801-A board is 27.5 kHz, the maximum clock rate that could be used to run the array board was 110 kHz (CLK input = 4 x Trigger Output).

Counters 1 and 2 on the 8253 were connected in series and both were also run as divide by N counters (Mode 2). These counters provided the start pulse for the array board and thus controlled the integration time. The minimum integration time that can practically be used is set by the time required to read out the complete array signal at the maximum data rate. For a 1024 element array at a data rate of 27.5 kHz, one readout cycle takes 38 msec which, therefore, is the minimum integration time.

The start pulse line is also connected to the external trigger port of the DT2801-A board and is used to synchronize the start of PDA readout with the start of data conversion. The Trigger pulse is provided by the driver/amplifier board and is connected to the external clock port of the DT2801-A. This timing pulse is used to synchronize data conversion with each diode readout.

The maximum integration time is limited by saturation of the array by the signal and/or the dark current. In order to maximize the integration capability of the array for weak signals, it is necessary to cool the array. Without cooling, dark current alone will saturate the array at an integration time of about 9 seconds. A cooling system for the array has been designed utilizing a Peltier effect cooling module (Melcor, Trenton, New Jersey) and a copper bus to conduct heat away from the array. A schematic diagram of the cooler is shown in Figure 2.4 and a photograph of the system is shown in Figure 2.5. The cold side of the Peltier cooler is coupled to the PDA by a copper bus which passes through the slot in the driver/amplifier board and contacts the back of the PDA chip. As mentioned earlier, this slot on the board is provided by the manufacturer. A thermal conductive paste is used to ensure good thermal contact of the cold copper bus with the array. The warm side of the Peltier device is in contact with a water cooled copper bus. With this design temperatures of approximately -20 degrees Celsius, at the array, can be achieved. Lower temperatures are possible if two or more Peltier cooling units are stacked in series. The Peltier cooler was operated at approximately 11 V and 4 amps making possible integration times of up to 100 seconds. To prevent condensation of water vapour and/or formation of ice on the PDA, the spectrometer is continually flushed with dry N₂.

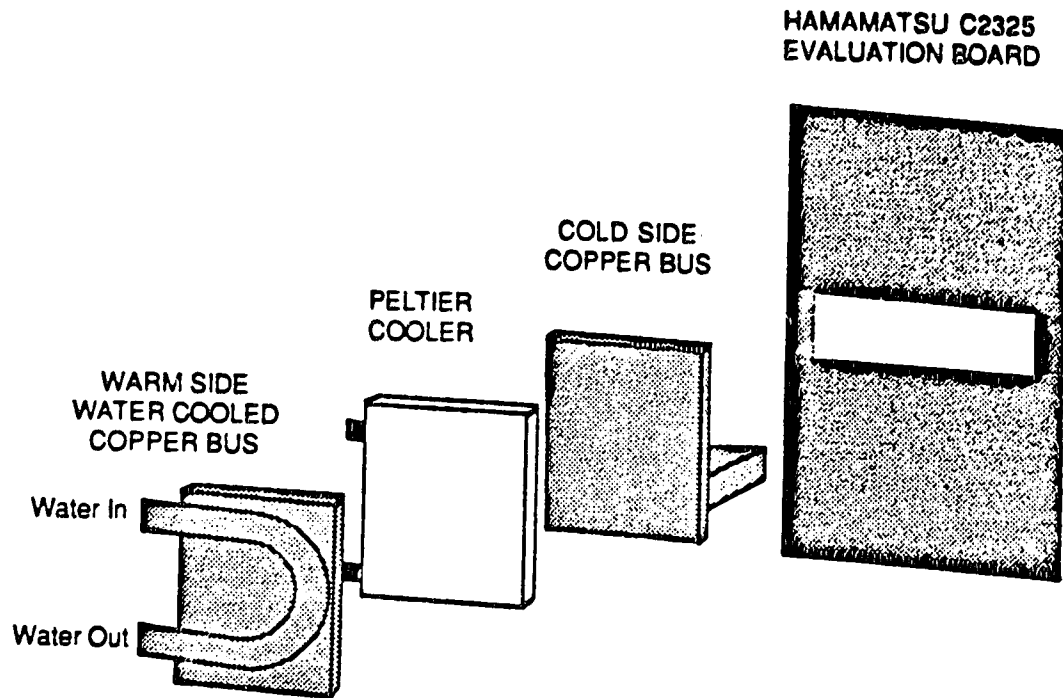
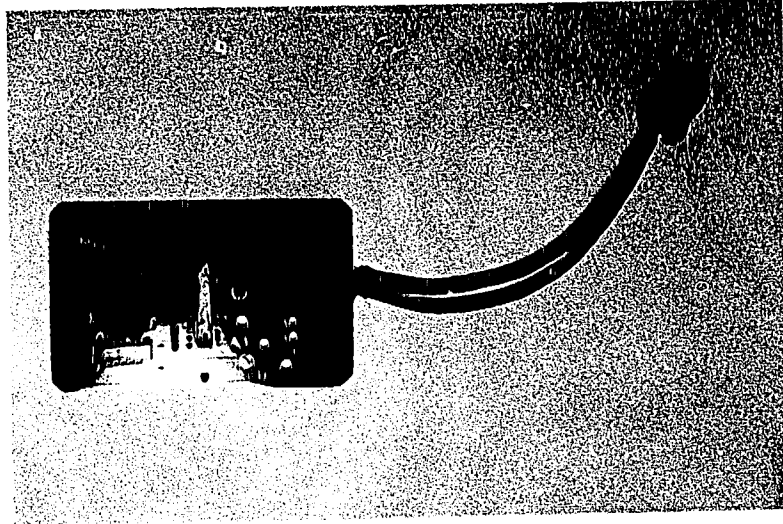


Figure 2.4 Hamamatsu C2325 driver/amplifier evaluation board with Peltier effect cooler and warm and cold side copper bus.

(a)



(b)

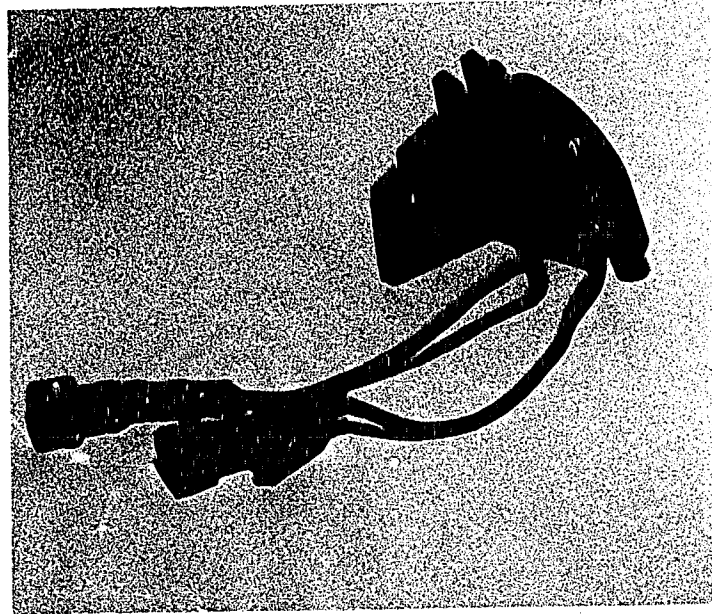


Figure 2.5 Photograph of a) Hamamatsu C2325 board and b) Peltier effect cooler with copper bus.

2.3 Reticon 1024S with RC1000 and RC1001 Boards

A new Reticon PDA system was also investigated in this study. The system consisted of a Reticon "S" series 1024 element PDA, an RC1000 mother board and an RC1001 satellite board. The RC1000 mother board is relatively large (~20 cm x 10 cm) however, the PDA sensor is mounted on the smaller (~10 cm x 5 cm) detachable satellite board (RC1001). A slot is provided in the satellite board for the easy interfacing of a cooling device to the back side of the array. It is recommended by the manufacturer that for low noise applications, the separation between the RC1000 mother board and the RC1001 satellite board be kept to a minimum. For this reason, the two boards were mounted together, along with the clock/timer interface electronics, directly in the spectrometer focal plane (Figure 2.6). Note the array location as shown in Figure 1.1.

The RC1000 mother board is provided with a fully self contained timing system and the PDA can be operated without any external, user supplied timing signals (Figure 2.7). The board is equipped with a variable frequency oscillator and an integration counter. The master clock oscillator controls the PDA clock frequency. The integration counter uses a series of divide by N counters to supply a PDA start pulse. The

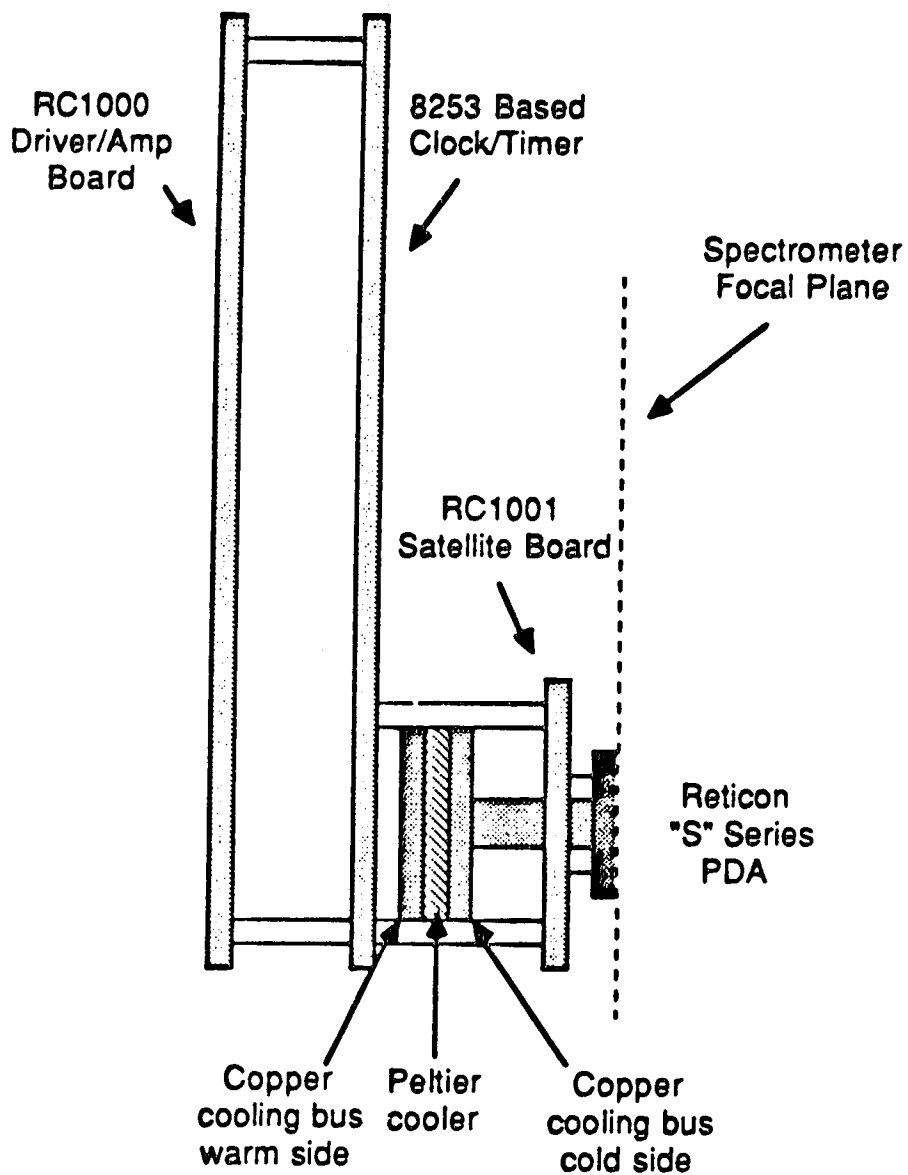


Figure 2.6 Side view of Reticon 1024S PDA with RC1000, RC1001, and 8253 clock/timer boards and Peltier effect cooling system.

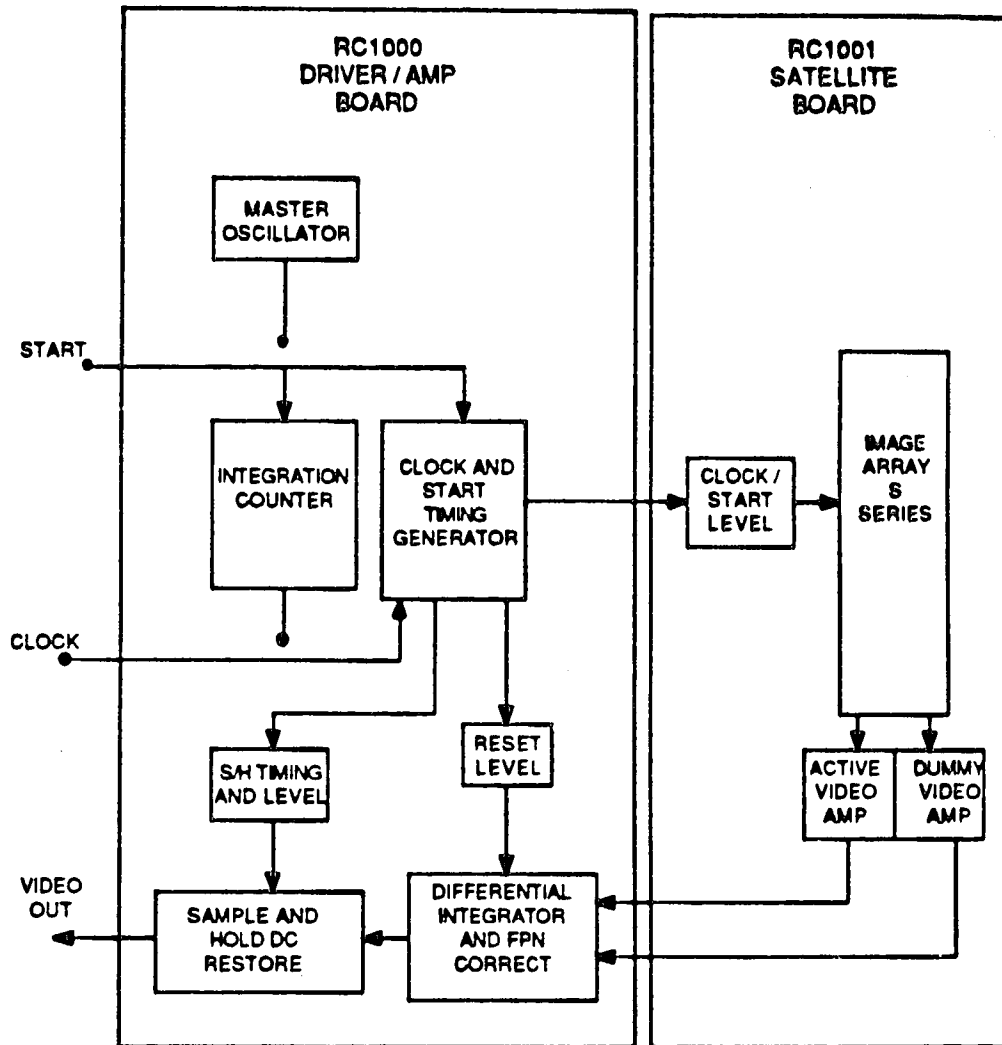


Figure 2.7 Schematic diagram of Reticon RC1000 and RC1001 driver/amplifier boards.

integration time is set by the user via a series of hardware switches located on the RC1000 mother board.

Using the switches, a maximum integration time of about 0.2 seconds can be obtained. For atomic spectrochemical measurements, integration times in the range of 0.05 seconds to 100 seconds are often required. For this reason and the difficulty in accessing the switches on the mother board, plus the fact that the master oscillator signal is not readily available to the user as an output, an external timing source was used to control the PDA.

Jumpers supplied by the manufacturer on the RC1000 board were set to by-pass the master oscillator and integration counter. The Intel 8253 clock/timer system described in the previous section was used to generate the start pulse and clock pulse for the Reticon PDA. The clock/timer interface was operated exactly as with the Hamamatsu system, with the exception, the clock frequency, set by counter 0 on the 8253, must be the actual clock frequency of the array and not four times the frequency. The clock frequency was set at 27.5 kHz. This clock signal to the PDA was also used as the external clock to control the ADC conversion rate. The time between start pulses, the integration time, must contain a multiple of 4 clock pulses. When the integration time is selected under software control, the time between start pulses is automatically adjusted by the computer program to contain a multiple of 4 clock pulses.

The cooling system used with the Reticon PDA was identical to the system described for the Hamamatsu PDA.

2.4 Reticon 1024S with RC1024S Board

Some comparative results are presented in this chapter, to measurements made with an E. G. & G. Reticon 1024S device used in conjunction with the older Reticon RC1024S evaluation circuit board. This is a sub-system that has been used in the laboratory for a number of years [2]. No satellite board is provided for the array as in the newer system just described and since the RC1024S evaluation circuit board is quite large (~21 cm x 11.5 cm) is not possible to directly mount this system in the focal plane of the EU-700 monochromator. In order to use this PDA system in conjunction with this monochromator a new exit folding mirror was mounted inside the monochromator about 10 cm in front of the normal exit folding mirror. This shown schematically in Figure 2.8. This new folding mirror (Mirror C in Figure 2.8) could be swung out of the spectrometer and the monochromator could be used in its normal configuration with a PMT detector. When the mirror was in place, the exit focal plane was brought out the side of the monochromator where there was room to mount the Reticon RC1024S evaluation circuit containing the 1024S array.

In contrast to the Hamamatsu evaluation circuit, the Reticon board contains the circuitry to provide the clocking

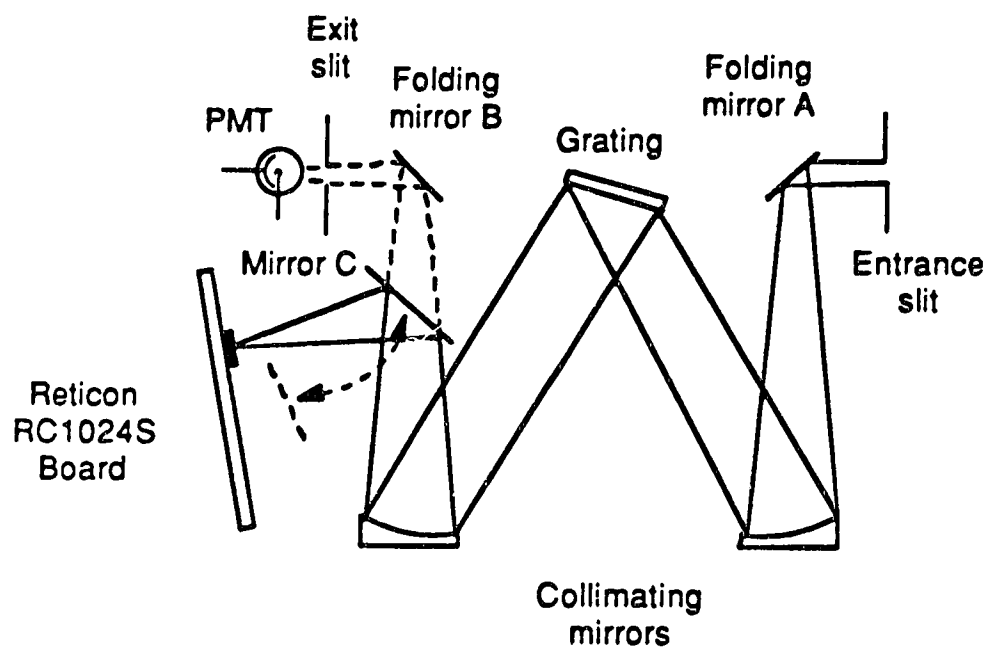


Figure 2.8 Schematic diagram of Czerny-Turner type monochromator with Reticon PDA and RC1024S evaluation board.

and start pulses to the array. However, only 12 bits of switch selectable divide by N counting is provided on board to generate start pulses. When running the array at 27 kHz data rates, this does not provide sufficiently long integration times. This problem is similar to that of the Reticon RC1000/1001 system discussed in the last section. Instead of using external clocking as described in the last section, the integration time was extended by adding two more 9316 4-bit binary counters to the timer on the RC1024S board [3]. Also an appropriate ADC clock signal is not provided on the pin outs of this board. We used the output of NAND gate 11 [4] and brought it out to connector pin W.

Finally, since the back of the array is not readily accessible, array cooling sub-systems were more difficult to mount and design than for the two newer systems just described. By double socketing the array, it is possible to mount a copper bus behind the array, with part of the bus extending out each end. Peltier effect cooling modules can then be mounted on each end, to cool the copper bus and hence the array. This system is shown schematically in Figure 2.9.

2.5 IBM-pc Data Acquisition System

The computer used with these systems was an IBM-pc, equipped with 640 kBytes RAM, 8087 math coprocessor, and AST Six-pack Plus expansion board. All software was written using the ASYST Scientific Software System (MacMillan Software, New

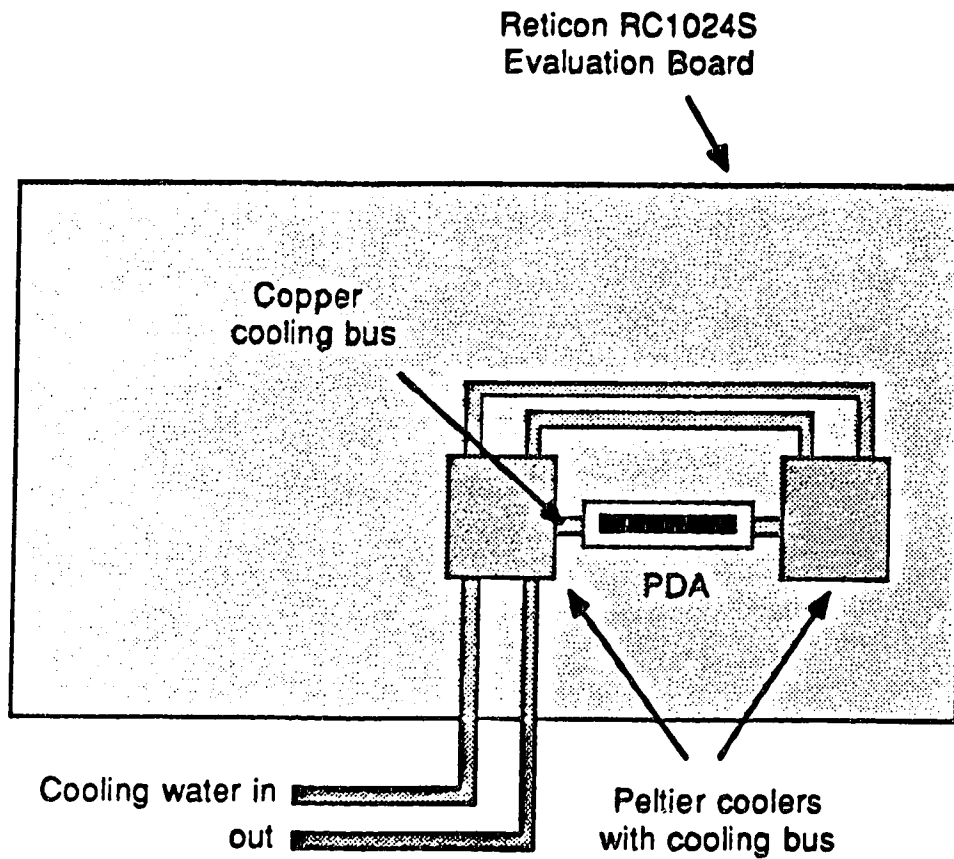


Figure 2.9 Schematic diagram of Reticon 1024S PDA and RC1024S evaluation board with Peltier effect cooling system.

York, New York) [5,6], which also supports the DT2801-A board. Although this software package requires the user to do a certain amount of programming in a FORTH-like language, it greatly simplifies the task of programming for data acquisition and control, and greatly enhances the speed and performance of the computer for data processing and graphics.

2.6 PDA Performance

In order to assess the performance of the PDA spectrometers as detectors for ICP-AES, a direct comparison among all systems was made using a single ICP source. For all measurements the ICP was operated at 1.25 kW. The argon gas flows were: outer gas 16 Lpm, intermediate gas 1 Lpm and central (nebulizer) 0.75 Lpm. The viewing height was 15 mm above the load coil and a 100 mm focal length quartz lens was used to produce a 1:0.5 reduced image of the plasma at the spectrometer entrance slit. Criteria considered in this comparison were sensitivity, spectral response, readout noise, dynamic range and detection limits.

The slope of the analytical calibration curve was used for the comparison of relative PDA sensitivities. Calibration curves were measured for Ca, Mn, Mg, Cd, and Zn over the concentration range 0.1 $\mu\text{g/mL}$ to 50 $\mu\text{g/mL}$. The intensity for each element at each concentration was calculated from the peak height of the spectral line in the PDA spectrum. The

peak height was converted to units of current, in order to make the slopes of the calibration curve independent of the integration time and the dynamic range of the PDA. The peak height is usually measured in ADC units (digital counts). To convert to current (pA), the peak as a fraction of PDA saturation is multiplied by the charge on the PDA at saturation, and divided by integration time. For example, 4095 digital counts is the PDA at saturation and the saturation charge for the Reticon 1024S PDA is 14 pC, therefore for a peak of 1000 counts, measured with an integration time of 10 seconds:

$$(1000 \text{ counts}/4095 \text{ counts}) \times 14 \text{ pC} / 10 \text{ seconds} = 0.34 \text{ pA}$$

The slopes of the calibration curves are tabulated in Table 2.1. For Ca 393.3 nm and Mg 279.6 nm all PDAs have approximately the same sensitivity. For Mn 257.6 nm, Cd 228.8 nm, and Zn 213.8 nm, the Hamamatsu PDA has better sensitivity. At the shortest wavelength, 213.8 nm, the Hamamatsu sensitivity is approximately 3 times greater than the other PDAs. This improvement in UV response can be attributed to the thinner silicon dioxide overcoat layer. The Hamamatsu array has a silicon dioxide layer 0.4 μm thick versus a 3 μm thick layer on the Reticon arrays. The thinner overcoat allows more UV photons to penetrate to the active silicon layer below and create electron hole pairs.

Table 2.1 PDA sensitivity, measured from slopes of analytical calibration curves.

Sensitivity [pA/($\mu\text{g/mL}$)]

Element	Line (nm)	Hamamatsu	Reticon RC1000	Reticon RC1024S
Ca	393.3	21	21	23
Mg	279.3	4.6	4.9	2.5
Mn	257.6	0.65	0.38	0.33
Cd	228.8	0.16	0.082	0.044
Zn	213.3	0.20	0.071	0.042

Some typical ICP spectral signals measured with the Hamamatsu array for a one second integration period are shown in Figure 2.10. Note that the concentration of Ca and Mg solutions was 1 $\mu\text{g/mL}$ but that the Zn concentration was 10 $\mu\text{g/mL}$. With a 25 second integration time, 100 ng/mL levels of Cd and Zn can be easily measured, as shown in Figure 2.11.

Noise in a PDA spectrum will originate from five sources: 1) ICP source fluctuations, 2) photon shot noise, 3) shot noise of the dark current, 4) noise due to the video amplifier, and 5) reset noise of the array pixels. Points 1 and 2 are dependent on the source, but points 3, 4, and 5 are related to the PDA and contribute to the array readout noise. If the array is cooled and if integration times are less than 2 seconds, dark current shot noise does not contribute significantly to the array readout noise [7]. Therefore, the major sources of array readout noise is amplifier noise and pixel reset noise. These two forms of noise occur at the time of array readout. Readout noise was determined by acquiring 16 dark current spectra at an integration time of 0.04 seconds. The standard deviation at each pixel was calculated and the mean standard deviation of the 1024 pixels was reported as the PDA readout noise. Readout noise is typically reported as charge or number of electrons, as these units are independent of integration time. The Reticon RC1024S evaluation circuit had a readout noise of 1.7×10^4 electrons. The Reticon RC1000/1001 system had a readout noise of 1.1×10^4 electrons.

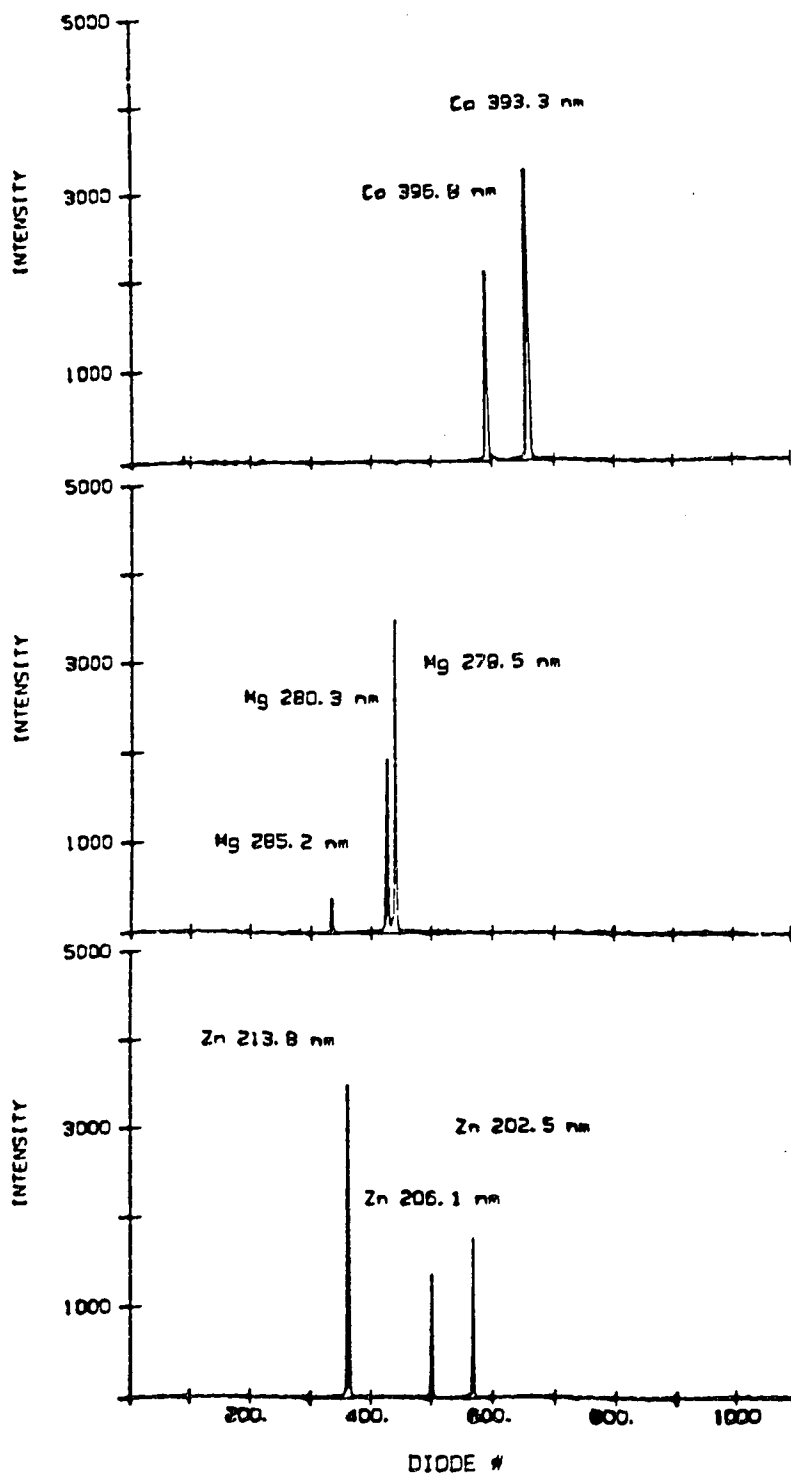


Figure 2.10 ICP-PDA spectra of a) 1 $\mu\text{g/mL}$ Ca, b) 1 $\mu\text{g/mL}$ Mg and c) 10 $\mu\text{g/mL}$ Zn measured with a 1 second integration time.

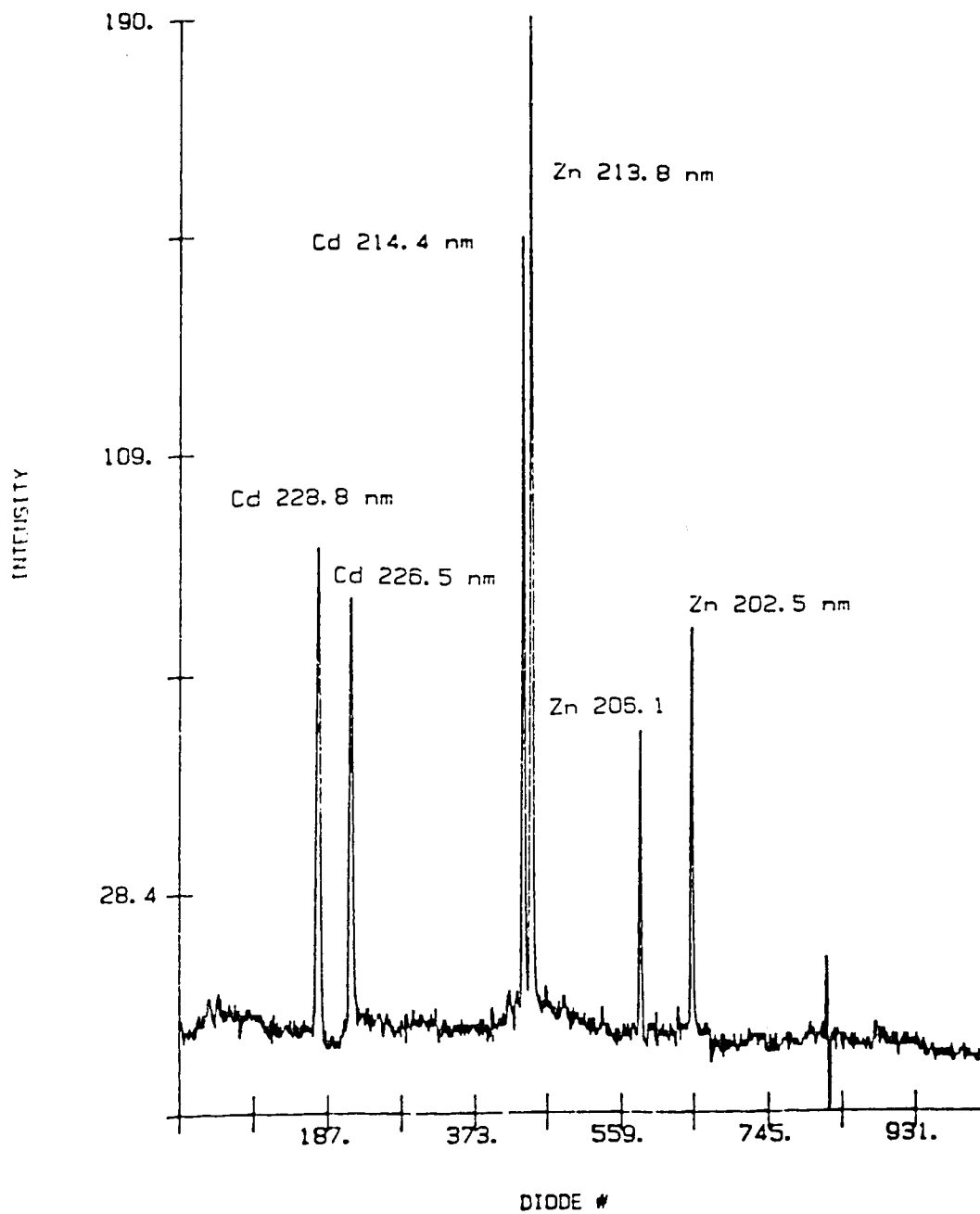


Figure 2.11 ICP-PDA spectrum of 100 ng/mL Cd and Zn measured with a 25 second integration time.

The Hamamatsu C2325 system had the highest readout noise of 2.1×10^4 electrons.

Since low noise PDA systems have been built with a readout noise of 1400 electrons [7], it is suspected most of the readout noise results from commercial amplifier boards which have not been optimized for low noise performance.

Dynamic range is defined as the ratio of the largest observable signal to the baseline noise. The largest observable signal is limited by the maximum charge on a photodiode at full reverse bias. The Reticon 1024S has a saturation charge of 14 pC and the Hamamatsu S2304-1024Q has a saturation charge of 7.5 pC. The baseline noise for a PDA is the readout noise. The Reticon RC1000/1001 system has a dynamic range of 8000. Dynamic range is often quoted in orders of magnitude, this is simply $\log_{10}(\text{dynamic range})$. Therefore, the Reticon RC1000/1001 dynamic range is 3.9 orders of magnitude. The Reticon RC1024S system dynamic range is 5200 or 3.7 orders of magnitude and the Hamamatsu PDA dynamic range is 2200 or 3.4 orders of magnitude. The PDA dynamic range is significantly less than the dynamic range of the PMT, which is typically greater than six orders of magnitude. A measurement approach is described in Chapter 3 involving the use of multiple integration times that can extend the PDA dynamic range to 6 orders of magnitude.

Finally, for their application in ICP-AES measurements, an important figure of merit for a PDA spectrometer is detection limits. The detection limits are given for a number

of elements in Table 2.2 for the three PDA system. The detection limits were determined for an integration time of 10 seconds. The standard deviation of the pixel at the spectral peak position was calculated for ten replicate blank PDA spectra and three times the standard deviation was used to calculate the detection limit. The detection limits for Ca and Mg are similar for all systems. Over the 300 to 400 nm wavelength range, the sensitivities of the Reticon and Hamamatsu PDAs are approximately equal and the limiting noise results from the spectral background of the ICP. For elements with emission lines further in the UV (Cd and Zn), the Hamamatsu PDA detection limits are superior by a factor of three. This improvement in detection limit is probably related to the improved UV response of the Hamamatsu PDA (Table 2.1), which has been attributed to the thinner silicon dioxide overcoat on the Hamamatsu array, as noted earlier.

2.7 Conclusions

In this chapter three PDA spectrometers for ICP-AES have been described and characterized. The Hamamatsu S2304-1024Q/C2325 and Reticon 1024S/RC1000/1001 PDA systems are compact and can be simply mounted, along with all interface electronics and Peltier cooling sub-system in the exit focal plane of a small monochromator.

The PDA spectrometer described in this chapter covers a relatively large spectral window, approximately 50 nm, but

Table 2.2 PDA detection limits measured with a 10 second integration time.

Detection Limit (ng/mL)

Element	Line (nm)	Hamamatsu	Reticon RC1000	Reticon RC1024S
Ca	393.3	1	1	1
Mg	279.3	1	1	0.9
Mn	257.6	5	11	9
Cd	228.8	10	25	30
Zn	213.3	9	27	30

to cover the full spectral range for lines emitted by the ICP (200-400 nm), at least four spectral windows must be sequentially scanned. The pixel spacing for the spectrometer is only 0.05 nm/pixel, but the spectral resolution is still limited by the spectrometer entrance slit width, grating dispersion, and focal length. The spectral resolution is about three pixels FWHM (0.16 nm) for an entrance slit of 30 μm .

The PDA spectrometers were designed to operate with an IBM-pc microcomputer and Data Translation DT2801-A I/O board. With the clock/timer interface that has been developed, all timing operations, including integration time, are under software control, thus allowing automated control of many aspects of spectrum acquisition, which will be discussed in the following chapter. The use of a microcomputer makes the PDA spectrometer much simpler to operate than the previous minicomputer systems [2].

Of the three PDA systems, the Hamamatsu S2304 PDA had the best UV response but, the Reticon RC1000/1001 system had the lowest readout noise. The improved sensitivity is related to the integrated circuit structure of the PDA, but for the most part, readout noise is related to the amplifiers on the driver/amplifier boards. In the future, it may be possible to reduce the readout noise of a PDA simply by changing the analog circuitry.

McGeorge [8] reported detection limits of 1 ng/mL for Ca (393.3 nm) and 4000 ng/mL for Zn (202.6 nm) with an ICP-PDA

spectrometer with a ten second measurement time. Salin and Horlick [2] reported detection limits of 1 ng/mL for Ca (393.3 nm) and 50 ng/mL for Zn (213.8 nm). These detection limits are close to the detection limits listed in Table 2.2, with the exception of the Zn 202.3 nm line. The reason for this difference is that the detector response falls off rapidly around 200 nm. Grabau and Talmi [9] reported detection limits of 0.04 ng/mL for Mn (257.6 nm), 0.2 ng/mL for Cd (228.8 nm), and 0.3 ng/mL for Zn (213.8 nm) with an ICP-PDA spectrometer with a 16.4 second integration time. These results are at least one order of magnitude better than any detection limits listed in Table 2.2. There are three points to consider when comparing the two sets of detection limits. First, differences in ICP operating conditions may cause improvements in detection limits. Second, longer integration times will improve detections, if the source of limiting noise is the detector readout noise, as is the case at the detection limit for lines less than 250 nm. Finally, the method of calculating the noise at the detection limit is important. Grabau and Talmi calculated the noise based on the standard deviation of ten neighbouring pixels near the peak. This noise has been called the intra-spectrum noise and has been shown to be less than the inter-spectra noise [8]. The inter-spectra noise is calculated by taking replicate PDA spectra and calculating the standard deviation at each diode and then finding the mean of all standard deviations.

In this chapter the basic characteristics of the PDA spectrometer have been defined in terms of wavelength coverage, pixel resolution, and dynamic range. In the following chapter data processing routines will be described which will maximize the pixel resolution within the given wavelength coverage, locate spectral lines, and maximize the dynamic range.

References

1. Intel MCS-80 Users Manual (with Introduction to MCS-85)
2. E. D. Salin and G. Horlick, *Anal. Chem.*, **52**, 1578, (1980)
3. R. G. Evans, PhD. Thesis, Department of Chemistry, University of Alberta, Edmonton, AB., (1983)
4. E. G. & G. Reticon, S-Series Solid State Line Scanners, Technical Data, (1978)
5. S. A. Bourman, *Anal. Chem.*, **57**, 983A, (1985)
6. M. Goldstein, *Research and Development*, February, 102, (1986)
7. R. W. Simpson, *Rev. Sci. Instrum.*, **50**, 730, (1979)
8. S. W. McGeorge, PhD. Thesis, Department of Chemistry, McGill University, Montreal, Que., (1985)
9. F. Grabau and Y. Talmi, "Multichannel Image Detectors" Vol.2, p.75, American Chemical Society, ACS Symposium Series 236, Washington, (1983)

Chapter 3

Data Processing for a Photodiode Array Spectrometer

3.1 Spectral Line-Diode Registry Effects with a PDA Spectrometer

3.1.1 Introduction

The interest in the PDA as a detector for ICP-AES stems from its ability to measure a number of spectral lines and background simultaneously, over a continuous spectral window. A PDA based spectrometer directly samples the wavelength axis of a spectrum, thus simplifying the acquisition, storage, processing, and display of the spectra with a digital computer. However, this sampling step may become a disadvantage when attempting to recover information from a PDA spectrum. Sampling of the spectral axis may result in errors in the determination of peak maximum locations, line shapes, and/or peak intensities.

Uncertainties in peak location are related to the nm/pixel rating of the PDA spectrometer [1]. Burton and

Blades [2] have shown differences exist in line shapes for ICP emission spectra measured with a scanning monochromator and PMT detector and with a PDA based spectrometer. Winge et al. [3] have shown that a 20 to 30% error in peak height may exist in a PDA spectrum. These errors can be attributed to the design and structure of the PDA elements and the process by which it samples the wavelength axis of a spectrum.

Kelly and Horlick [4] have discussed the effects of digitization for a number of general cases. In this section, we will describe digitization effects for a PDA spectrometer and how sampling errors can be avoided or corrected. In a large part, these errors result, not from improper sampling, but from improper processing of the sampled spectral signal when recovering peak parameter information.

3.1.2 PDA Sampling Process

Before beginning a discussion of sampling errors, a brief description of the PDA sampling process is necessary. The sampling of an image in the focal plane of a spectrometer by a PDA can be described in two steps (Figure 3.1) [5]. The first involves a convolution of the spectral image in the focal plane (Figure 3.1a) with the geometric response function (GRF) of a single PDA element (Figure 3.1b). The trapezoid form of the GRF arises from the fact that the PDA is constructed of alternating p-type and n-type silicon regions [1,6,7]. In the second step the convolved image

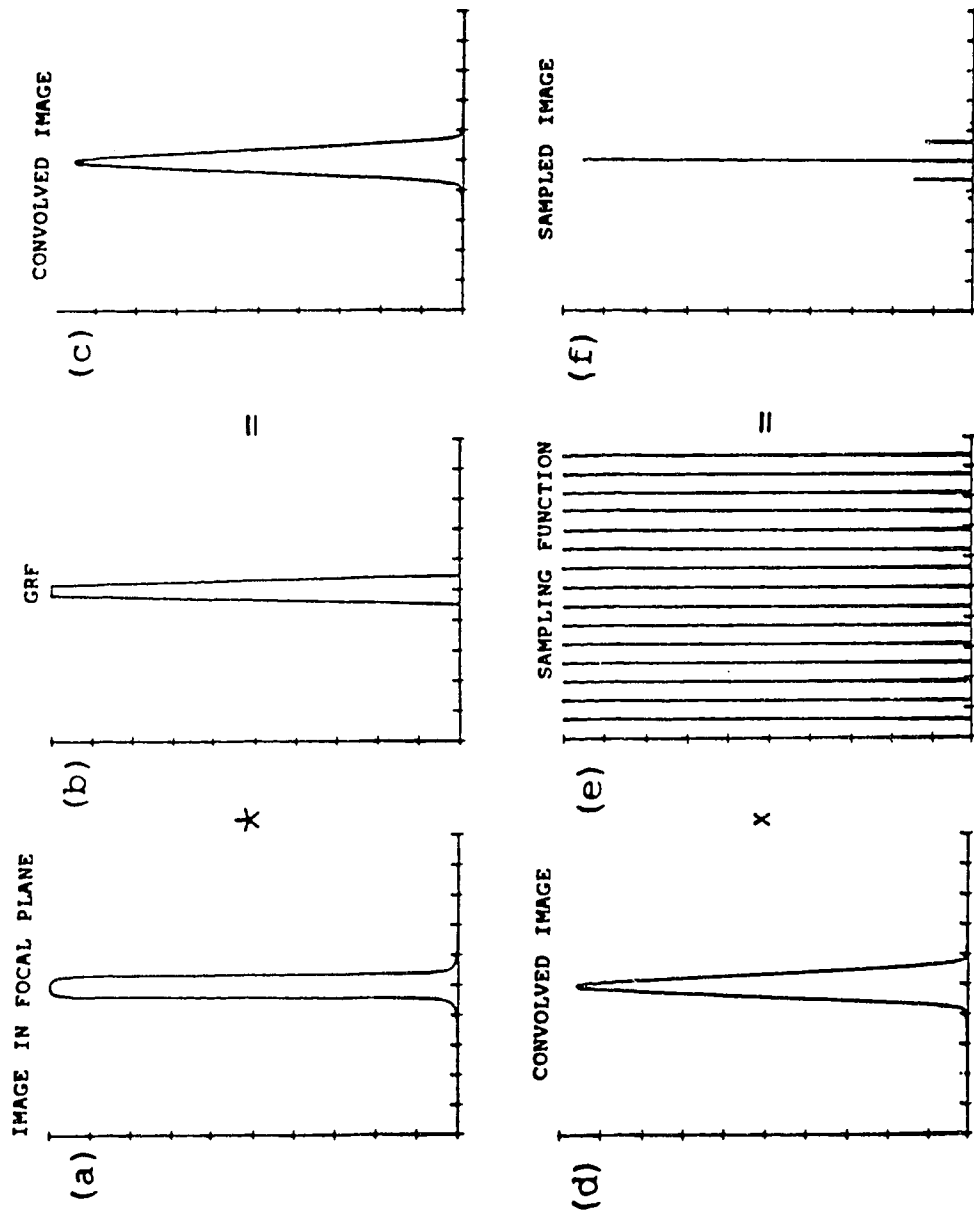


Figure 3.1 Illustration of the sampling of a spectral image by a PDA detector (see text for discussion).

(Figure 3.1d) is multiplied by a series of delta functions, spaced at Δx , the center-to-center spacing of the individual diodes, i.e. the sampling function (Figure 3.1e). The result is the sampled image (Figure 3.1f) which is the observed PDA spectrum.

This explanation clarifies two important points concerning the PDA. First, the GRF of the PDA is wider than the pixel spacing. Therefore, the pixels overlap and there are no gaps between pixels. Light is integrated across the full width of the PDA.

Second, as pointed out by Burton and Blades [2], the shape of a spectral line measured with a PDA spectrometer differs from the line shape of a spectral line measured with a scanning PMT based spectrometer. The line shape measured by the scanning monochromator is result of the convolution of the spectral image in the focal plane and the rectangular exit slit. The line shaped measured by the PDA spectrometer is a convolution of the spectral image and the trapezoidal GRF. This result is important if the fundamental spectral line shape is required from a PDA spectrum and the instrumental contribution to the total line shape must be removed.

3.1.3 Recovery of Spectral Information

The simplest method of obtaining an analog spectrum from sampled data is a linear interpolation. In this method a straight line is drawn to connect the points in the PDA spectrum. An error in peak intensity may occur, depending on the phase of the sampling function relative to the position of the image of the spectral line in the focal plane. This error has been called a spectral line-diode registry effect [3]. This registry effect is illustrated in Figure 3.2. For the spectrum shown in Figure 3.2a, the peak of the Mn 279.4 nm line falls between the centers of two adjacent pixels, i.e. the peak position is "out of phase" with the sampling function. The Mn 279.8 nm line (Figure 3.2a) is centered on a pixel or is "in phase" with the sampling function. The Mn 280.1 nm line (Figure 3.2a) is between these two extreme cases. For the spectrum shown in Figure 3.2b, the grating has been shifted by a small amount. Now the Mn 279.4 nm line is centered on a pixel, the Mn 279.8 nm line falls between two PDA diodes, and the Mn 280.1 nm line is again, between the two cases. The relative intensities for the Mn 279.4, 279.8 and 280.1 nm lines in Figure 3.2a are 1.0:0.90:0.58 and in Figure 3.2b are 1.0:0.66:0.50. Clearly from this example, the relative phase of the sampling function may be a problem if relative intensities are required, or if the grating is moved during an analysis, either by thermal expansion of

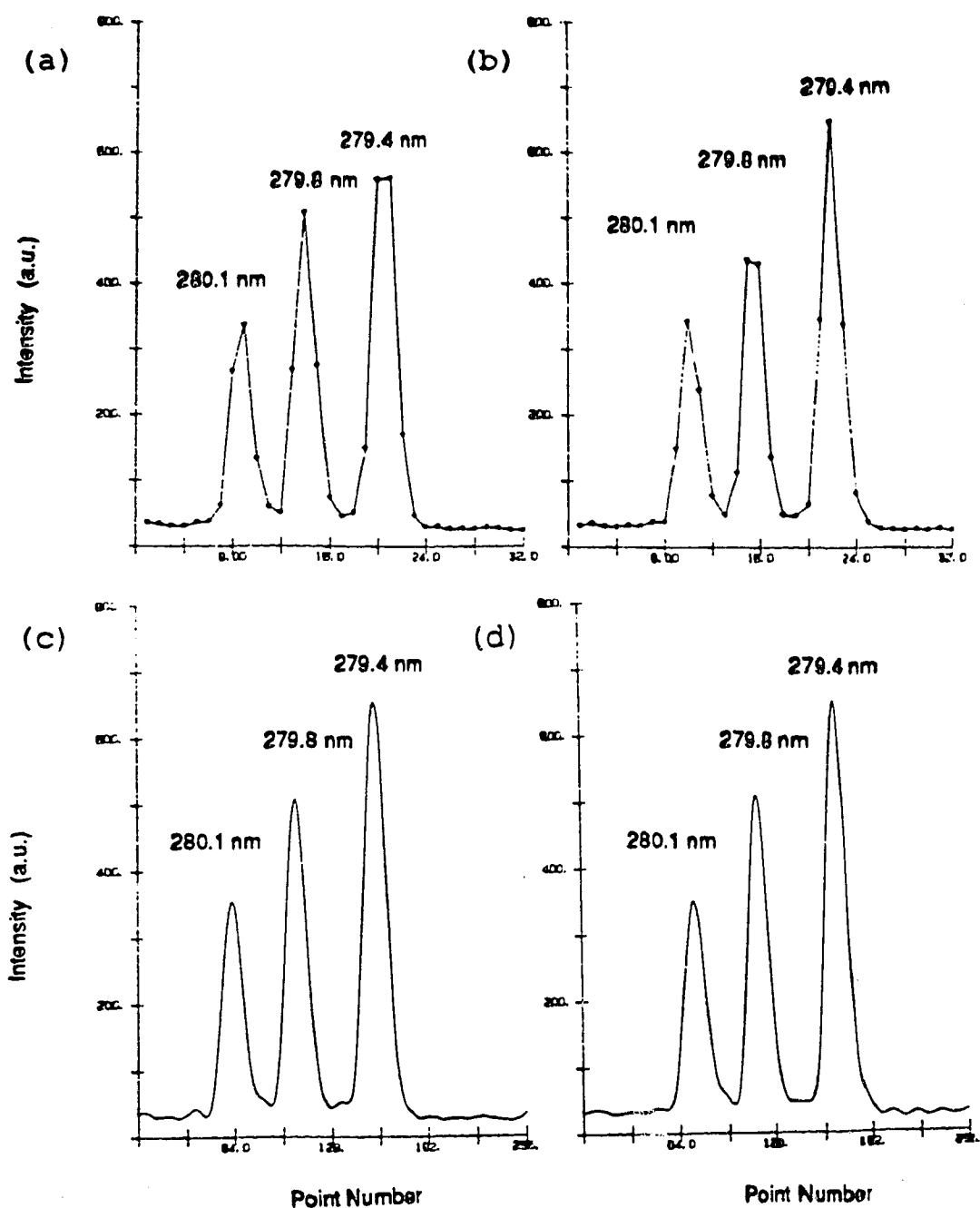


Figure 3.2 a) 32 pixels of Mn PDA spectrum, b) as in a) with small shift in grating position, c) Fourier domain zero filled spectrum of a), d) Fourier domain zero filled spectrum of b).

spectrometer parts or by scanning to another spectral window and back. The magnitude of the error may be reduced by increasing the width of the spectrometer entrance slit or by summing pixels across the peak, the latter is equivalent to measuring the peak area. Both solutions result in a decrease in spectral resolution. The problem is not one of under sampling. The spectra shown in Figure 3.2a and Figure 3.2b are both correctly sampled from the point of view of the sampling rate or the density of data points along the spectral axis relative to the spectral line widths. The problem is that linear interpolation is not the correct procedure for recovery of the signal information from the sampled set of data points.

This problem is not unique to PDA sensor based spectrometers. The identical effect will be observed when recording a spectrum with a stepper-motor controlled scanning monochromator with a PMT detector. In this case, the problem can be corrected by reducing the size of the grating steps, and hence over sampling the spectral axis. It is, of course, not possible to arbitrarily decrease the diode-to-diode spacing in a PDA spectrometer. However, instead of over sampling, it is possible to interpolate correctly the sampled data set. As hinted at above, the root of the spectral line-diode registry effects is the use of linear interpolation. It is clearly stated in basic sampling theory that recovery of signal information from a sampled data set should be achieved by convolution with an appropriately wide $(\sin x)/x$ function

[4,8]. An easy and efficient way to implement this interpolation is by a method known as Fourier domain zero filling [9,10].

Fourier domain zero filling (Figure 3.3) involves calculating the Fourier transform (Figure 3.3b) of the PDA spectrum (Figure 3.3a) and adding zeros to increase the length of the array from $1/\Delta x$ to $2^n(1/\Delta x)$, where n is an integer (Figure 3.3c). The ASYST Fourier transform algorithm, as with most others, requires that the data array has a multiple of 2^n data points. The inverse Fourier transform results in a spectrum with points spaced at $\Delta x/2^n$ (Figure 3.3d) and interpolated along the line shape determined by the original PDA spectrum.

The results of zero filling the two Mn spectra are shown in Figure 3.2. The relative peak heights are now 1.0:0.77:0.52 for the spectrum shown in Figure 3.2c and Figure 3.2d. The spectra now appear to be identical. Comisarow and Melka [11] have shown that Fourier domain zero filling to increase the size of the data array by four times will reduce the peak height error to less than 2%.

As noted earlier, Winge et al. [3] illustrated some problems with spectral line-diode registry effects with spectra acquired with a PDA based spectrometer. In particular they noted problems in accurate peak height measurements. In light of the results presented in this section, their problems appear to result from a failure to interpolate correctly their sampled spectral data. That is, they relied

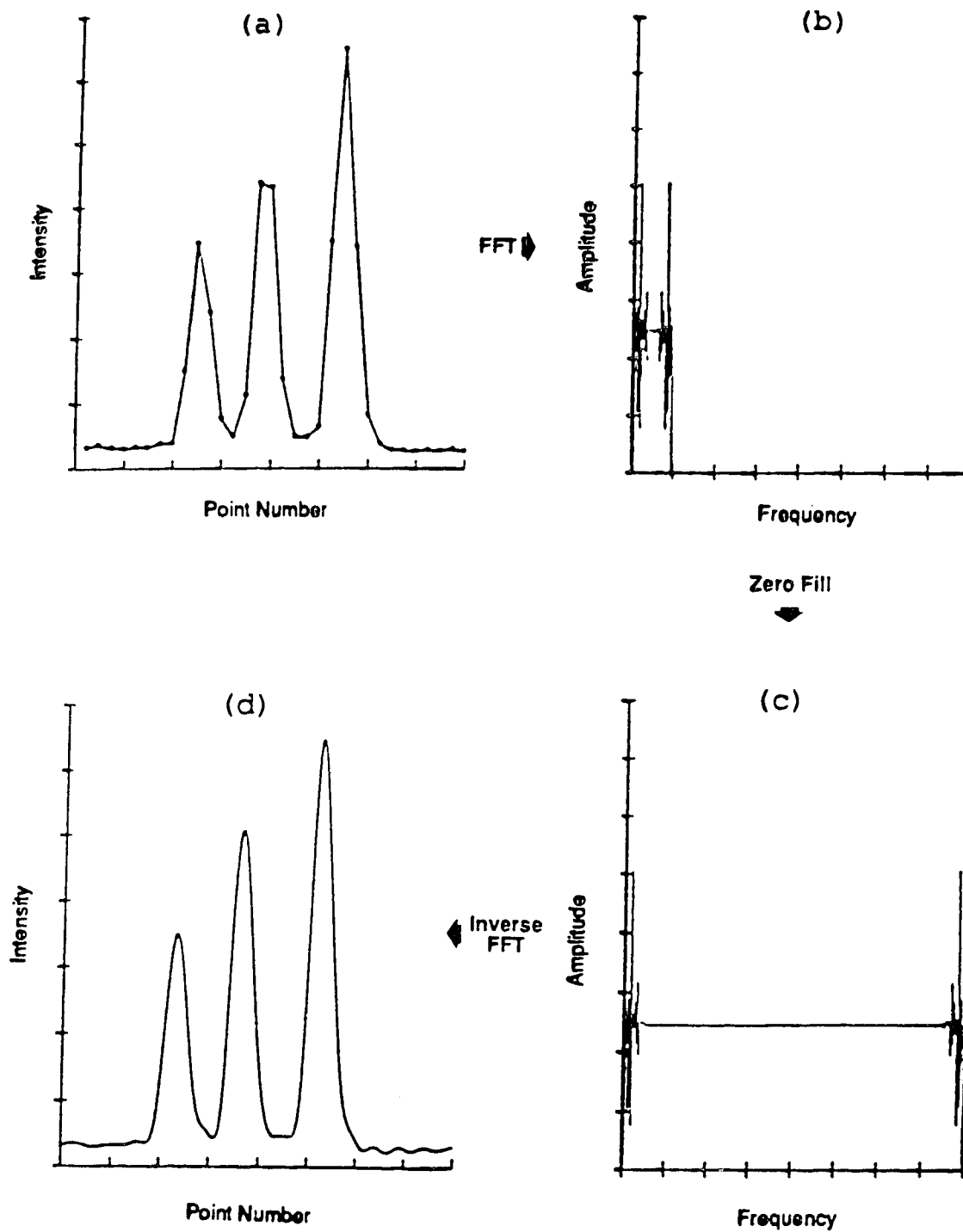


Figure 3.3 Fourier domain zero filling procedure (see text for discussion).

on linear interpolation. To illustrate their problem, they took a series of PDA spectra while slowly stepping the grating of the spectrometer. At each step a spectrum was acquired and the peak height of the Hg 253.65 nm line was determined and plotted against grating position. We have repeated this experiment with the ICP emission line of Mn at 279.4 nm and the result is shown in Figure 3.4. The valleys of the lower curve correspond to the center of the spectral peak falling between two diodes. The peaks in the lower curve correspond to the spectral peak aligned with a diode center. The upper line is the peak height of the same spectral line, except every spectrum has been Fourier domain zero filled by four times and apodized with a Gaussian line shape. Note that the valleys no longer exist. Thus, the spectral line-diode registry effect as discussed and illustrated by Winge et al. [3] does not exist and is a consequence of improper interpolation of sampled data set.

It is important to note that, although Fourier domain zero filling will correct sampling (spectral line-diode registry) errors, it does not allow one to ignore Shannon's sampling theorem [8]. Shannon's sampling theorem states that a signal must be sampled at a rate (the Nyquist frequency) at least as high as twice the highest frequency in the spectrum. In other words, the Fourier transform of the spectrum must be zero at the Nyquist frequency. The Nyquist frequency for a PDA spectrum corresponds to the point at $1/(2\Delta x)$. Whether or

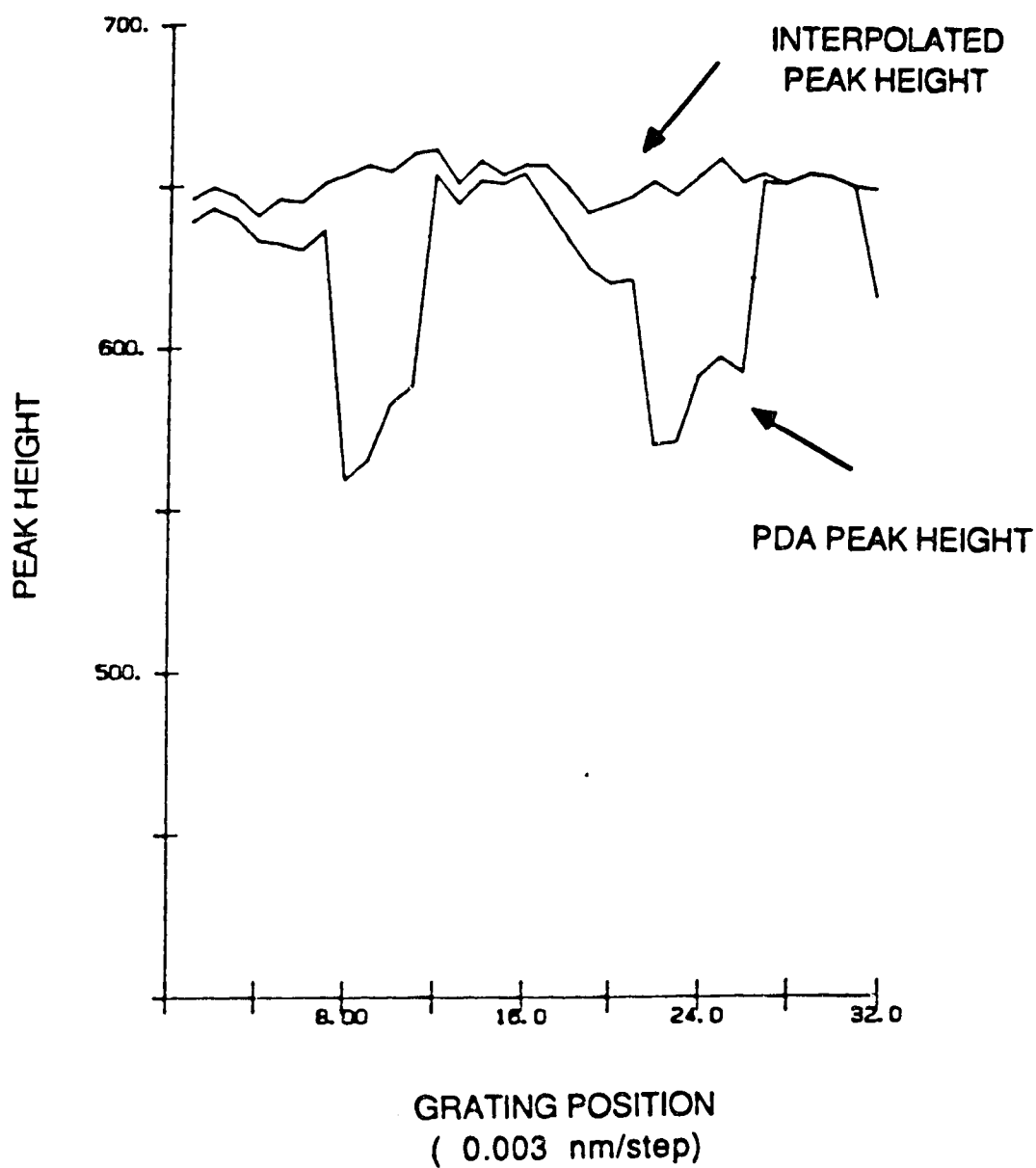


Figure 3.4 Peak height of Mn 279.4 nm line in PDA spectra as a function of grating position, lower curve, raw PDA spectra, upper curve, zero filled PDA spectra.

not this criterion is met depends on the entrance slit width and the shape of the image in the focal plane.

In the case of a narrow slit width, a spectral line will be narrow and as a result will be under sampled. The Fourier transform of the line will contain high frequency components and will not reach zero at the Nyquist frequency (f_N) and aliasing will result. This case is shown in Figure 3.5 using a HeNe laser as the source. The Fourier transform of this spectral line, acquired using a 100 μm slit, is shown in Figure 3.5a. The intensity is close to zero at the Nyquist frequency. This is also illustrated in Figure 3.3b for the Fourier transform of the Mn triplet. However, if the slit width is reduced to 10 μm and the HeNe laser line is reacquired and transformed, the resulting function is far from being zero at the Nyquist point (Figure 3.5b). Zero filling in this situation can result in the generation of significant spurious sidelobes in the zero filled spectrum.

This problem is specifically illustrated for a Mg doublet spectrum acquired with the PDA spectrometer with a slit width of 30 μm . This spectrum is shown in Figure 3.6a. The result of the application of Fourier domain zero filling to this spectrum is shown in Figure 3.6b and the generation of spurious sidelobes is clearly evident. The side lobes can be reduced by either increasing the slit width or by apodizing the Fourier domain spectrum, i.e. truncating the Fourier transform of the spectrum to force it to zero at the Nyquist frequency. An example of a spectrum apodized by

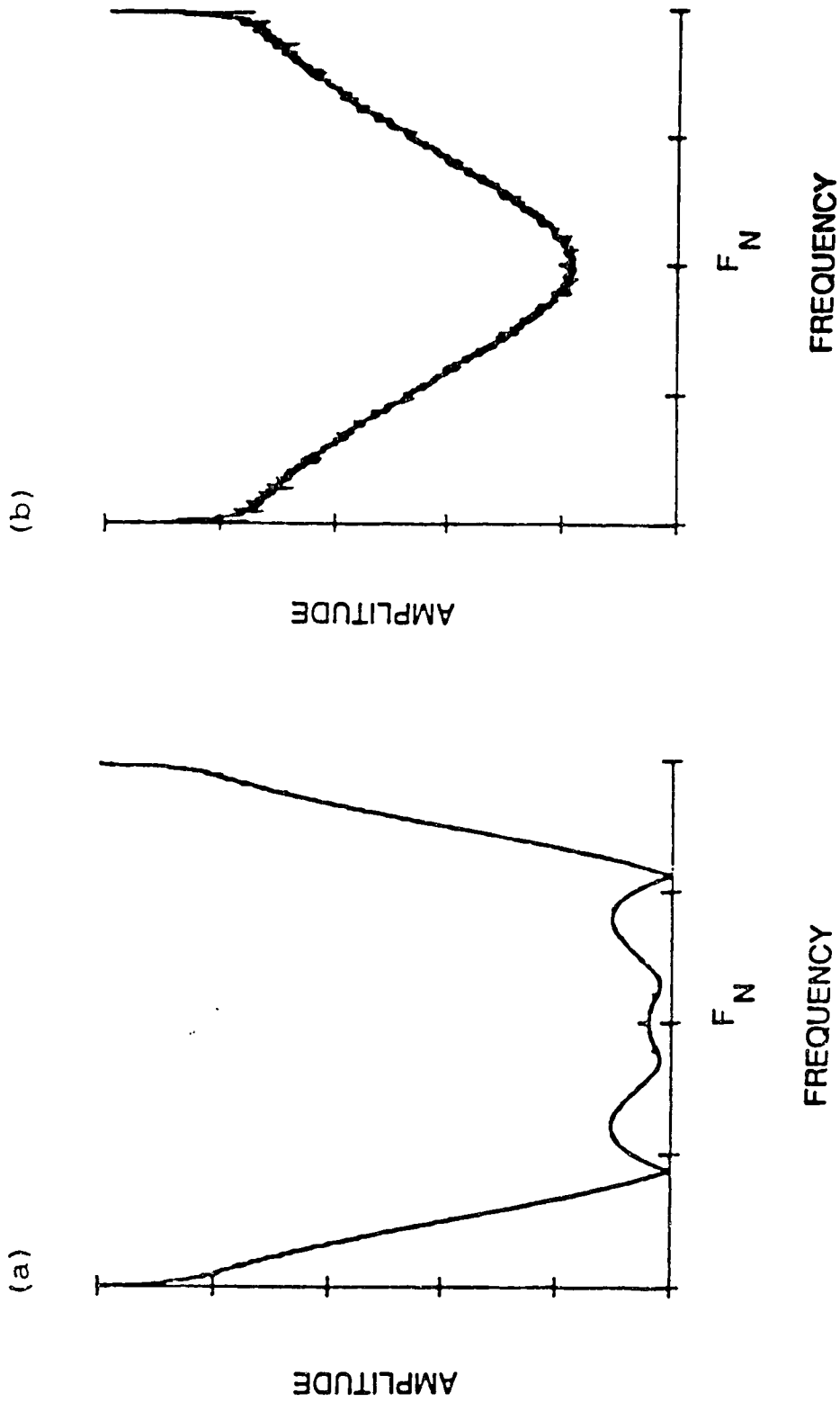


Figure 3.5 Fourier transform of HeNe laser line with a) 100 μm entrance slit width and b) 10 μm entrance slit width.

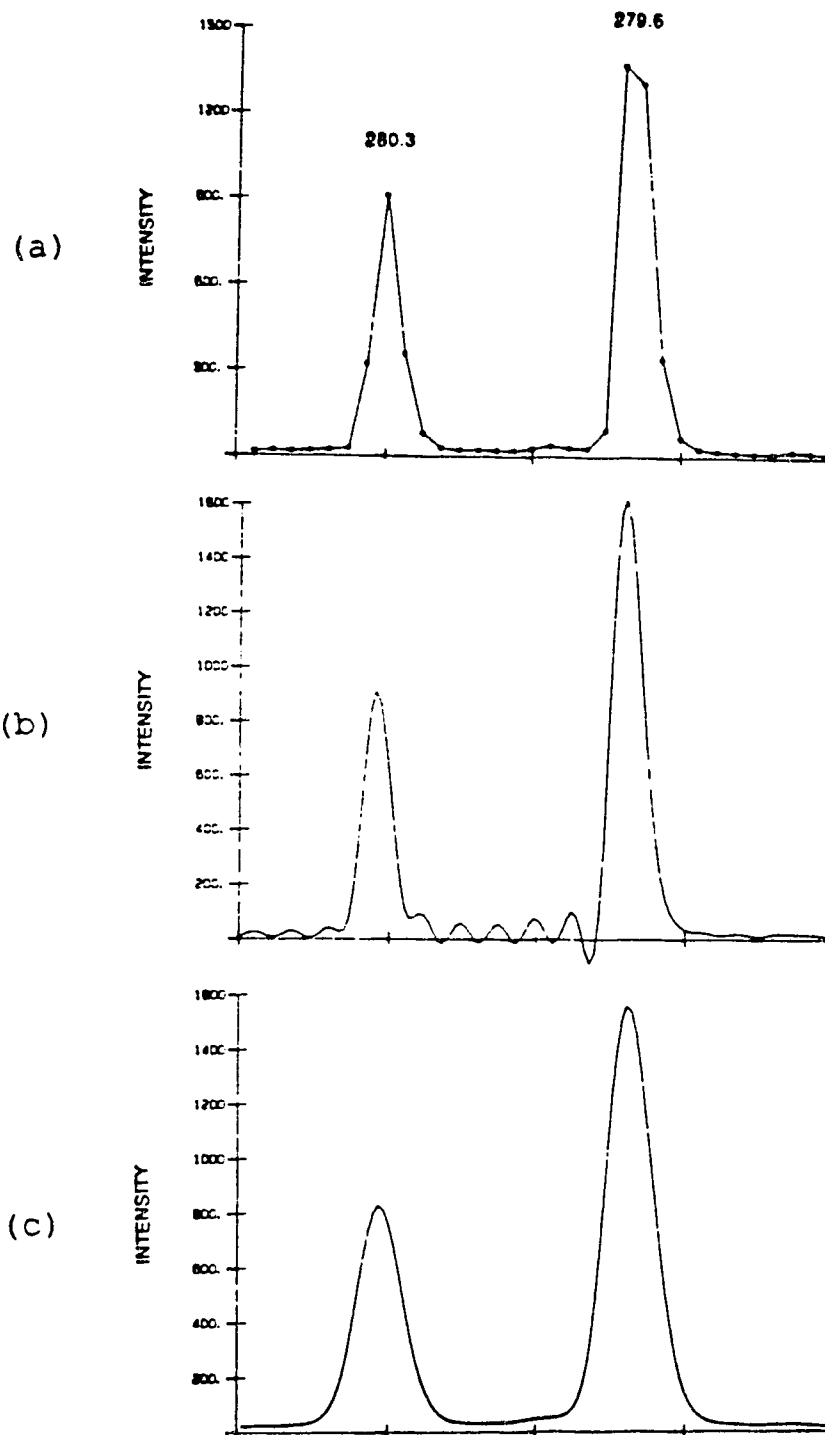


Figure 3.6 a) 32 pixels of Mg spectrum acquired with $30\ \mu\text{m}$ entrance slit width, b) zero filled spectrum of a), c) zero filled spectrum of a) with apodization with Gaussian peak shape.

multiplying the Fourier transform of the spectrum with a Gaussian line shape, is shown in Figure 3.6c. The sidelobes are removed, but at a sacrifice of resolution.

Fourier domain zero filling will also improve the accuracy in locating the peak maximum [10]. This effect will be illustrated in the following section.

3.2 Wavelength Calibration

3.2.1 Introduction

The ICP is an energetic source and as a result, the emission spectrum may contain several thousand lines, from both neutral and ionic emitting species. This fact can make qualitative identification of spectral lines from an unknown sample a difficult problem. Ideally, a spectrometer with a wavelength uncertainty of 5 pm or less is desired to identify unknown lines in a complex spectrum. For a PDA spectrometer, the wavelength uncertainty is determined by the pixel spacing of the detector and the reciprocal dispersion of the monochromator. The PDA spectrometer described in Chapter 2, has a pixel spacing of 25 μm and a reciprocal dispersion of approximately 2 nm/mm, resulting in a wavelength uncertainty of +/- 0.05 nm (50 pm). Although this uncertainty is significantly larger than that desirable for reliable wavelength assignment of unknown lines, the spectrometer may

be used effectively to locate selected lines of known elements in a spectrum.

Before a line can be located, the spectra, which up until now have been presented with diode number across the horizontal axis, must be calibrated in terms of wavelength.

3.2.2 Primary Wavelength Calibration

The initial calibration of the wavelength axis involves three steps. First, an emission spectrum of a known element or group of elements, with several emission lines in the selected spectral window, is acquired. For this example, an ICP emission spectrum of 1000 $\mu\text{g/mL}$ Fe will be used, with the spectral window centered at approximately 375 nm (Figure 3.7).

The second step involves identifying and locating a number of lines in the spectrum. Initially, estimates of the wavelength and the relative intensities are made and this information is compared with data from reference tables [12-14]. Once the identification of the lines has been confirmed, the diode number and wavelength for each peak maximum is tabulated.

A plot of wavelength versus diode number for the peaks (Figure 3.8) is fit to a straight line. The slope of the line is the dispersion in nm/diode and the y axis intercept is the wavelength at diode number 0. With this information,

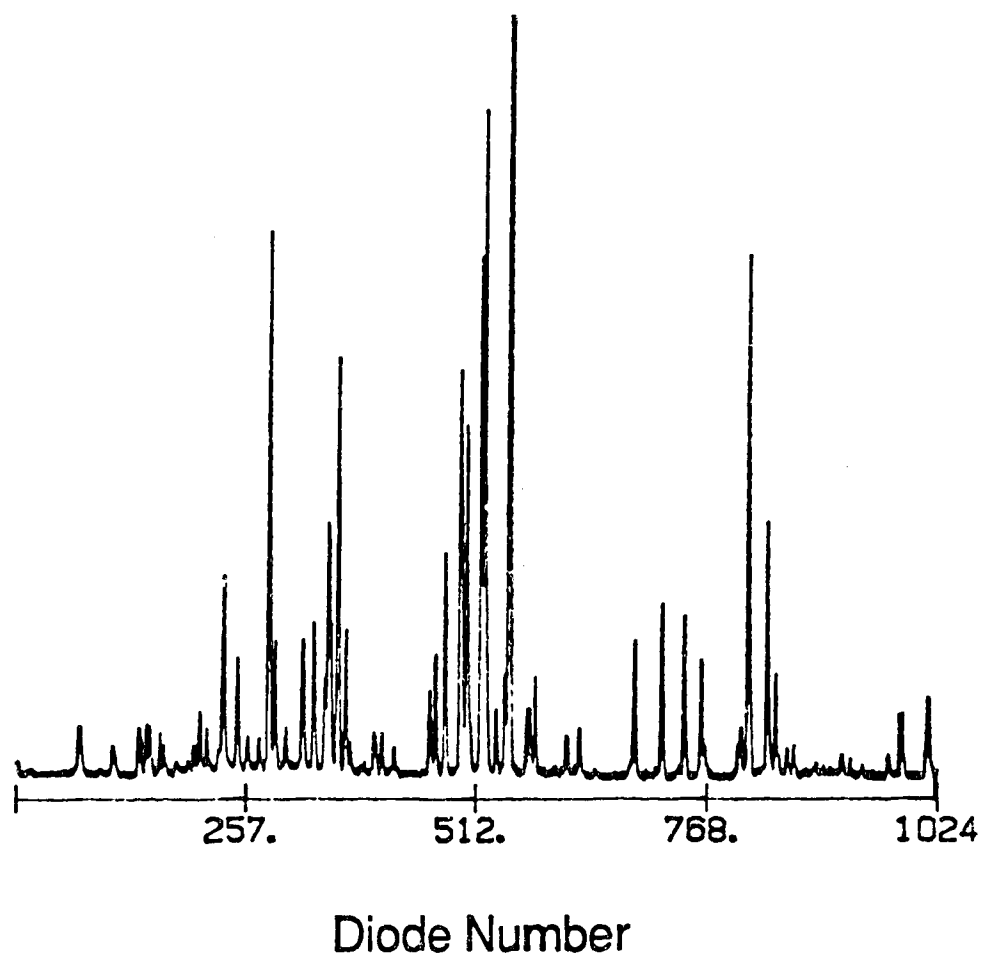


Figure 3.7 Fe I ICP-PDA spectrum, centered at 374 nm.

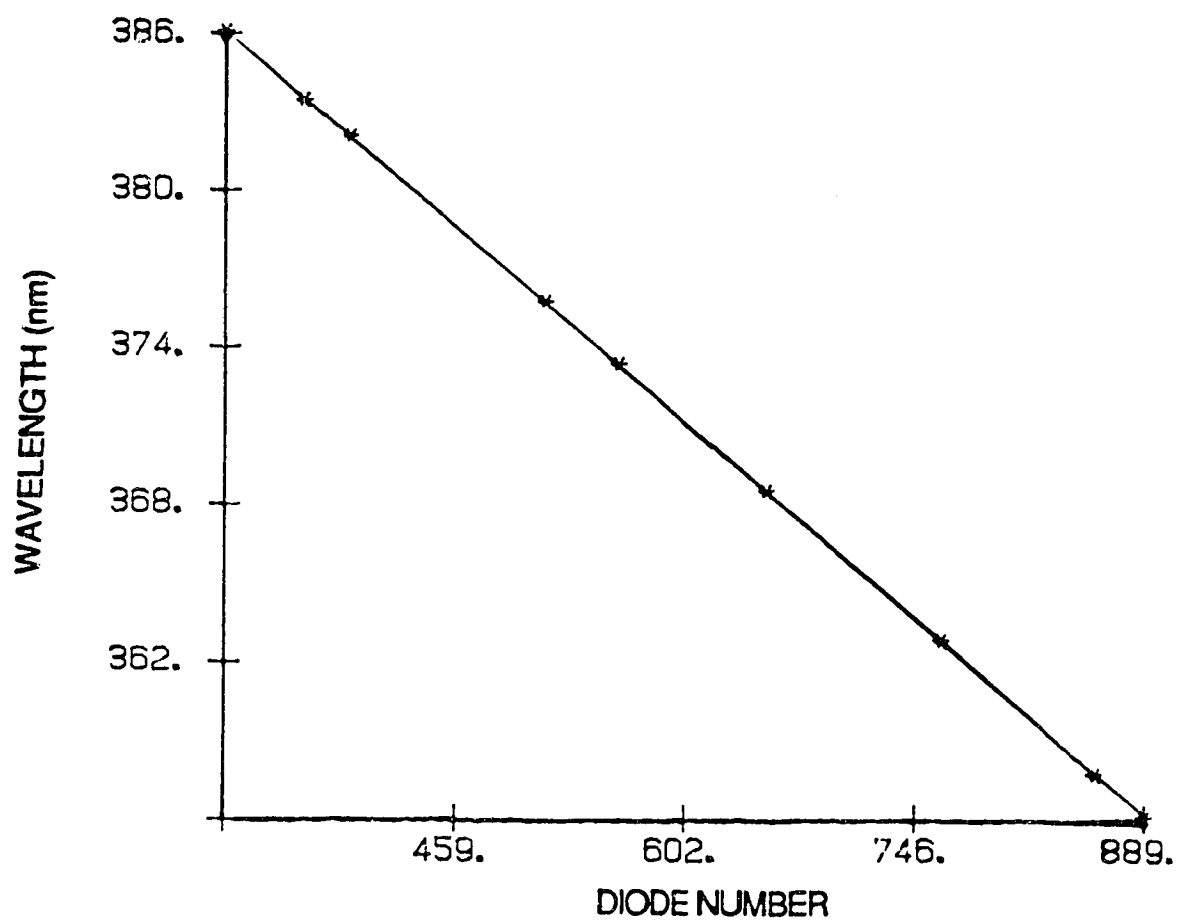


Figure 3.8 Wavelength calibration plot, peak position as wavelength versus peak position as diode number.

it is possible to calculate the wavelength at any point in that spectral window, given the diode number at that point.

It should be noted that this procedure assumes a constant dispersion across the spectral window. Although reciprocal dispersion is wavelength dependent, over the relatively small spectral window and within the given diode spacing of the PDA, the dispersion can be assumed constant.

Once the slope and intercept information have been obtained, the procedure for locating spectral lines can be computer controlled. The wavelengths of all sought for lines are entered into the computer. Each wavelength is converted to a diode number and the diode number is used to locate a small region of the spectrum in which the peak search will take place. The size of the region can be controlled by the user. A large search region may result in the selection of the wrong peak and too small a search area may miss the peak maximum. Typically, the search area is two to three times the FWHM for the peak. Once the search area has been identified, the ASYST command LOCAL.MAXIMA is used to identify the diode number of the peak maximum and the intensity. The peak maximum is then converted back to a wavelength. The results of a peak search for 20 Fe I lines are tabulated in Table 3.1. All errors in peak maximum are within one pixel spacing (0.054 nm).

The zero filling routine described in Section 3.1 of this chapter can be used to reduce the uncertainty in locating peak maxima. The interpolation allows for a more

Table 3.1 Error in peak maximum location for Fe I lines using peak search routine.

Peak Wavelength (nm)	Measured (nm)	Error (nm)
385.991	386.026	-0.035
384.105	384.088	0.017
382.042	382.044	-0.002
381.584	381.572	0.012
378.788	378.742	0.046
376.719	376.698	0.021
376.379	376.332	0.048
375.823	375.808	0.016
374.556	374.550	0.006
373.713	373.659	0.054
373.486	373.449	0.038
372.762	372.716	0.046
370.557	370.515	0.042
368.746	368.733	0.013
367.991	367.947	0.044
364.784	364.750	0.034
363.146	363.126	0.020
361.877	361.868	0.009
360.886	360.924	-0.038
358.119	358.147	-0.028

precise identification of the peak position [10]. A 256 point region of the Fe I spectrum from 388 to 375 nm was Fourier domain zero filled (four times) to 1024 points. Primary calibration was performed and 10 lines were included in the peak search (Table 3.2). The maximum peak position uncertainty is now reduced to less than 0.01 nm.

3.2.3 Secondary Wavelength Calibration

Once the grating is moved to a new spectral window, the calibration procedure must be repeated, using a new set of emission lines. On returning the grating to a previously calibrated window, recalibration will be required, unless the grating can be precisely repositioned to reproduce the exact wavelength to diode correspondence that existed when the spectral window was originally calibrated. Even without moving the grating, thermal expansion of optical components in the spectrometer over time may necessitate recalibration of the spectral window. Since returning the grating to an exact position is impractical due to mechanical limitations of the scanning system, and the calibration procedure can be time consuming and tedious, a simple and rapid method for recalibrating a spectral window is required. The method that has been developed is based on the cross correlation of a calibrated and uncalibrated spectrum.

Once a spectral window has been calibrated, the spectrum, slope, and intercept information are stored on

Table 3.2 Error in peak maximum location for Fourier domain
zero filled Fe I spectrum.

Peak Wavelength (nm)	Measured (nm)	Error (nm)
385.991	385.996	-0.005
382.042	382.038	0.004
381.584	381.580	0.004
378.788	378.785	0.003
376.719	376.721	-0.002
376.379	376.381	-0.002
375.823	375.819	0.004
374.556	374.565	-0.009
373.713	373.716	-0.003
373.486	373.494	-0.008

disk. When recalibration is required, a new spectrum of the sample used to do the primary calibration is acquired. The information previously saved on disk is retrieved and the cross correlation of the new spectrum and the spectrum used for primary calibration is calculated.

An Fe I spectrum that has been calibrated using the primary calibration procedure is shown in Figure 3.9a. For the spectrum shown in Figure 3.9b the grating has been moved, resulting in an approximate 10 nm shift in the position of the spectral window. The cross correlation of the two spectra was calculated and is plotted in Figure 3.9c. The largest peak in the cross correlation spectrum indicates the point where the two spectra correlate best. The number of points this peak is shifted from the $\tau = 0$ point is the amount that the two spectra are shifted relative to one another. This value is then applied as a correction to the intercept used in the calibration. With the corrected intercept and the slope from the primary calibration, the wavelength at any point in the new spectrum can now be calculated, given the diode number and providing that the shift in position is not so large that a significant change in dispersion results. The position of a spectral window can be reproduced within one or two nanometers relatively easily, therefore a 10 nm shift would be considered a large shift.

Eighteen lines were located in an Fe I spectrum, calibrated with the secondary calibration procedure. For two

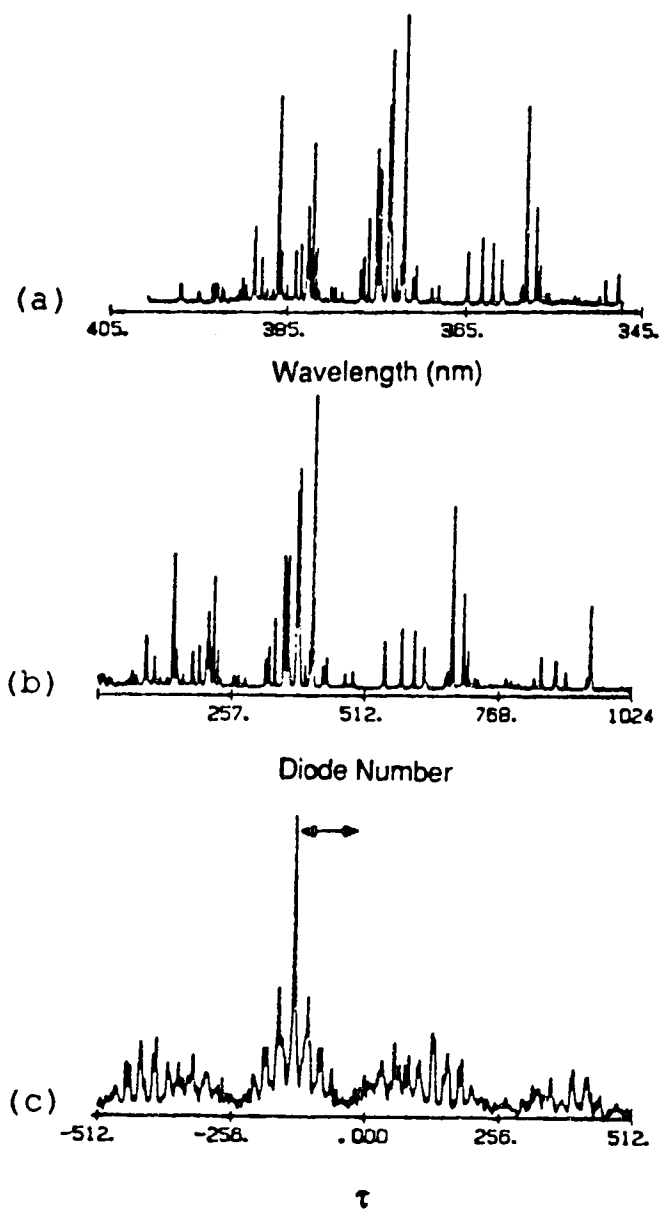


Figure 3.9 a) Fe I spectrum with primary calibration of wavelength axis, b) Fe I spectrum as in a) with small grating shift, c) cross correlation of a) and b).

shifts in spectral window, the maximum error was less than 0.054 nm, the spacing of one pixel (Table 3.3).

Thus, once a primary calibration has been performed, it is not necessary to repeat that time consuming process. A library of calibrated windows can be acquired and saved on disk and when a calibration is required, the secondary calibration procedure can be used. The secondary calibration requires no intervention by the user and is completed in about 15 seconds. This technique can be applied equally as well to zero filled spectra.

3.3 Dynamic Range

The ICP provides emission intensities linearly related to analyte concentration over a range of six orders of magnitude. To take full advantage of this property of the ICP, the detection system must have a linear response over an equal or greater range. PMT based spectrometers, generally, have been able to cover such a range. PDAs, on the other hand, have been criticized as having a working range limited to only two to three orders of magnitude.

The first difficulty with PDAs and dynamic range is how to define dynamic range. The simplest definition is the single pixel, single integration time dynamic range, defined as the ratio of the largest observable signal to the signal equivalent to the baseline readout noise. For the Reticon PDA described in Chapter 2, the maximum readout noise is limited

Table 3.3 Error in peak maximum location using secondary calibration procedure for Fe I spectrum

Peak Wavelength (nm)	-12 nm Shift Error (nm)	+8 nm Shift Error (nm)
384.105	-0.035	0.018
382.042	-0.054	-0.002
381.584	-0.040	0.012
378.788	-0.007	-0.007
376.719	0.021	0.021
376.379	-0.005	0.048
375.823	0.016	0.016
374.556	0.006	0.006
373.713	0.002	0.054
373.486	0.038	0.038
372.762	0.046	0.046
370.557	0.042	0.042
368.746	0.013	0.013
367.991	0.044	-0.008
364.784	0.034	-0.018
363.146	0.020	-0.032
361.877	0.009	-0.043
360.886	0.014	-0.038

by the saturation charge of 14 pC (3800 counts) (Figure 3.10). The baseline readout noise is approximately 0.0055 pC (1.5 counts) for a five second integration time. The result is a dynamic range of 2500. This measure is valid for shorter integration times, as for longer integration times the dark current and spectral background increases reducing the dynamic range with respect to the signal.

A second definition of dynamic range, specific to image sensors, is the intraspectral dynamic range. The intraspectral dynamic range is the largest observable signal divided by the signal equivalent to the background noise in the same spectrum. Effects such as blooming, the spread of charge from a saturated diode to nearby diodes, spectrometer stray light, and veiling glare, a series of internal reflections in the quartz window and SiO₂ overglass, which spreads light across the PDA, may cause the intraspectral dynamic range to be less than the single pixel dynamic range. It has been shown that blooming is not significant in PDAs [15] and the problem of veiling glare has not been observed in our system. Therefore, the intraspectral dynamic range is approximately equal to the single pixel dynamic range.

Talmi and Simpson [16] have described a variable integration time mode of operation for extending the dynamic range of a PDA absorbance spectrometer. With this method a series of PDA spectra are acquired for a single spectral measurement. Each spectrum in the series is acquired at a different integration time. Integration times are selected so

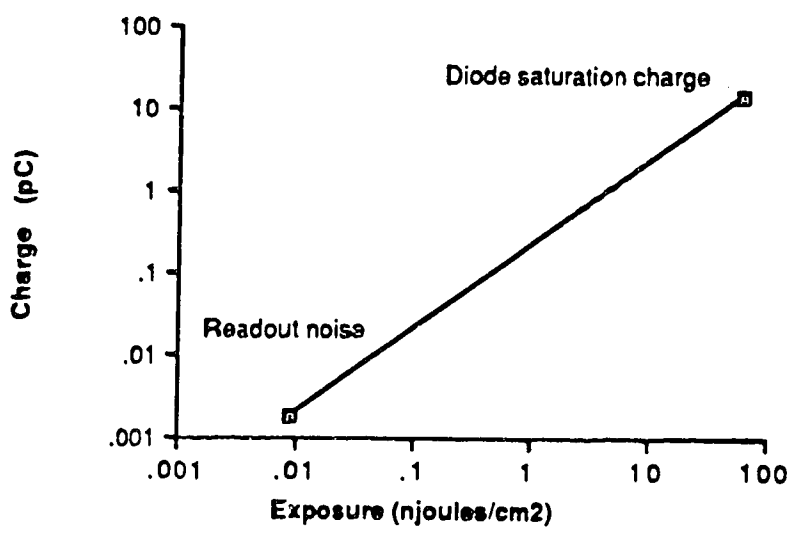


Figure 3.10 Dynamic range for Reticon PDA with 5 second integration time.

that for each peak in the spectrum, the peak maximum is between 50 and 100% of the saturation level of the PDA. Between 50 and 100% of saturation, a peak will be at the optimum signal to noise ratio. Spectra with shorter integration times are used to observe the intense spectral features and at longer integration times where the intense signals have saturated the PDA, the weaker signals can be observed.

Aiello and Enke [17] have described a wide dynamic range detector for optical rotatory dispersion spectroscopy. This method is very similar to the one just described, in that it also uses multiple integration times to measure a spectral signal. The first PDA spectrum is acquired for time t . Then for the same sample, another spectrum is acquired for time $2t$, then $4t$, up to $2^{(n-1)}t$, where n is the number of integration times. By systematically increasing integration time in this manner, each region of the PDA will be measured at its optimum signal level, regardless of the level of illumination at any position on the PDA. The dynamic range improvement with this method was $2^{(n-1)}$ and the total measurement time is approximately twice the longest integration time. The full improvement in dynamic range may not be realized if dark current becomes significant at longer integration times.

Wirsz and Blades [18] have developed an extension to the variable integration time mode. After a series of spectra are acquired at a range of integration times, non-saturated

pixels from all spectra are selected and scaled according to integration time. The points are then combined to produce a single spectrum. The result is a single spectrum that contains points from all spectra, each point displayed is acquired at the optimum integration time. There are a number of advantages to combining points into one spectrum. First, the size of the memory required to store the data is reduced. Points containing no quantitative information, i.e. low intensity or saturated points, are discarded and only points obtained at optimum integration times are retained.

Second, further data processing and spectral interpretation are simplified. Zero filling and peak search procedures need only to be performed on one spectrum.

This method was adapted for use with our PDA spectrometer. Since integration time was already under software control, the variable integration time mode could easily be implemented as a fully automated procedure. The acquisition, sorting, and scaling of the data can be done with a single keystroke.

If the method is valid there must be a reciprocity between video signal and integration time. To ensure that the linearity of the signal with integration time existed, the emission at 422 nm from a Ca hollow cathode lamp was measured at integration times ranging from 0.042 to 40.0 seconds. The net signal intensity was plotted versus integration time (Figure 3.11). The slope of the plot is 0.97 (+/- 0.01),

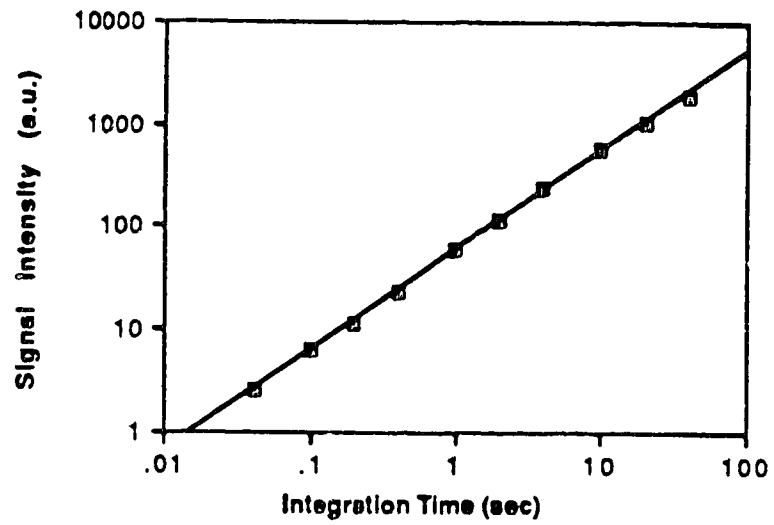


Figure 3.11 Peak height of 422 nm line of a Ca hollow cathode lamp, as a function of PDA integration time.

indicating a linear relationship between signal and integration time.

As dark current will also contribute to the total signal, it therefore must also be linear with respect to the integration time. Figure 3.12 indicates that dark current is not linearly related to integration time. Despite the nonlinearity, the method of multiple integration times may still be used if a dark current spectrum is subtracted at each integration time.

With the method developed for our PDA spectrometer, up to 10 different integration times may be selected. Once integration times are entered into the computer, a background or dark current spectrum is acquired at each integration time. The foreground or analytical spectrum can then be acquired. Data processing starts with the spectrum with the shortest integration time. The spectrum is searched for all points above a preset saturation level. If any are found, they are background subtracted and transferred to the final spectrum. All subsequent spectra are searched, in order, for new saturated points. If a saturated point is found, the corresponding point in the previous spectrum (spectrum with shorter integration time) is background subtracted, scaled according to integration time, and stored in the final spectrum. Finally, for the longest integration time spectrum, all remaining unsaturated points are background subtracted, scaled, and transferred to the final spectrum. Processing time requires approximately 15 to 30 seconds per spectrum.

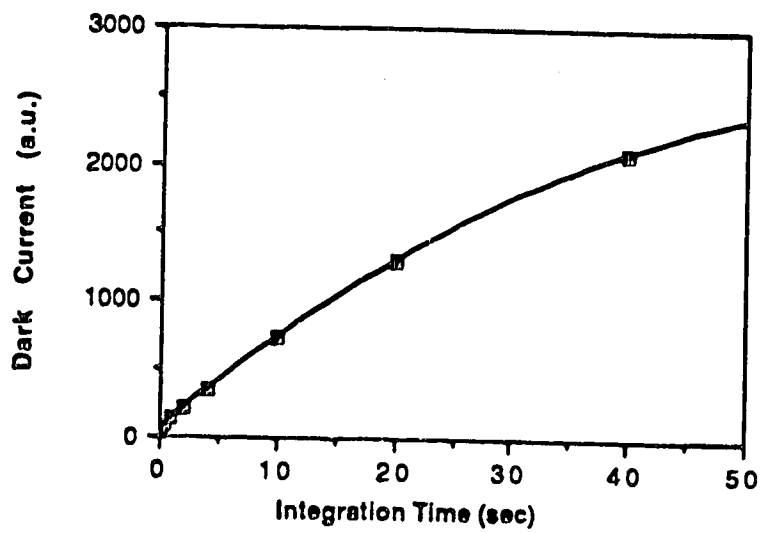


Figure 3.12 PDA dark current as a function of PDA integration time.

A solution containing 0.1 $\mu\text{g/mL}$ Mn and 10 $\mu\text{g/mL}$ Mg was prepared by serial dilution of 1000 $\mu\text{g/mL}$ stock solutions. This sample is an example of a low concentration of a weak emitter in the presence of a high concentration of a strong emitter. Two ICP emission spectra of the sample were acquired (Figure 3.13). The first (Figure 3.13a) is the spectrum acquired at the single integration time of 0.083 seconds. The second (Figure 3.13b), a spectrum with multiple integration times of 0.083, 0.16, 0.32, 0.64, 1.28, 2.56, 5.12, and 10.2 seconds. At first inspection, the two spectra appear to be identical, but when the vertical scale is expanded 10 times (Figure 3.14), only noise is visible in the baseline of the single integration time spectrum. On expanding the vertical scale 100 times (Figure 3.15) the Mn lines become clearly visible in the multiple integration spectrum. Only when expanded 1000 times (Figure 3.16) does the level of baseline noise in the multiple integration time spectrum become apparent. The dynamic range in this multiple integration time spectrum is approximately 2×10^5 .

The longest practical integration time is 100 seconds, the upper limit set by dark current and spectral background. The shortest integration time is 0.042 seconds, the lower limit set by the time required to readout the PDA. Therefore, the maximum dynamic range that could be achieved with multiple integration times would be 4×10^6 or 6.6 orders of magnitude.

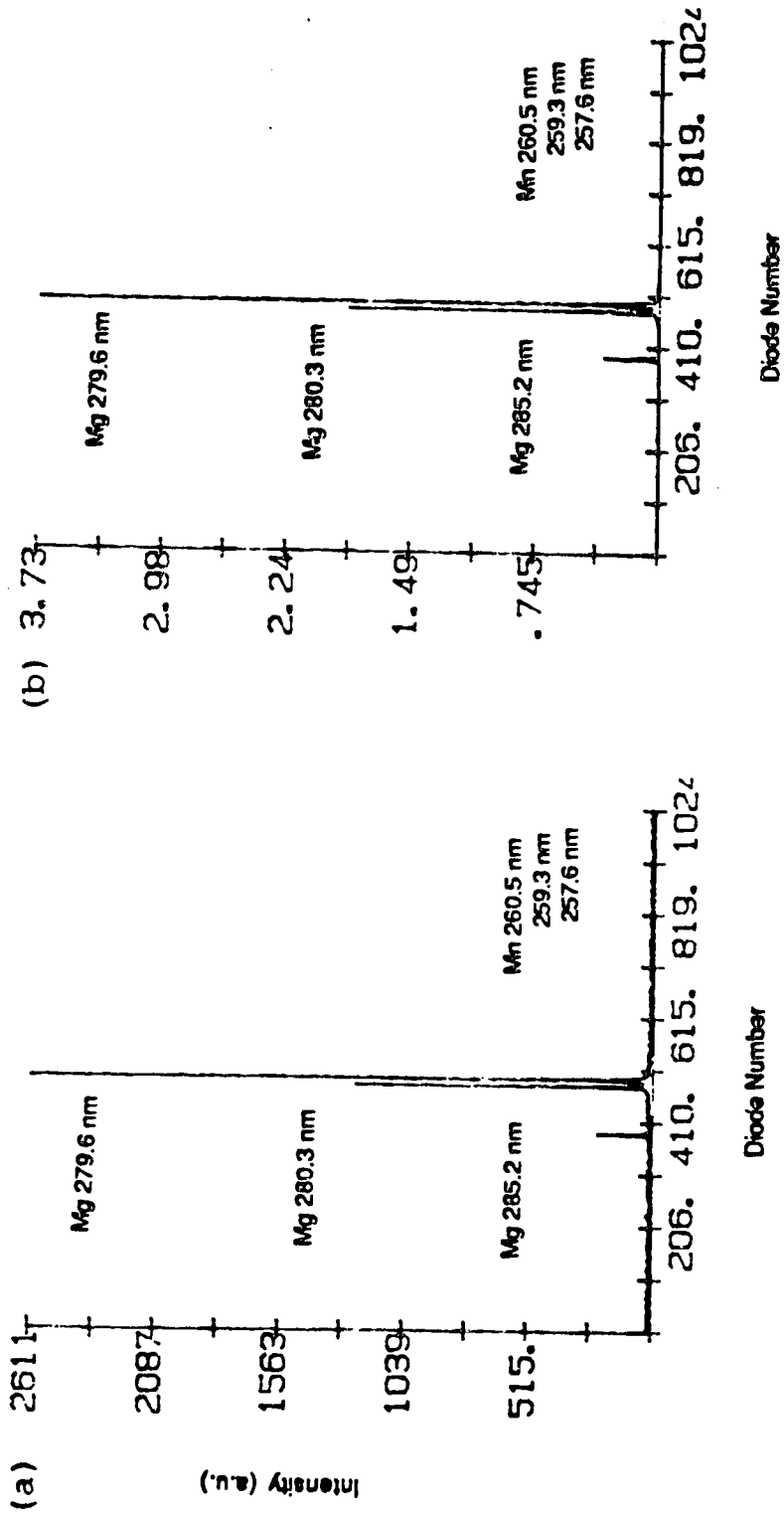


Figure 3.13 ICP-PDA spectrum of 10 $\mu\text{g/mL}$ Mg and 0.1 $\mu\text{g/mL}$ Mn with a) a single integration time and b) multiple integration times.

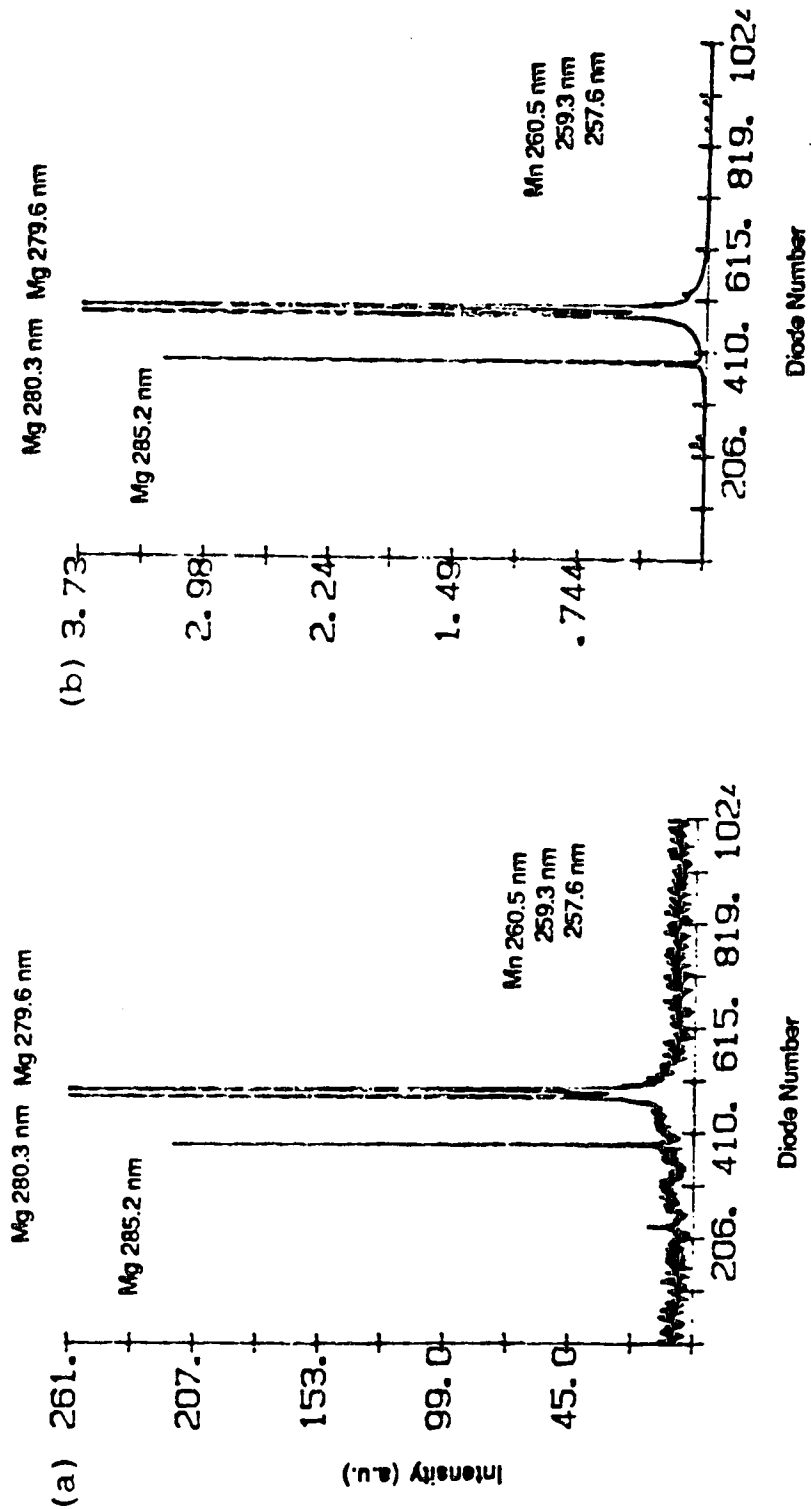


Figure 3.14 ICP-PDA spectra as in Figure 3.13 with vertical scale expanded 10 times.

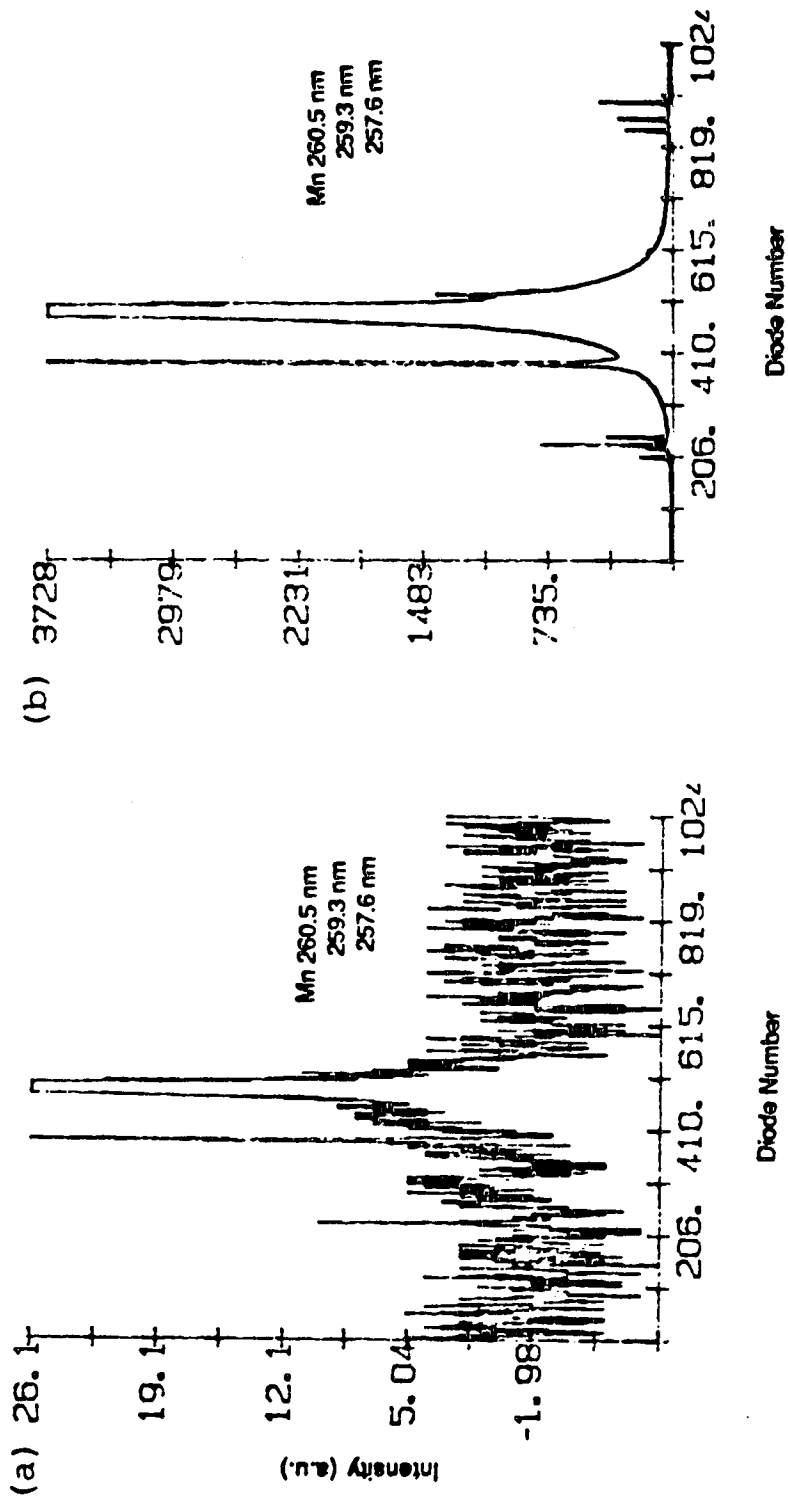


Figure 3.15 ICP-PDA spectra as in Figure 3.13 with vertical scale expanded 100 times.

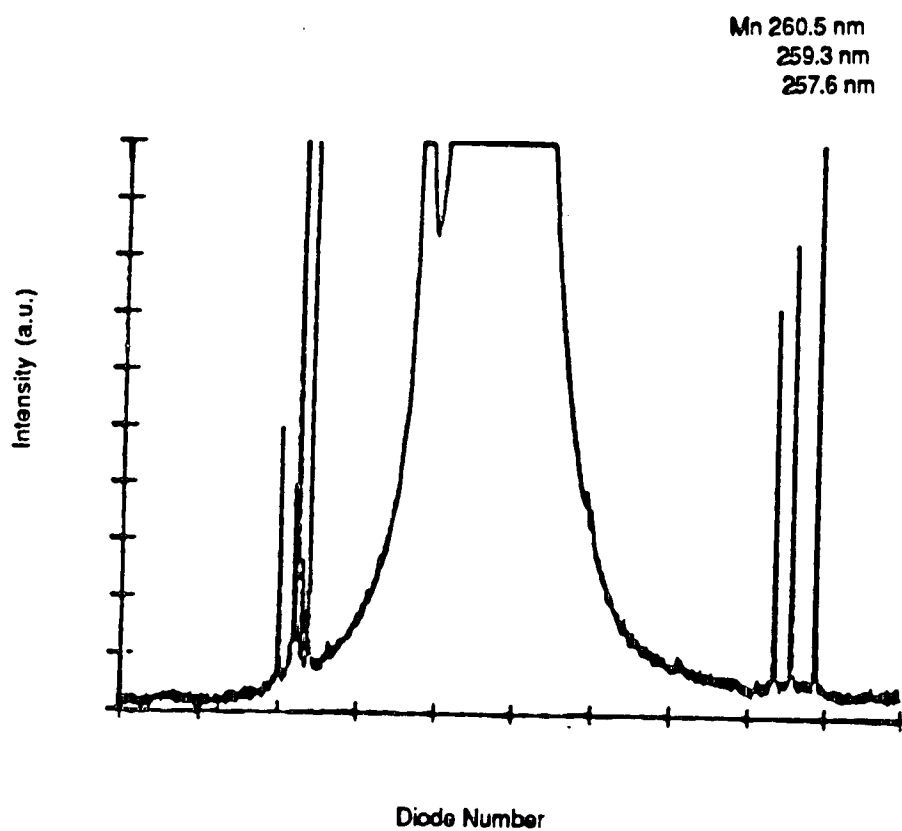


Figure 3.16 ICP-PDA multiple integration time spectrum in Figure 3.13 with vertical scale expanded 1000 times.

3.4 Conclusions

If the PDA spectrometer is used to acquire peak ratios for fundamental studies, or if the grating of the spectrometer is moved to select another spectral window, intensity errors can result. These errors are not due to the sampling of the spectrum by the PDA, but from using a simple linear interpolation to recover the sampled data. Fourier domain zero filling is described and implemented as a simple and rapid procedure for the proper interpolation of PDA sampled spectra. The zero filling routine was shown to eliminate the spectral line-diode registry effect and allow accurate determination of the peak intensity. The zero filling procedure has been fully automated and requires only five seconds of processing time on the IBM-pc with ASYST software.

In a routine ICP-AES analysis, using a single spectral window in a PDA spectrometer, the procedure used to interpolate the spectrum is not required, but if peak ratios are desired, or if the spectral window must be moved and then replaced, then Fourier domain zero filling is required.

An ICP emission spectrum may contain several lines and because of the complex nature of the spectrum, the spectral axis must be calibrated in terms of wavelength if spectral lines are to be located. The calibration of the wavelength axis is a tedious and time consuming procedure, and because

of the limited wavelength coverage of a PDA spectrometer calibration of several spectral windows may be required. The secondary calibration procedure for the calibration of the spectral axis has been described. The method is rapid, requiring only 15 seconds to complete and requires only minimal operator skill.

The single integration time dynamic range of the PDA is only 3.4 orders of magnitude and is not sufficient for most ICP-AES analysis. The method of multiple integration times was shown to increase the intraspectral dynamic range to 6.6 orders of magnitude. Also by compressing the multiple integration time data into a single spectrum the storage, processing, and interpretation of the spectra is simplified.

The data processing routines, Fourier domain zero filling, wavelength calibration, and multiple integration times extend the measurement capabilities of the PDA spectrometer for ICP-AES. Since all techniques are under complete computer control, the operator skill required to operate a PDA spectrometer is reduced. These processing techniques will be used in the following chapter in a method using relative line intensities to obtain excitation temperatures in the ICP. The measurement of excitation temperatures would not be possible with the PDA spectrometer described in Chapter 2 without all of the data processing techniques described in this chapter.

References

1. S. W. McGeorge and E. D. Salin, *Anal. Chem.*, **57**, 2740, (1985)
2. L. L. Burton and M. W. Blades, *Appl. Spectrosc.*, **42B**, 513, (1987)
3. R. K. Winge, V. A. Fassel, and D. E. Eckels, *Appl. Spectrosc.*, **40**, 461, (1986)
4. P. C. Kelly and G. Horlick, *Anal. Chem.*, **45**, 518, (1973)
5. D. F. Barbe and S. B. Canpana, "Solid State Imaging", Ed. P. G. Jespers, F. Van DeWiele, and M. H. White, NATO Advanced Study Institute Series, Series E: Applied Science, No.16, Noordhoff-Leyden, (1976)
6. S. W. McGeorge and E. D. Salin, *Spectrochim. Acta*, **41B**, 327, (1985)
7. E. G. & G. Reticon, Product Description S-Series Solid State Line Scanners, Sunnyvale, CA., Publication 97250, (1978)
8. R. N. Bracewell, "The Fourier Transform and Its Application", McGraw-Hill, New York, (1965)
9. P. R. Griffith, *Appl. Spectrosc.*, **29**, 11, (1975)
10. G. Horlick and W. K. Yuen, *Anal. Chem.*, **48**, 1643, (1976)

11. M. B. Comisarow and J. D. Melka, *Anal. Chem.*, **51**, 2198, (1979)
12. A. N. Zaidel, V. K. Prokof'ev, S. M. Raiskii, V. A. Slaonyi, and E.Ya. Shreider, "Tables of Spectral Lines", IFI/Plenum, New York, (1970)
13. R.K. Winge, V. J. Peterson, and V. A. Fassel, *Appl. Spectrosc.*, **33**, 206, (1979)
14. M. L. Parsons, A. Forster, and D. Anderson, "An Atlas of Spectral Interferences in ICP Spectroscopy", Plenum Press, New York, (1980)
15. G. Horlick and E. G. Coddington, "Contemporary Topics in Analytical and Clinical Chemistry" Vol.1, D.M. Hercules ed., Plenum Press, (1977)
16. Y. Talmi and R. W. Simpson, *Appl. Optics*, **19**, 1401, (1980)
17. P. J. Aiello and C. G. Enke, "Multichannel Image Detectors" Vol.2, p.57, American Chemical Society, Washington, (1983)
18. D. F. Wirsz and M. W. Blades, *Appl. Spectrosc.*, **41**, 1383, (1987)

Chapter 4

Excitation Temperature Measurements with a PDA Spectrometer

4.1 Introduction

Current research in the field of ICP-AES can be divided into two general areas: 1) ICP applications and development, which involve research aimed at directly improving the analytical performance of the ICP. Examples of such research include new sample introduction techniques, spectrometer design, and method development. 2) Fundamental studies or plasma diagnostics which aims consider "... the identification and quantitative description of the relevant mechanisms and plasma species that are responsible for excitation, de-excitation, and ionization." [1]. To work toward the goal of understanding the plasma at a fundamental level, a number of plasma properties must be measured. These parameters include electron density, particle energy, distribution temperatures, degree of ionization, and gas flow dynamics.

PDA spectrometers have been extensively used for diagnostic studies of the ICP [2-15]. To study a single

plasma property, peak shape information, intensities of several lines and background, and intensities at a number of spatial locations may be required. The multichannel capabilities of the PDA greatly facilitate such measurements, by reducing experimental time and effort required. In the case of diagnostic studies, operating conditions can be selected to minimize the PDA disadvantages. Concentration of the element of interest can be increased to ensure a sufficiently intense signal and spectral lines can be selected so that no spectral interferences occur.

One of the most commonly measured plasma parameters in diagnostic studies is the excitation temperature (T_{exc}). T_{exc} describes the distribution of an analyte species among its electronic energy levels and is useful in describing the condition of the plasma as an emission source.

T_{exc} is described by the Boltzmann distribution:

$$n(p) = n_a [g_p / Z_a(T)] \exp(-E_p / kT_{exc}) \quad (1)$$

where $n(p)$ is the concentration of atoms (or ions) in energy level p , g_p is the statistical weight of level p , $Z_a(T)$ is the partition function of the atom (or ion) a , E_p is the excitation energy of level p , and k is the Boltzmann constant.

T_{exc} can be measured spectroscopically by a number of methods and an excellent summary of many of the methods is provided by Boumans [16]. The method of relative line

intensities is experimentally the most practical and is, therefore the most commonly used. To use this method we must first consider the equation describing the emission intensity (I_{pq}) of an optically thin source:

$$I_{pq} = [(l/4\pi)n(p)A_{pq}hc]/\lambda_{pq} \quad (2)$$

where l is the path length, A_{pq} is the transition probability for the transition from level p to q , λ_{pq} is the wavelength of the emitted radiation, h is Planck's constant, and c is the velocity of light. If we rearrange this equation to solve for $n(p)$ and substitute into the Boltzmann equation, we can relate emission intensity and T_{exc} .

$$I_{pq} = (l/4\pi)n_a [g_p/Z_a(T)] A_{pq} (hc/\lambda_{pq}) \exp(-E_p/kT_{exc}) \quad (3)$$

Next, if we further rearrange this equation and take the natural logarithm of both sides:

$$\ln(I_{pq}\lambda_{pq}/g_p A_{pq}) = -E_p/kT_{exc} + \ln[n_a l hc / 4\pi Z_a(T)] \quad (4)$$

we have an equation that has the form of a straight line. If $\ln(I_{pq}\lambda_{pq}/g_p A_{pq})$ is plotted versus E_p for a number of lines of one element, the slope of the line will be $-1/kT_{exc}$. The advantage this method has over others is: first, if all lines are close in wavelength, calibration of the optical system is

not required, and second, the actual concentration of the emitting species is not required.

Emission lines selected for use in the temperature measurement should have accurately known transition probabilities, be close in wavelength, and cover a range of excitation energies, to improve the precision of the temperature measurement. Fe is the most commonly used element for determining T_{exc} , as its emission spectrum consists of many lines and the transition probabilities have been well documented [17, 13].

These requirements create some experimental difficulties. Several lines and background must be recorded for each single temperature and, since T_{exc} may vary with spatial observation zone and ICP operation parameters, several temperatures may be required in a single study. Therefore, several hundred individual intensity measurements may be required in a single study. It may take several hours to make all the required measurements with a scanning monochromator. Direct reading polychromators are normally set up to detect only one line per element and it is not practical to realign the spectrometer to measure several lines of one element.

Lines with a wide range of excitation energies will have intensities that extend over a wide range. Therefore, an optical system with a wide dynamic range is required. The spectrometer must be capable of high resolution to ensure that all lines will be adequately resolved. Finally, since

relative intensities are required, the method must be able to accurately measure peak heights within a spectrum.

The multichannel capabilities of the PDA can greatly reduce the time required to make an excitation temperature measurement. An appropriate section of the Fe spectrum with background information can be acquired with a PDA spectrometer in a few seconds. The multiple integration time mode, described in Chapter 3, enables the PDA to accommodate the wide range of emission intensities. Although our PDA spectrometer is not capable of high resolution, a narrow entrance slit will provide medium resolution, adequate to resolve several appropriate Fe lines. As demonstrated in Chapter 3, narrow slits can result in peak intensity errors, therefore zero filling is necessary to obtain the relative peak intensity.

4.2 Results and Discussion

Excitation temperatures were calculated based on emission intensities from both the atom and ion lines of iron (Table 4.1). The atom lines (Fe I) were located in a 50 nm spectral window centered at approximately 370 nm (Figure 4.1). Ion lines (Fe II) were located in a window centered at 260 nm (Figure 4.2). All spectra were acquired using an entrance slit of 30 μm . Due to memory constraints, array sizes are limited to 1024 points. Therefore, each spectrum is subdivided into 256 point regions. Each region can then be

Table 4.1 Iron lines, excitation energies, and transition probabilities used for calculation of excitation temperature.

Wavelength (nm)	Excitation Energy (eV)	gA ($\times 10^8 \text{ sec}^{-1}$)
Fe I		
385.99	3.21	0.796
382.04	4.10	6.16
381.58	4.73	8.15
371.99	3.33	1.79
361.88	4.42	5.09
360.89	4.45	4.16
Fe II		
275.57	5.48	21.1
273.96	5.51	15.4
271.44	5.55	3.86
266.66	8.07	24.1
266.44	8.04	26.5
261.19	4.79	8.71
260.71	4.84	6.63
258.59	4.79	6.64

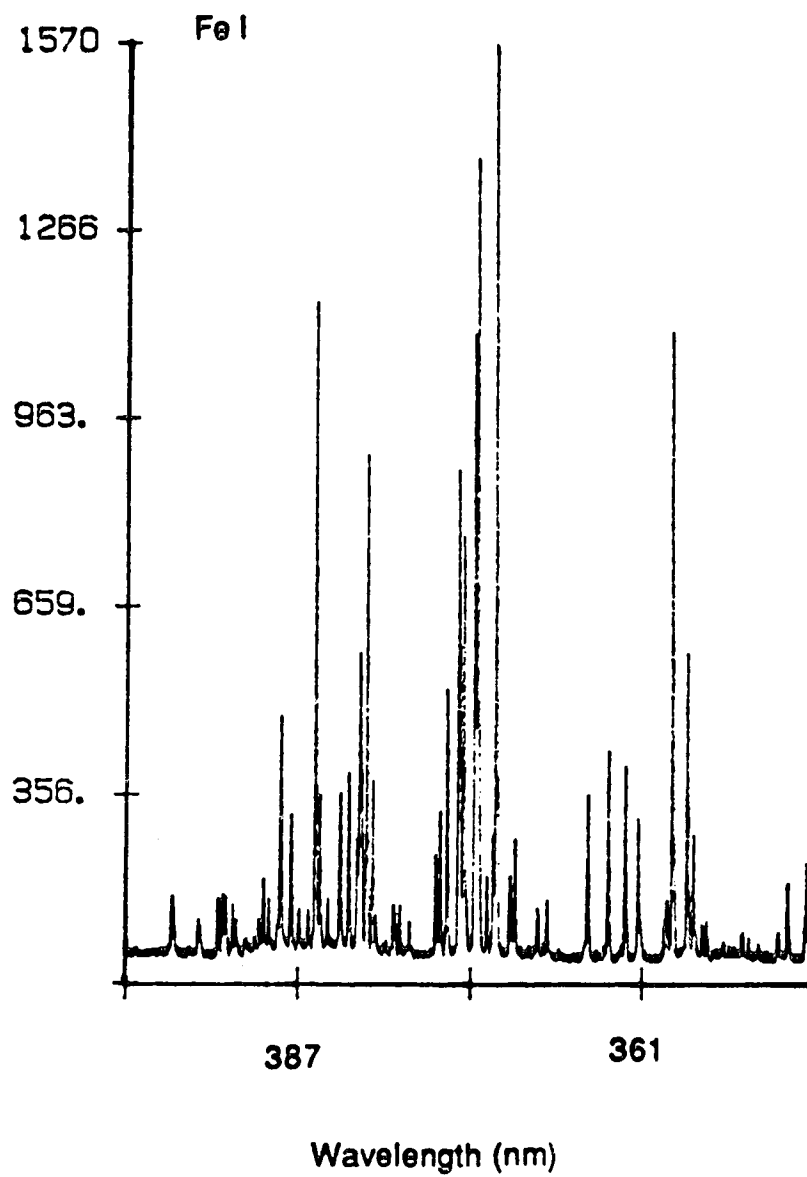


Figure 4.1 Fe I spectrum centered at 370 nm, used in calculation of excitation temperature.

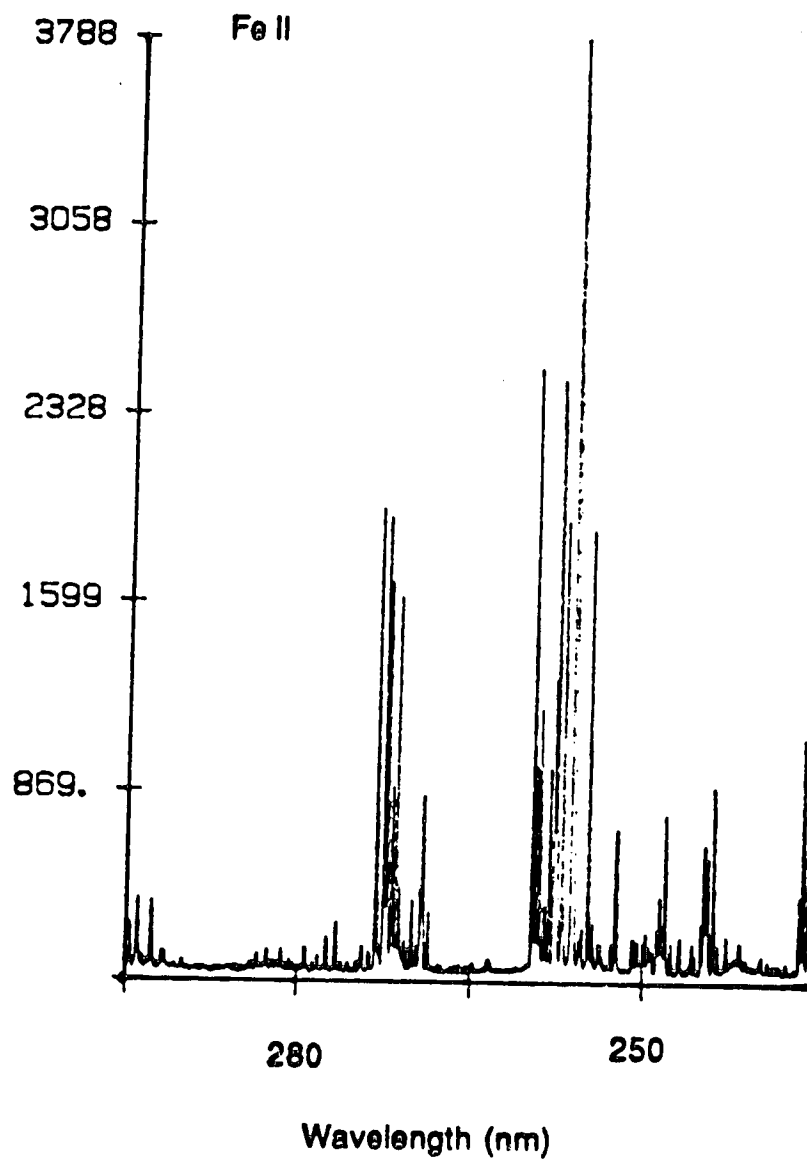


Figure 4.2 Fe II spectrum centered at 260 nm, used in calculation of excitation temperature.

zero filled four times to the maximum 1024 points. The separation of the Fe I lines across the spectral window required that three zero filled region be used (Figure 4.3). Two windows were required for Fe II (Figure 4.4). The wavelength axis for each region is calibrated using the procedure described in Chapter 3.2. The wavelength, excitation energy, and transition probability for each line were entered into the computer. The peak search routines located all lines and calculated net intensities for each line. The intensities, with the transition probabilities, wavelengths, and excitation energies are entered into equation (4) to yield the Boltzmann plot (Figure 4.5). The slope is calculated and T_{exc} is extracted from the result.

Once the wavelength calibration, Fe wavelengths, transition probabilities, and excitation energies have been entered into computer memory and stored on disk, the entire procedure can be performed with a single keystroke. The acquisition, peak search, and Boltzmann plot fit are all performed transparent to the user. Not including acquisition time, the T_{exc} calculation requires about 40 seconds or less, depending on the number of zero filled windows.

The speed at which T_{exc} can be measured allows one to measure T_{exc} at several experimental conditions. The method was used to find T_{exc} as a function of RF power and central (nebulizer) gas flow rate for both atoms and ions. A 5 mm observation zone, 15 mm above the load coil was selected. The

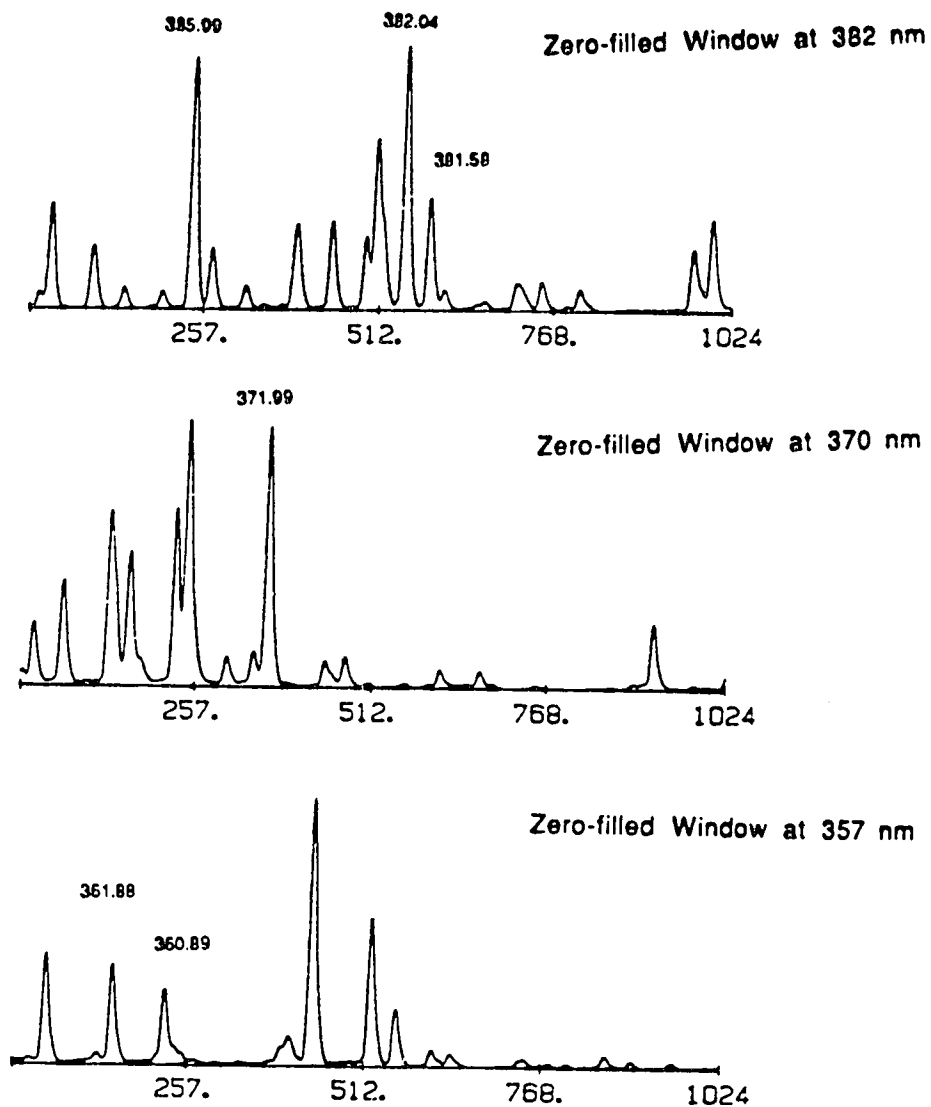


Figure 4.3 Zero filled spectra for Fe I spectrum from Figure 4.1.

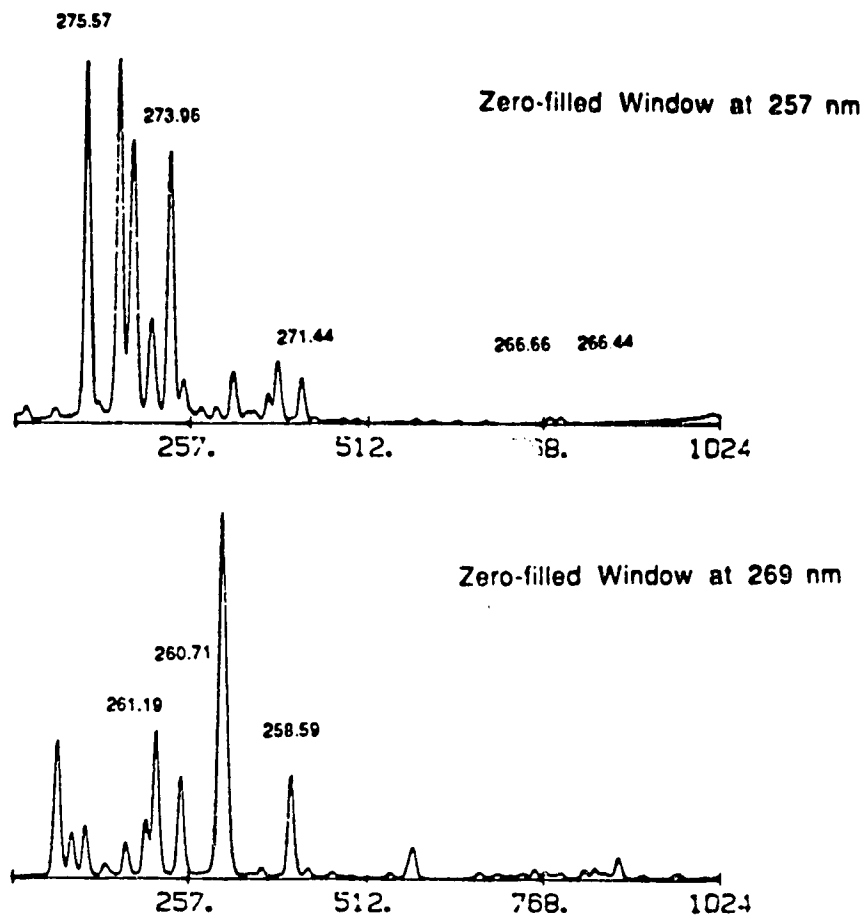


Figure 4.4 Zero filled spectra for Fe II spectrum from Figure 4.2.

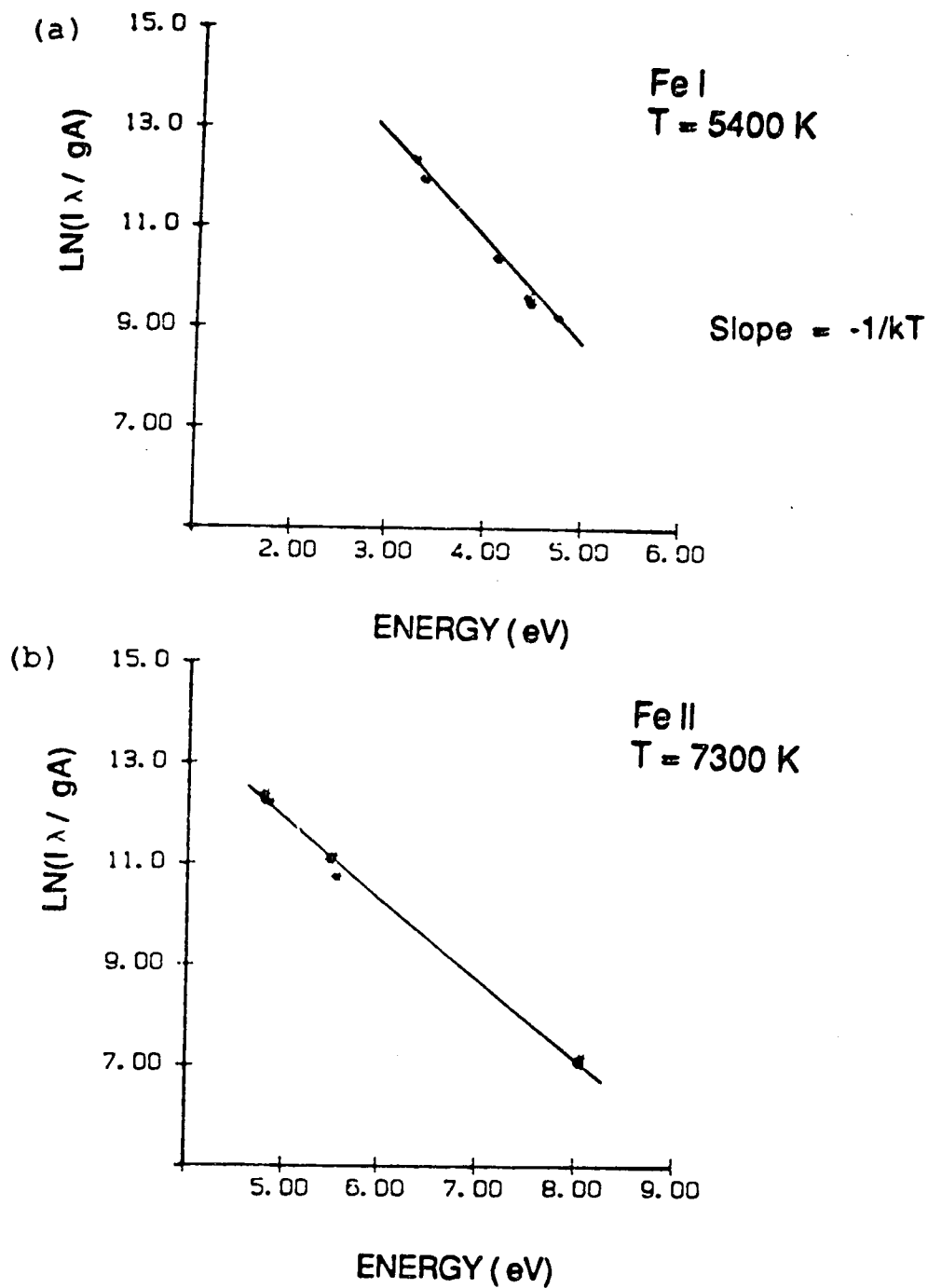


Figure 4.5 Boltzmann plot for a) Fe I lines and b) Fe II lines.

RF power was varied from 0.75 to 2.0 kW. The central (nebulizer) gas flow rate was varied from 12 to 32 psi.

Increasing RF power puts more energy into the plasma and T_{exc} was observed to increase (Figure 4.6). Increased central (nebulizer) gas flow rate decreases T_{exc} for both ions and atoms. The central channel of the plasma discharge expands with the increasing flow of nebulizer gas, thus cooling the plasma and lowering T_{exc} . This experiment required approximately two hours to complete. The grating position was moved only once, to switch from the Fe I window to the Fe II window. To perform the same experiment with a scanning monochromator, the grating would have to be moved a total of 1404 times. If 10 seconds is required to scan from peak to peak and locate the peak maximum, scanning times alone would be almost four hours. If each peak is measured for only 10 seconds the total experimental measurement time would be at least eight hours.

With the capability to simply and rapidly measure T_{exc} , T_{exc} becomes a parameter that can be used on a routine basis to optimize or characterize a plasma source. As the ICP is changed or modified, the nature of the source will change and emission intensity data alone are not sufficient to evaluate changes in the excitation process. For example, miniature or low flow torches have been developed for the ICP to reduce Ar consumption [19]. A change in emission intensity relative to the conventional ICP may be a result of the reduction in size or, a change in energy of the new plasma. T_{exc} measurements

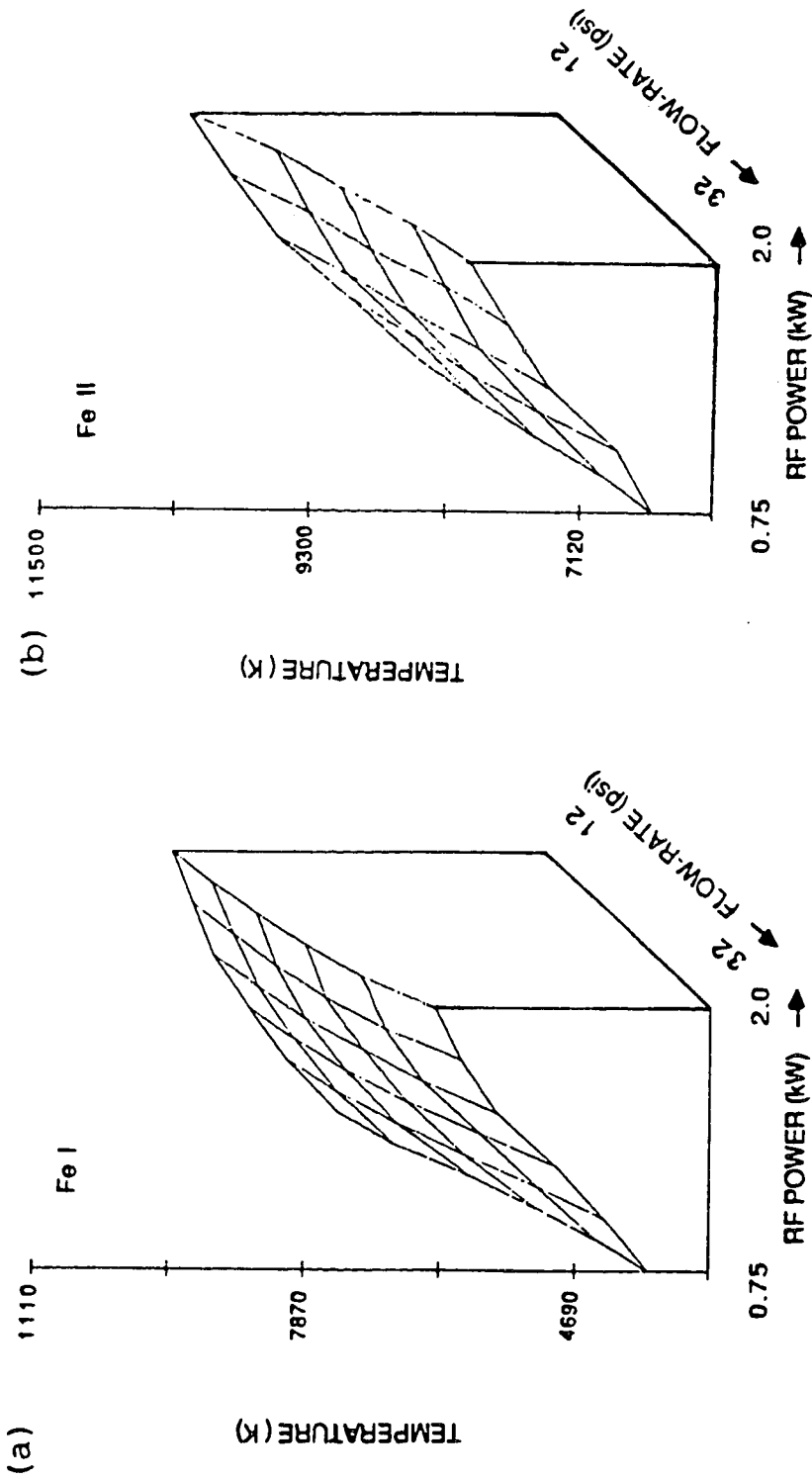


Figure 4.6 Excitation temperature as function of RF power and central (nebulizer) gas flow rate for a) Fe I lines and b) Fe II lines.

are required to determine which effect causes an intensity change.

A similar example is the mixed gas ICP. As a foreign gas, such as N_2 , He, H_2 , or air is introduced into the plasma, enhancements in emission intensity for different elements are observed [20]. Without T_{exc} , it is difficult to determine changes in the excitation process that result when a foreign gas is introduced.

T_{exc} may also be used as an estimate for other distribution temperatures in the ICP. For example, in studying the source of metal oxide formation in ICP-mass spectrometry (ICP-MS), it is uncertain as to whether the oxides originate in the ICP discharge or are formed via ion reactions in the mass spectrometer. A distribution temperature of metal oxide species, based on oxide bond strength can be calculated with the ICP-MS. If this temperature is close to an optically determined T_{exc} , it is probable that the oxide formation occurs in the plasma. On the other hand, if the oxide temperature is much less than T_{exc} , this would be evidence that oxide formation occurs in the mass spectrometer.

References

1. M. W. Blades, B. L. Caughlin, Z. H. Walker, and L. L. Burton, *Prog. Anal. Atom. Spectrosc.*, **10**, 57, (1987)
2. M. W. Blades and G. Horlick, *Spectrochim. Acta*, **36B**, 861, (1981)
3. M. W. Blades and G. Horlick, *Spectrochim. Acta*, **36B**, 881, (1981)
4. E. H. Choot and G. Horlick, *Spectrochim. Acta*, **41B**, 889, (1986)
5. M. W. Blades and G. Horlick, *Appl. Spectrosc.*, **34**, 696, (1980)
6. N. Furuta and G. Horlick, *Spectrochim. Acta*, **37B**, 53, (1982)
7. E. H. Choot and G. Horlick, *Spectrochim. Acta*, **41B**, 907, (1986)
8. B. L. Caughlin and M. W. Blades, *Spectrochim. Acta*, **39B**, 1583, (1984)
9. B. L. Caughlin and M. W. Blades, *Spectrochim. Acta*, **40B**, 579, (1985)
10. B. L. Caughlin and M. W. Blades, *Spectrochim. Acta*, **40B**, 987, (1985)

11. B. L. Caughlin and M. W. Blades, *Spectrochim. Acta*, **40B**, 1539, (1985)
12. L. L. Burton and M. W. Blades, *Appl. Spectrosc.*, **40**, 256, (1986)
13. Z. Walker and M. W. Blades, *Spectrochim. Acta*, **41B**, 761, (1986)
14. B. L. Caughlin and M. W. Blades, *Spectrochim. Acta*, **42B**, 353, (1987)
15. Z. Walker and M. W. Blades, *Spectrochim. Acta*, **42B**, 1077, (1987)
16. P. W. J. M. Boumans, "Inductively Coupled Plasma Emission Spectroscopy" Pt.1, Wiley-Interscience, New York, (1987)
17. J. M. Bridges and R. L. Kornblith, *Astrophys.*, **192**, 793, (1974)
18. W. Whaling, Technical Report 84A, Kellogg Radiation Laboratory, California Institute of Technology, (1985)
19. G. M. Hieftje, *Spectrochim. Acta*, **38B**, 1465, (1983)
20. S. Greenfield and D. T. Burns, *Anal. Chim. Acta*, **113**, 205, (1980)

Chapter 5

Fiber Optic Entrance Slit for a PDA Spectrometer

5.1 Introduction

The ICP is a spatially inhomogeneous emission source and therefore, when attempting to characterize the emission conditions of the ICP, measurements must be made at a number of spatial positions. To perform a spatially resolved measurement, either the source or the monochromator must be moved one position at a time, to view a different spatial region of the plasma. Both the ICP source and the monochromator tend to be large instruments and are therefore difficult to move in an accurate and reproducible manner under computer control.

With introduction of the PDA spectrometer, spatially resolved emission data became relatively easy to acquire [1-3]. By mounting the PDA vertically in the exit focal plane of a monochromator, as shown in Figure 1.3 in Chapter 1, vertical emission profiles can be obtained in a single readout of the PDA, without moving either the source or the monochromator. Lateral emission profiles of the ICP can be

obtained by rotating this PDA spectrometer 90 degrees, on to its side. With the PDA spectrometer in either the vertical or lateral orientation, a spatial region of the plasma source can be very well defined, but only one wavelength can be monitored at a time. If more than one spectral line is required, the grating must be moved to select other spectral lines, one at a time.

In the case of an excitation temperature measurement, as described in Chapter 4, intensity measurements at several wavelength positions are required. For such a measurement, it is more efficient to have the PDA mounted horizontally in the spectrometer focal plane, as shown in Figure 1.1 of Chapter 1, to record the spectral data simultaneously and measure the spatial positions one at a time. With the PDA spectrometer in the spectral configuration, the problem of moving the source or the monochromator to obtain the spatially resolved data once again returns. To overcome this problem, we have employed a fiber optic cable to couple the light from the ICP source to the spectrometer. The input end of the fiber optic cable can be placed in virtually any position and, often in positions where it would be impossible to mount an entire spectrometer. Also, once positioned, the input end of the cable can be easily and reproducibly moved to provide the spatial profiling capabilities.

5.2 Instrumentation

The fiber optic cable was a spot-to-slit, 1 meter quartz cable, obtained from General Fiber Optic Inc. (Cedar Grove, NJ, 07009). The cable consisted of several smaller optical fibers, each 100 μm in diameter. At one end of the cable the individual fibers are grouped together in a circular bundle, 1 mm in diameter. At the other end of the cable, the fibers are stacked to give a slit shape, 100 μm by 5 mm. The first folding mirror on the PDA spectrometer was removed and the slit end of the cable was mounted directly in the entrance focal plane of the spectrometer, as shown in Figure 5.1. The slit end of the fiber optic now becomes the entrance slit of the spectrometer.

The circular input end of the fiber optic cable was mounted on a manually controlled X-Y translation stage. With this stage, the cable could be moved in 0.1 mm increments. A 150 mm focal length, quartz lens was used to form a 1:1 image of the plasma and the translational stage with the fiber optic cable was placed in this image plane.

5.3 Spatial Profiling

To test the spatial accuracy of the translational stage, the system in Figure 5.2 was assembled. Light from the tungsten bulb was collimated with a 150 mm focal length lens.

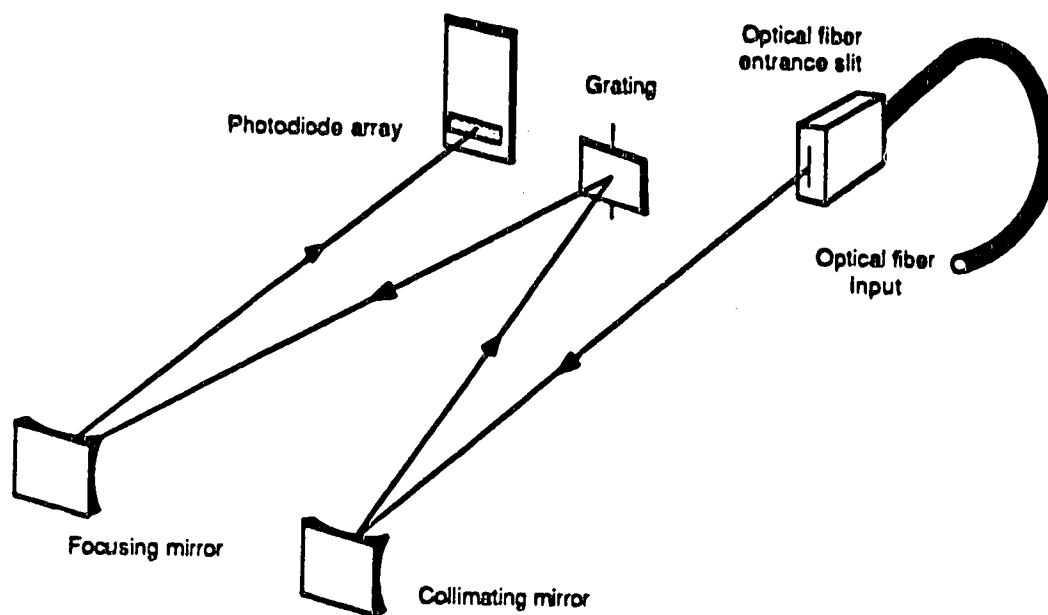


Figure 5.1 Schematic diagram of Czerny-Turner type monochromator with PDA detector and fiber optic cable input.

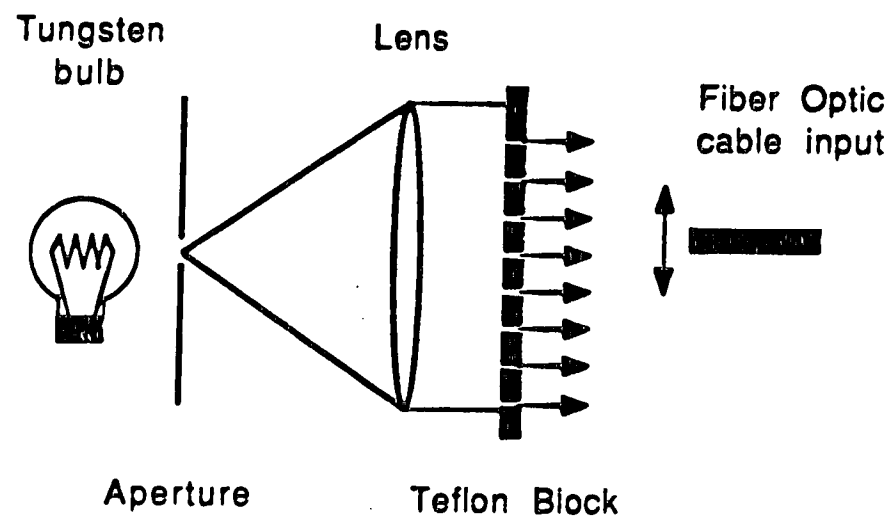


Figure 5.2 Schematic diagram of apparatus to test the spatial profiling accuracy of the fiber optic cable.

A teflon block was placed in front of the collimated beam. The teflon block had a series of 1 mm diameter holes, spaced at 2.5 mm intervals in a vertical row down its center. With the manual positioner, the fiber optic cable was moved up the back of the block, in 0.2 mm increments. The spectrometer was centered at 800 nm and the average intensity across the 50 nm region was measured at a each spatial interval. The fiber optic cable was moved a total of 7 mm, then returned to the starting position and the scan was repeated.

The width of the peaks in Figure 5.3 are not exactly 1 mm, the diameter of the holes in the block. This result does not mean the fiber optic cable is inaccurate in making spatial measurements, but rather the measured profile is actually the convolution of the light pattern and the circular shape of the optical fiber. Also imperfect collimation of the light may also distort peak shapes. The separation of the peaks is 2.5 mm, indicating excellent spatial accuracy. Due to the shape and size of the optical fiber, spatial resolution is approximately 1 mm.

The two replicate profiles correspond very well along the spatial axis, indicating excellent positioning reproducibility.

The spatial profiling capabilities of the PDA spectrometer with fiber optic input was demonstrated using the ICP. A 1:1 image of the ICP was formed at the fiber optic cable input. The spectrometer was centered at approximately 400 nm. At this position, both the Sr II (421.55 nm) line and

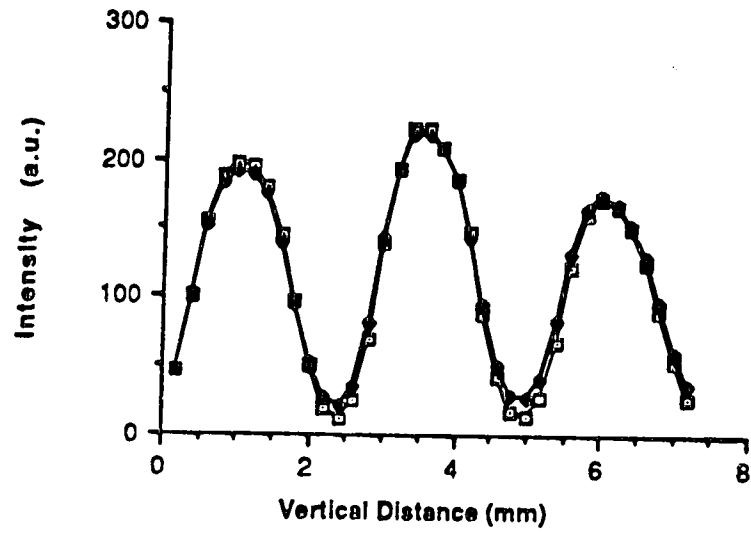


Figure 5.3 Spatial profile of light pattern from Teflon block.

the Sr I (460.73 nm) line could be detected. The fiber optic cable was positioned at the point corresponding to 5 mm above the load coil. The cable was moved in 2 mm increments, to cover the range 5 to 19 mm above the load coil. The procedure was repeated for RF powers of 1.1, 1.3, and 1.5 kW. The shape of the profiles and the position of the maximum emission intensity in Figure 5.4 correlates well with vertical spatial emission profiles previously measured for the ICP [2].

5.4 Spectral Resolution

Before implementing the fiber optic input, resolution and light throughput could be varied by controlling the entrance slit width. Now, both parameters are fixed, as the slit shape of the fiber optic cable can not be changed. No longer being able to control light throughput is not a major problem, as light levels can be compensated for by varying the integration time of the PDA.

Loss of control of resolution, however, does create some difficulties. The resolution of the PDA spectrometer with the fiber optic input was compared to the resolution achieved at a variety of slit widths with the same spectrometer before the fiber optic cable was installed. A Mn spectrum obtained with a slit width of 100 μm had the same resolution as the spectrum acquired with the fiber optic cable (Figure 5.5). Since 100 μm is the width of the fiber optic slit, the fiber

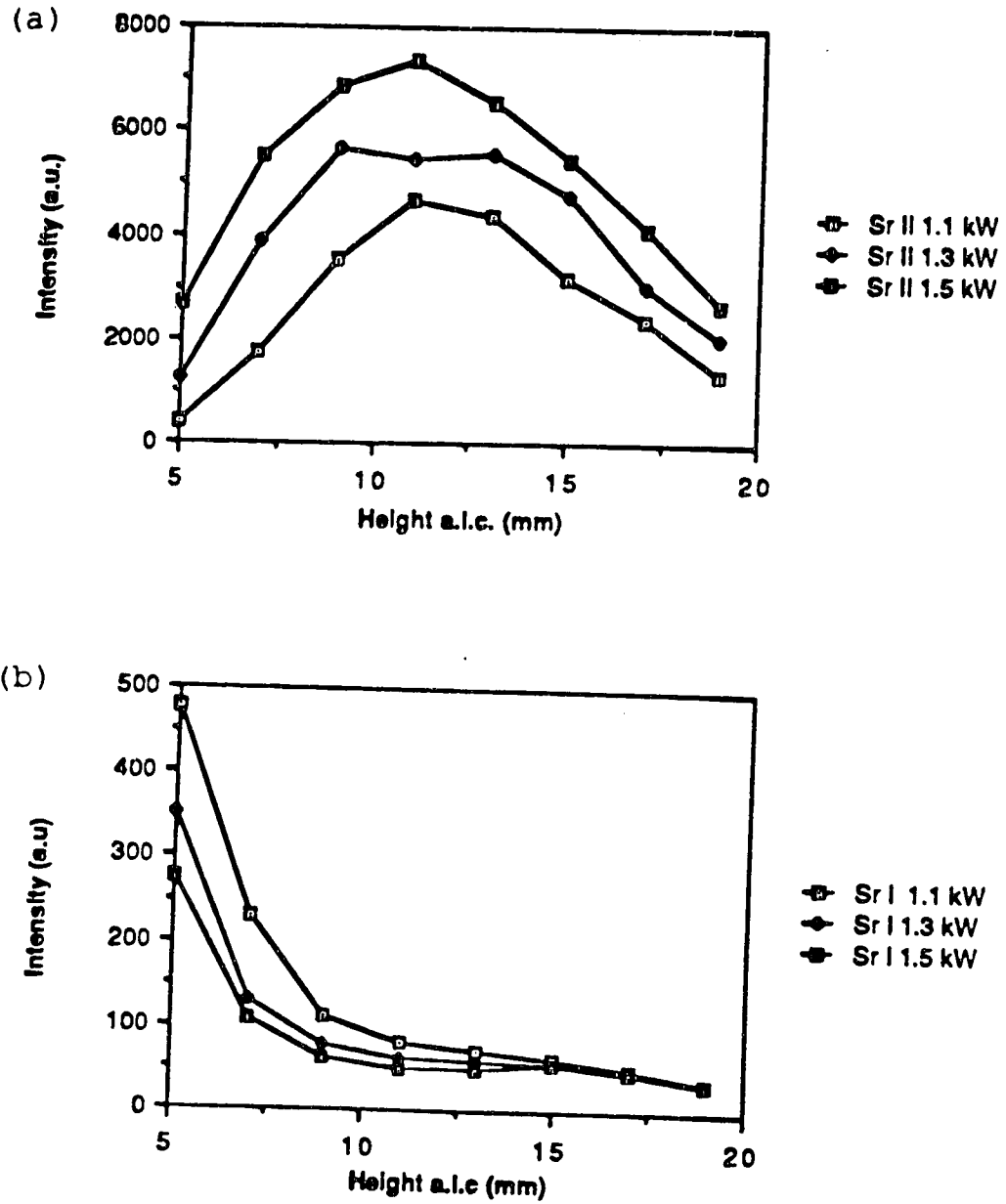


Figure 5.4 Spatial emission profile of the ICP for a) Sr II and b) Sr I.

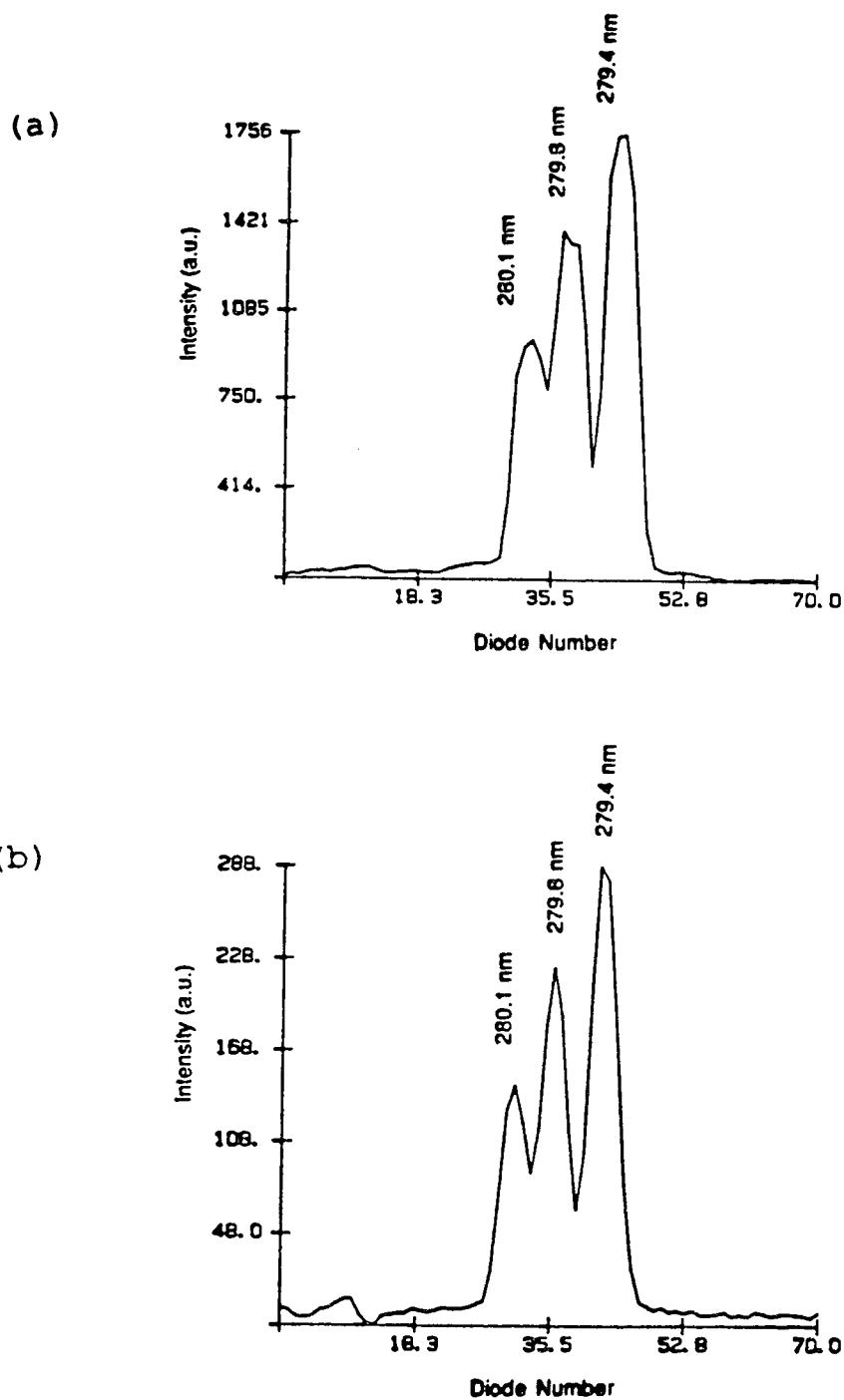


Figure 5.5 ICP-PDA spectrum of Mn triplet measured with a) convention entrance slit PDA spectrometer (100 μm slit width) and b) PDA spectrometer with fiber optic input.

optic input performs very much like the conventional entrance slit.

It was mentioned in Chapter 4 that a 30 μm slit width was required to resolve many of the lines in an Fe spectrum used for excitation temperature measurements. Now with resolution limited by the width of the fiber optic entrance slit, some of the lines could no longer be resolved. Unfortunately, this means that T_{exc} measurements are hampered when the fiber optic input is used. Either resolution must be improved or other lines selected. Resolution could be improved by three methods without changing the fiber optic cable.

- 1) Replace the current grating with one with greater dispersion. By increasing dispersion, the spectral window available to the PDA would be reduced.

- 2) Place a variable slit after the fiber optic entrance slit. Another slit would further reduce the light throughput and significantly reduce the instrument sensitivity.

- 3) Use digital filtering to deconvolve the spectra. Resolution enhancement techniques are, generally, more difficult to successfully implement in the case of atomic spectra than for IR spectra. The reasons for this is twofold. First, the natural line width of an emission line is narrower than or approximately equal to the spectral bandpass of the spectrometer, and it is inherently difficult to deconvolve beyond the instrument resolution [4]. Secondly, the signal to noise ratio of ICP spectra are typically lower than found for

IR spectra and successful deconvolution requires good signal to noise ratios.

5.5 Spectral Throughput

A major concern while designing the fiber optic system was loss in sensitivity. To measure the degree of attenuation caused by the fiber optic cable, spectra of Ca, Mg, Cd, and Zn were acquired with the PDA spectrometer before the fiber optic cable was installed. A 100 μm entrance slit was used for all measurements.

After the fiber optic cable was installed, the same solutions were run using the identical ICP and optical imaging parameters. The degree of attenuation was calculated by taking the net intensities of peaks from spectra obtained with the fiber optic spectrometer and dividing them by the net intensities of the peaks from the spectra obtained with the slit spectrometer. These results are summarized in Table 5.1. The attenuation at longer wavelengths (Ca 393. nm) is approximately 40% (Table 5.1). At shorter wavelengths the attenuation becomes more severe. The fall off of throughput roughly corresponds to the UV transmission characteristics of the quartz cable. The loss in net intensities must be compensated for by using longer PDA integration times.

Table 5.1 Attenuation of light throughput by fiber optic cable.

Element	Wavelength (nm)	Attenuation
Ca	396.8	0.37
	393.3	0.41
Mg	285.2	0.20
	280.3	0.24
	279.6	0.24
Cd	228.8	0.17
	226.5	0.16
	214.4	0.12
Zn	213.8	0.12
	206.1	0.09
	202.5	0.06

5.6 Conclusions

128

The loss of sensitivity and resolution restrictions, further limits the applicability of this PDA spectrometer for trace analysis of unknown samples. But the increased flexibility in optical coupling and simplicity of spatial profiling, along with the simultaneous multi-wavelength capability, opens up several new applications for this type of PDA spectrometer. Many of these new applications will be described in the following chapters.

References

1. T. E. Edmonds and G. Horlick, *Appl. Spectrosc.*, **31**, 536, (1977)
2. M. W. Blades and G. Horlick, *Appl. Spectrosc.*, **34**, 696, (1980)
3. M. W. Blades, *Appl. Spectrosc.*, **37**, 371, (1983)
4. G. Horlick, *Appl. Spectrosc.*, **26**, 395, (1972)

Chapter 6

Simultaneous Optical and Mass Spectrochemical Measurements on an ICP

6.1 Introduction

Since the mid 1970's, the ICP has been widely used as a source for atomic emission spectroscopy and recently, the ICP has become popular as a source for mass spectrometry [1,2]. Analyte ions from the ICP discharge are extracted into a quadrupole mass spectrometer for mass analysis. ICP-mass spectrometry (ICP-MS) offers a number of advantages over conventional ICP-AES. Detection limits for ICP-MS are typically 100 to 1000 times lower than the detection limits achieved with ICP-AES [3]. The ICP-MS can rapidly determine a large number of elements in the periodic table, making the technique ideal for qualitative analysis. The ICP-MS has the capability to obtain isotope distribution information, a capability not readily available to ICP-AES. Isotope information can be used for isotope dilution analysis or isotopically labeled tracer studies. The ICP-MS spectra are simpler than the corresponding atomic emission spectra. An

elemental mass spectrum will consist mainly of the singly charged ion and its isotopes. An atomic emission spectrum, on the other hand, may contain thousands of spectral lines, all from a single element.

The number of publications on the development and application of ICP-MS as an analytical technique has steadily increased in the last few years. Recently the field of elemental mass spectrometry has been included as a separate subject covered by the Analytical Chemistry Fundamental Reviews [4]. However, in the course of research into ICP-MS, some disadvantages of ICP-MS have also been realized.

As mentioned earlier, ICP-MS can achieve low detection limits, but the technique is not capable of determining the major components in a sample. If concentrations exceed 10 $\mu\text{g/mL}$, the detector can be damaged by the high ion current. Therefore, a dilution step is required if concentrations of major constituents are desired.

Simple spectra were initially stated as an advantage for ICP-MS over ICP-AES. Simple spectra implied that spectral overlap should be uncommon in ICP-MS. On the contrary, a spectral overlap in a mass spectrum can be a more serious problem than in an emission spectrum. Spectral interferences in ICP-MS can be divided into four categories: 1) spectral overlaps from basic background species, such as argon, water, and air, 2) interelement spectral overlaps, 3) matrix induced molecular overlaps, and 4) spectral overlaps due to argon-matrix related species. If we consider the major isotopes of

ten elements often determined in an elemental analysis (Si, Al, Fe, Ca, Na, K, Mg, Ni, Cu, and Zn) we can see some of the effects of spectral interferences in ICP-MS.

The basic background species in the ICP arise from the plasma discharge, entrained air and/or water and often result in intense peaks in the ICP-MS spectra. The major background species are N_2^+ , Ar^+ , ArO^+ , $ArOH^+$, and Ar_2^+ [5]. Examples of background species interference on the top ten elements are N_2^+ overlapping with Si^+ , $^{38}ArH^+$ overlapping with K^+ , Ar^+ overlapping with Ca^+ , and ArO^+ overlapping with Fe^+ .

Interelement spectral overlaps include isobaric overlaps and element oxides, element hydroxides, and doubly charged species overlapping with the analyte peak [6]. The oxides, hydroxides, and doubly charged species can be relatively abundant in the ICP, and can cause serious interferences. Examples of this type of overlap include Sc^{2+} and $^{46}Ca^{2+}$ on Na^+ , $^{48}Ca^{2+}$ on Mg , MgO^+ on Ca^+ , CaO^+ on Fe^+ , $^{42}CaO^+$ on Ni^+ , $^{47}TiO^+$ on Cu^+ , and $^{48}CaO^+$ and TiO^+ on Zn^+ .

The third type of spectral interference results from the ions, oxides, and hydroxides formed from matrix elements in solution. The source of the highest concentration of matrix elements is usually the acid used to dissolve the sample [5]. The matrix interference that occurs will, therefore depend on the acid used to dissolve the sample. For example, if H_2SO_4 is used to dissolve a sample, SO_2^+ and S_2^+ will overlap on Zn^+ .

The final type of spectral interference results from species formed between Ar and matrix elements in high concentrations. In samples with high Na concentration, such as sea water, a peak from ArNa^+ will be detected and this peak will overlap Cu^+ .

Another problem associated with the ICP-MS is matrix effects [7]. Generally, a high concentration of a matrix element in solution will cause a suppression in analyte signal. The suppression is more serious for matrix elements with higher masses and light analyte elements are affected more seriously. A high concentration (1000 $\mu\text{g/mL}$) of a heavy matrix element may cause a 50% or greater suppression of the analyte signal.

Medium and long term signal stability is also a problem with ICP-MS. Relative standard deviations of up to 13%, for a 30 minute period, have been reported [8]. As a result, internal standards are required for most quantitative analysis with the ICP-MS.

It is difficult to determine definitively, which individual technique, ICP-MS or ICP-AES, is superior, but it is clear that the two techniques can be complementary. ICP-MS with low detection limits is excellent for trace and ultra-trace analysis, ICP-AES is capable of determinations at the trace, minor, and major levels.

To identify if a spectral overlap exists in an ICP-MS spectrum, a determination must be made at more than one isotope. If the measured concentrations of the two isotopes

for a single element are not the same, then a spectral overlap at one of the isotopes exists. This procedure is not possible to carry out for mono-isotopic elements such as Be, Na, Sc, Mn, Co, Al, P, Y, Nb, Rh, Bi, Au, Cs, Ta, and La. In these cases ICP-AES could be used to confirm a spectral overlap.

To correct for a spectral overlap, the contribution of the interfering species to the total signal must be determined. For example, to correct for the interference of TiO^+ on Zn^+ at mass 64, the concentration of Ti must first be determined. From this concentration, the contribution of TiO at mass 64 can be calculated and subtracted from the total signal, leaving only the signal due to Zn^+ . The most serious spectral overlaps will result from the major components in the sample. Therefore, it is important to have a quantitative measure of the major sample components. As noted earlier, it is often not possible to quantitatively determine major components in a sample by ICP-MS without a dilution step. In such a case it would be advantageous to determine the major components with ICP-AES.

For the case of the CaO^+ overlap on Fe^+ , the concentration of Ca is required to correct for the CaO signal at mass 56. The determination of Ca with ICP-MS is hampered by the interference of Ar^+ on Ca^+ . Ar^+ is a very intense signal at mass 40 and therefore, it is not possible to determine either Ca or Ar with ICP-MS to provide the correction for Fe^+ at mass 56. In this case a determination

of Ca by ICP-AES would be required to provide a correction for of the CaO interference on Fe.

ICP-AES is relatively free from matrix effects and the long term stability is such that internal standards are not normally required. By making simultaneous optical and mass spectrochemical measurements some insight into the sources of the matrix effects and drift in ICP-MS may be gained.

6.2 Instrumentation

The ICP-MS used in this study was a Sciex Elan 250. Its operation has been described previously [9]. The optical channel was the PDA spectrometer with the fiber optic input cable as described in Chapter 5. A quartz lens (100 mm focal length) was attached, via a specially adapted lens mount, to a beam supporting the quadrupole spectrometer. The translational stage with the fiber optic input was mounted directly on the outer housing of the Elan. The lens was positioned 20 cm from the mass spectrometer sampling cone, and the fiber optic input was 20 cm from the lens, resulting in a 1:1 image of the plasma at the fiber optic input (Figure 6.1). All emission data were acquired and processed with the IBM-pc. Mass spectral data were acquired with the Elan system. There was no electronic synchronization of the two systems. All spectra were acquired at the same time under manual control.

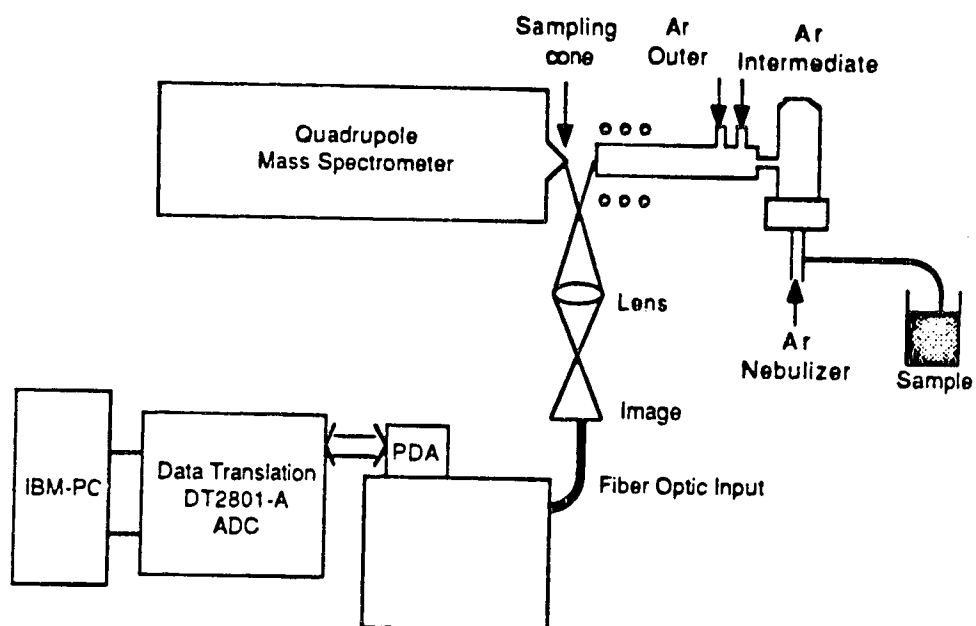


Figure 6.1 Schematic diagram of experimental system for simultaneous optical and mass spectrochemical measurements.

Alignment of the optical system with a HeNe laser was not possible because of the configuration of the mass spectrometer. Therefore, to determine the location of the central channel of the ICP, a vertical spatial emission profile was determined (Figure 6.2). Both atom and ion lines of Sr (Figure 6.3) were measured in a single spectral window with the PDA spectrometer. The vertical scale on the horizontal axis of the plot in Figure 6.2 is the reading from the micrometer on the fiber optic translational stage. The central channel was found at micrometer reading 15.5 mm. The fiber optic cable was positioned at this height for all subsequent measurements. The distance from the sampling cone to the load coil was 15 mm for all measurements. Optical measurements were made 1 mm in front of the sampling cone (14 mm from load coil), unless otherwise specified.

6.3 Effect of Plasma Operating Parameters on Optical and Mass Spectrochemical Signals

The effects of central (nebulizer) gas flow rate and RF power on Sr ion mass (Sr^+), Sr ion emission (Sr II), and Sr atom emission (Sr I) signals were investigated. The effect of central gas flow rate on the Sr^+ mass signal at 1.1 kW RF power is plotted in Figure 6.4. The Sr^+ mass signal has a sharp peak in the flow rate plot with the maximum value at 0.95 Lpm. The effect of power on the Sr^+ mass signal is

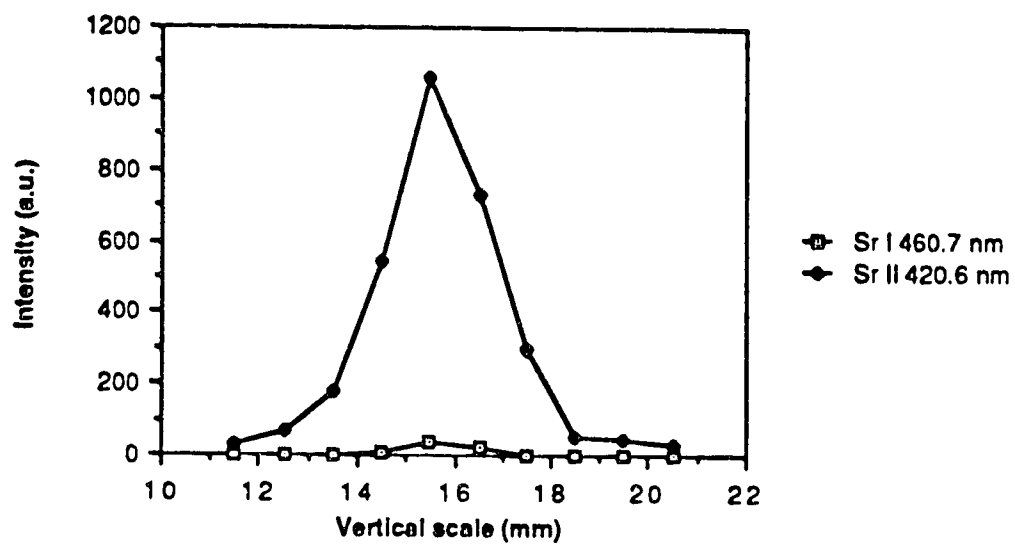


Figure 6.2 Vertical spatial emission profile (lateral across the ICP) for Sr II and Sr I.

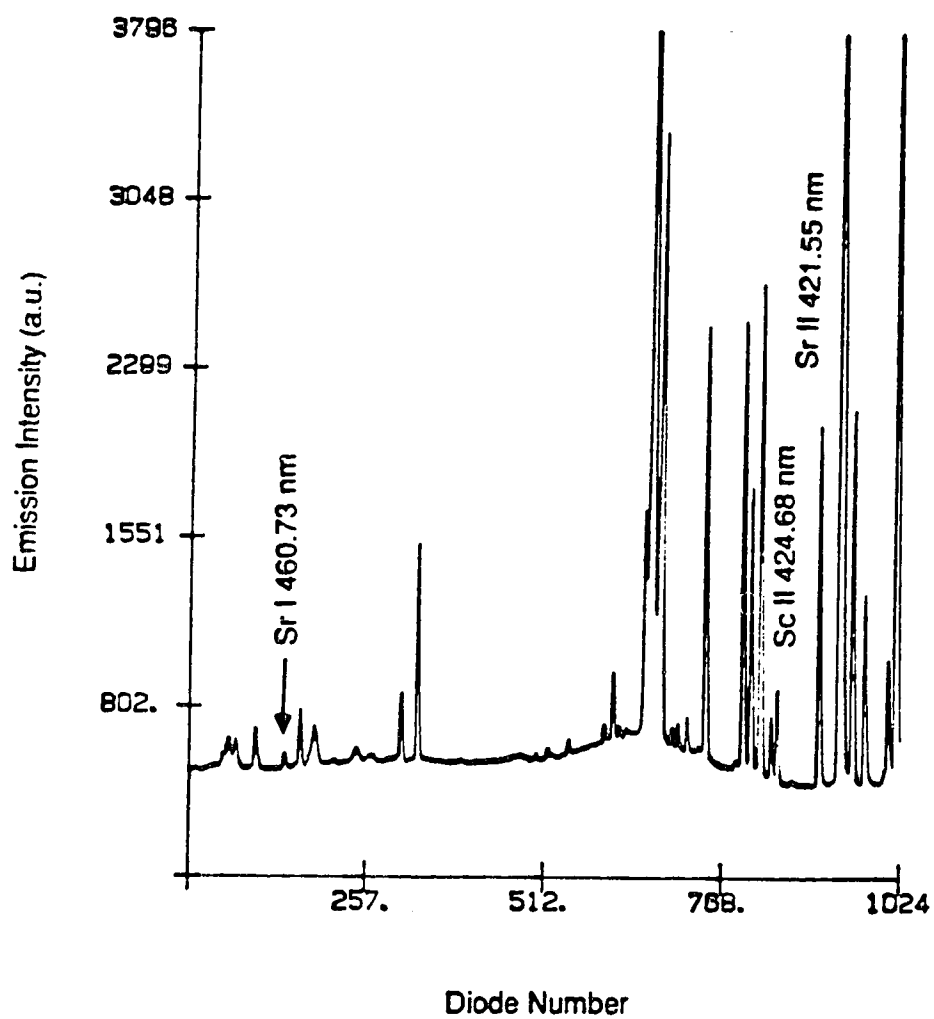


Figure 6.3 ICP-PDA spectrum of 1 $\mu\text{g/mL}$ Sr and Sc, with spectrometer centered at approximately 440 nm.

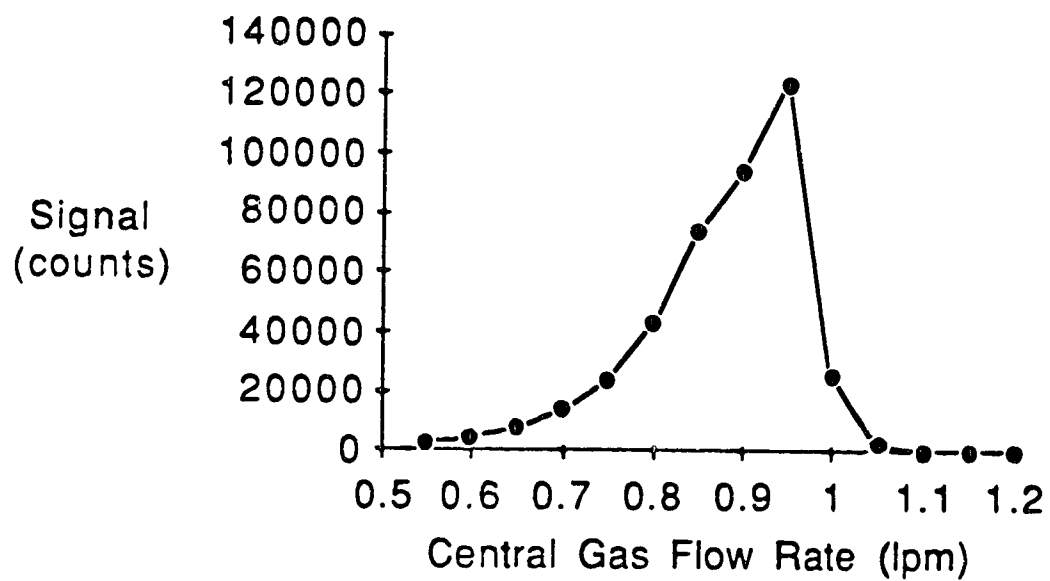


Figure 6.4 Sr^+ mass signal as a function of central gas flow rate at 1.1 kW RF power.

plotted in Figure 6.5. The general peak shape of the central gas flow rate plots are maintained at all RF powers, but the position of optimum central gas flow rate shifts to higher flow rates. At 1.1 kW, the optimum flow rate was 0.95 Lpm, at 1.3 kW, the optimum flow rate was 1.05 Lpm, and at 1.5 kW, the optimum flow rate increased to 1.1 Lpm. The net signal also increases with power, but only if the signal is measured at the optimum flow rate for that power.

The Sr II emission signal also goes through a maximum value as central gas flow rate is increased (Figure 6.6). The maximum signal occurred at approximately 0.7 Lpm at 1.1 kW, and as power is increased the flow rate for optimum emission signal also increased (Figure 6.7). The net emission signal also increased with power, but unlike the Sr⁺ mass signal, it increased with power at all flow rates measured.

If the Sr⁺ mass signal and Sr II emission signal are plotted together on the same flow rate axis (Figure 6.8), it is clear that the optimum central gas flow rates for mass and optical measurements occur at different flow rates for all powers studied.

The effect of optical viewing zone on emission intensity was also investigated. The sampling cone to load coil distance was held constant at 15 mm while the fiber optic input cable was moved away from the sampling cone toward the load coil in 1 mm increments. At each spatial point, the central gas flow rate was varied to obtain a flow rate profile for Ba II emission, as in Figure 6.6. The emission

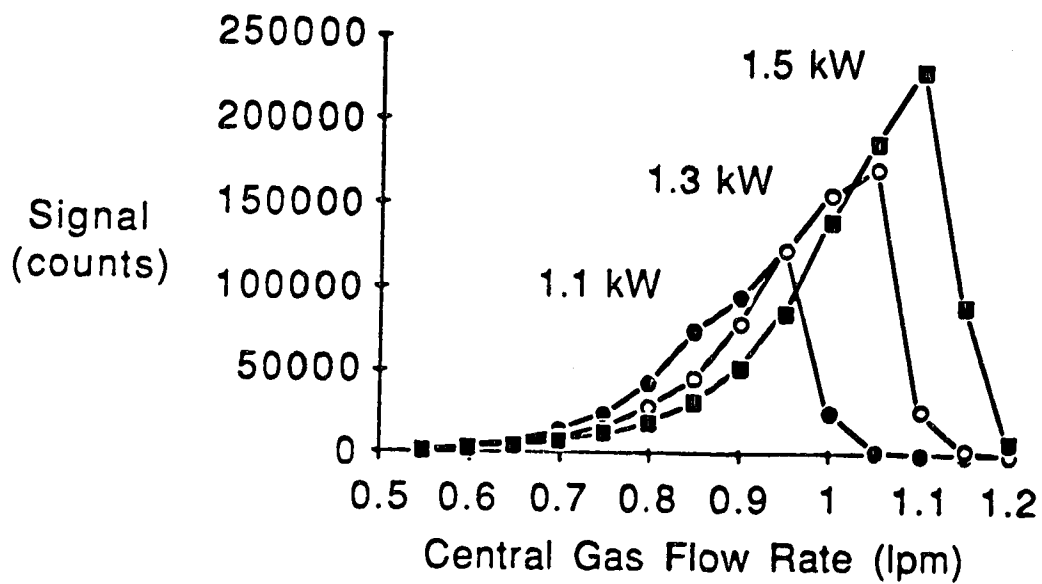


Figure 6.5 Sr⁺ mass signal as a function of central gas flow rate at 1.1, 1.3, and 1.5 kW RF powers.

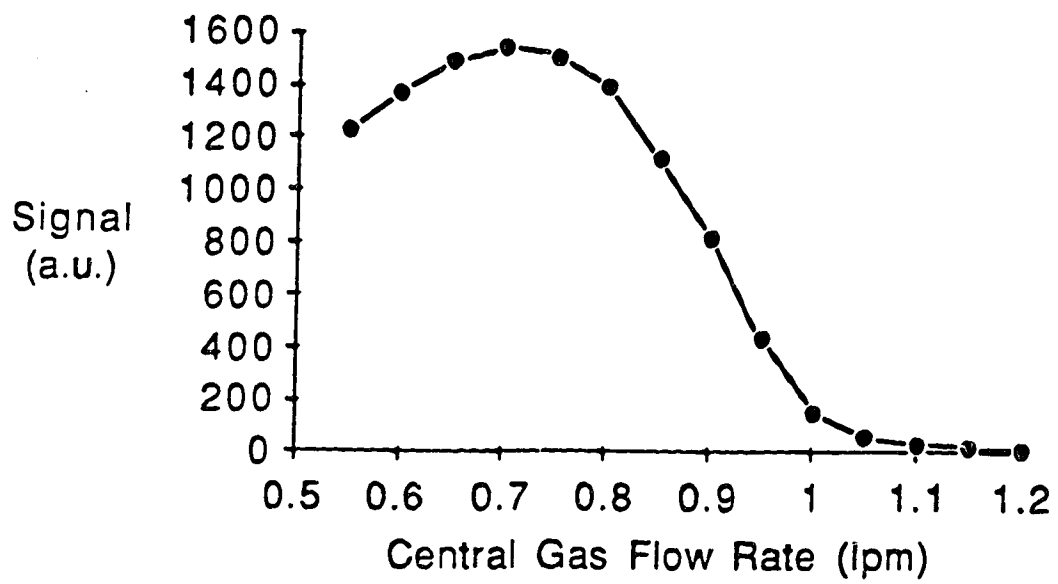


Figure 6.6 Sr II emission signal as function of central gas flow rate at 1.1 kW RF power.

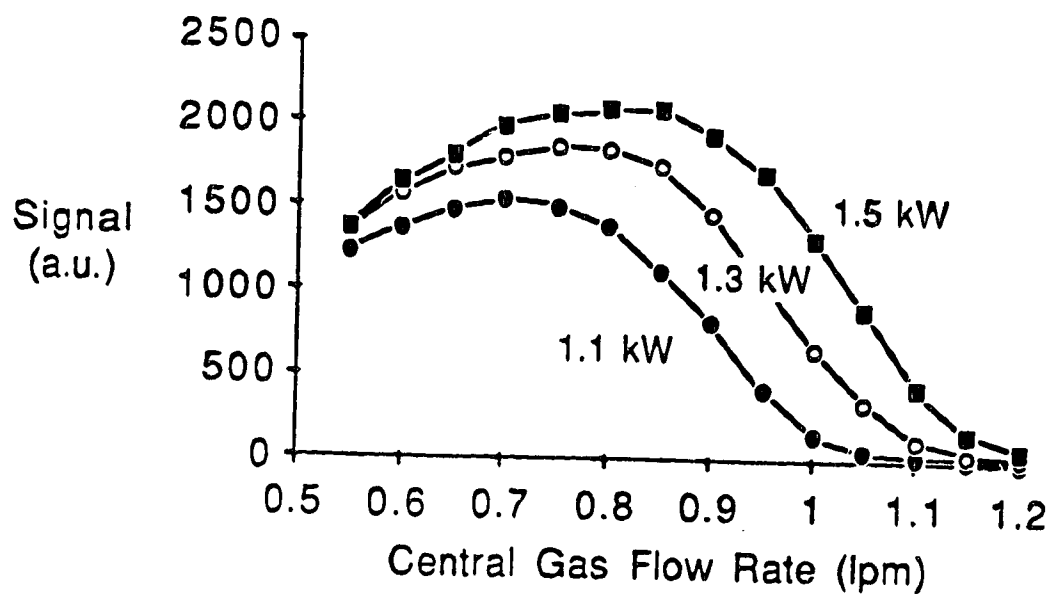


Figure 6.7 Sr II emission signal as function of central gas flow rate at 1.1, 1.3, and 1.5 kW RF powers.

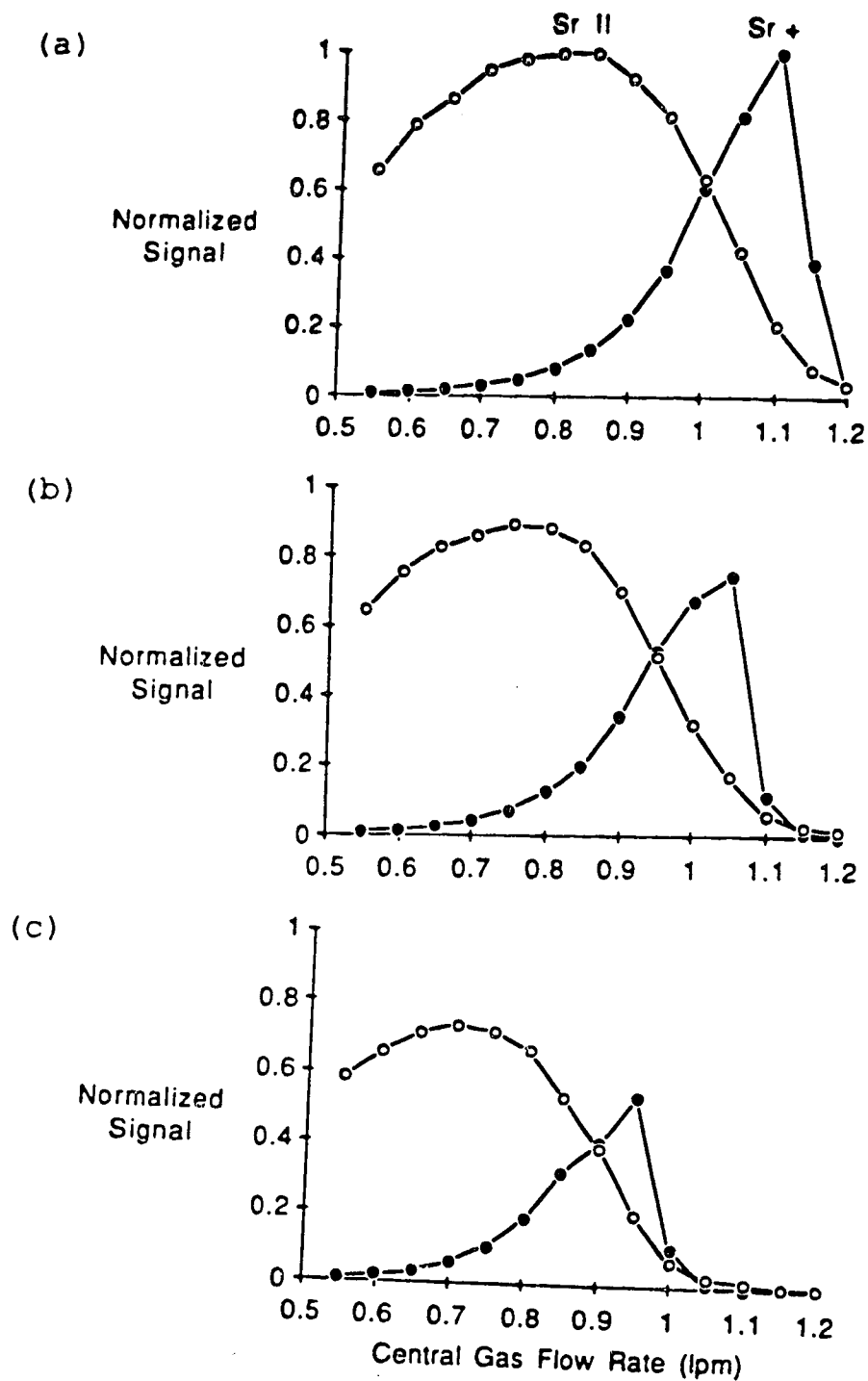


Figure 6.8 Sr II emission and Sr⁺ mass signals as function of central gas flow rate at a) 1.5, b) 1.3, c) 1.1 kW RF power.

intensity at all flow rates less than 0.9 Lpm increased as the observation zone moved from 1 to 4 mm from the sampling cone (Figure 6.9). At flow rates above 0.9 Lpm, no increase in emission intensity was observed. Therefore, changing the spatial observation zone does not improve the emission channel sensitivity at the higher central channel flow rates required for optimum mass channel sensitivity.

In terms of analytical applications, these results indicate that a single flow rate, power, or spatial position does not exist for optimum simultaneous optical and mass measurements. The sensitivity of one channel must be sacrificed to optimize the other.

Another interesting feature of the flow rate plots are the shapes of the curves for the emission and mass data. Emission flow rate profiles are much broader than the corresponding mass profiles, in all cases. To fully explain this response, species densities and electron densities at each flow rate would be required. Clearly, the mass signal is much more dependent on the plasma operating conditions than is the emission signal. This result may be significant when comparing the long term stability of the two systems.

The central gas flow rate plots for Sr^+ mass, Sr II emission, and Sr I emission, at 1.1 kW, 1.3 kW, and 1.5 kW RF power, are shown in Figure 6.10. The maximum Sr I emission signal occurs at a central gas flow rate of approximately 1.1 Lpm, higher than the optimum for either the Sr II or Sr^+ signals for all RF powers.

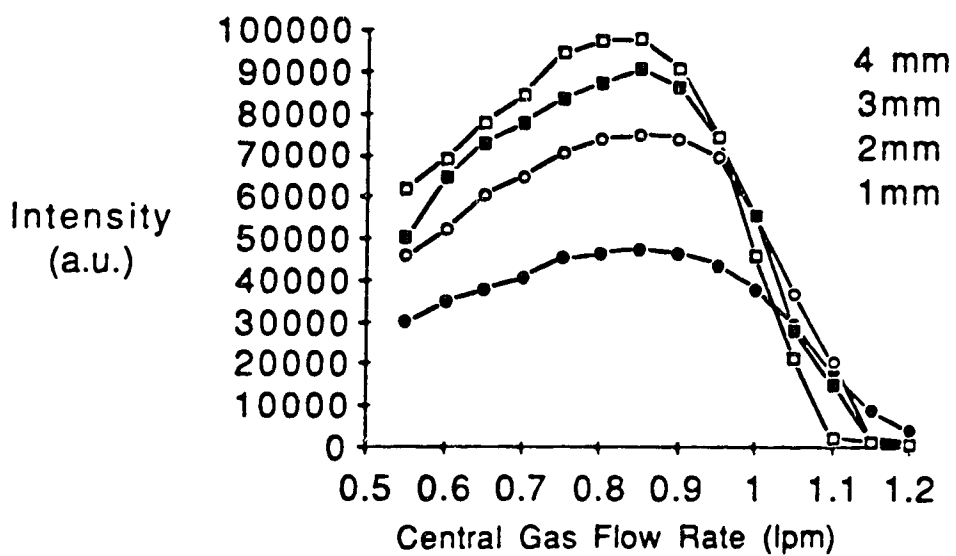


Figure 6.9 Ba II emission as a function of central gas flow rate at observation zones 1, 2, 3, and 4 mm from the sampling cone.

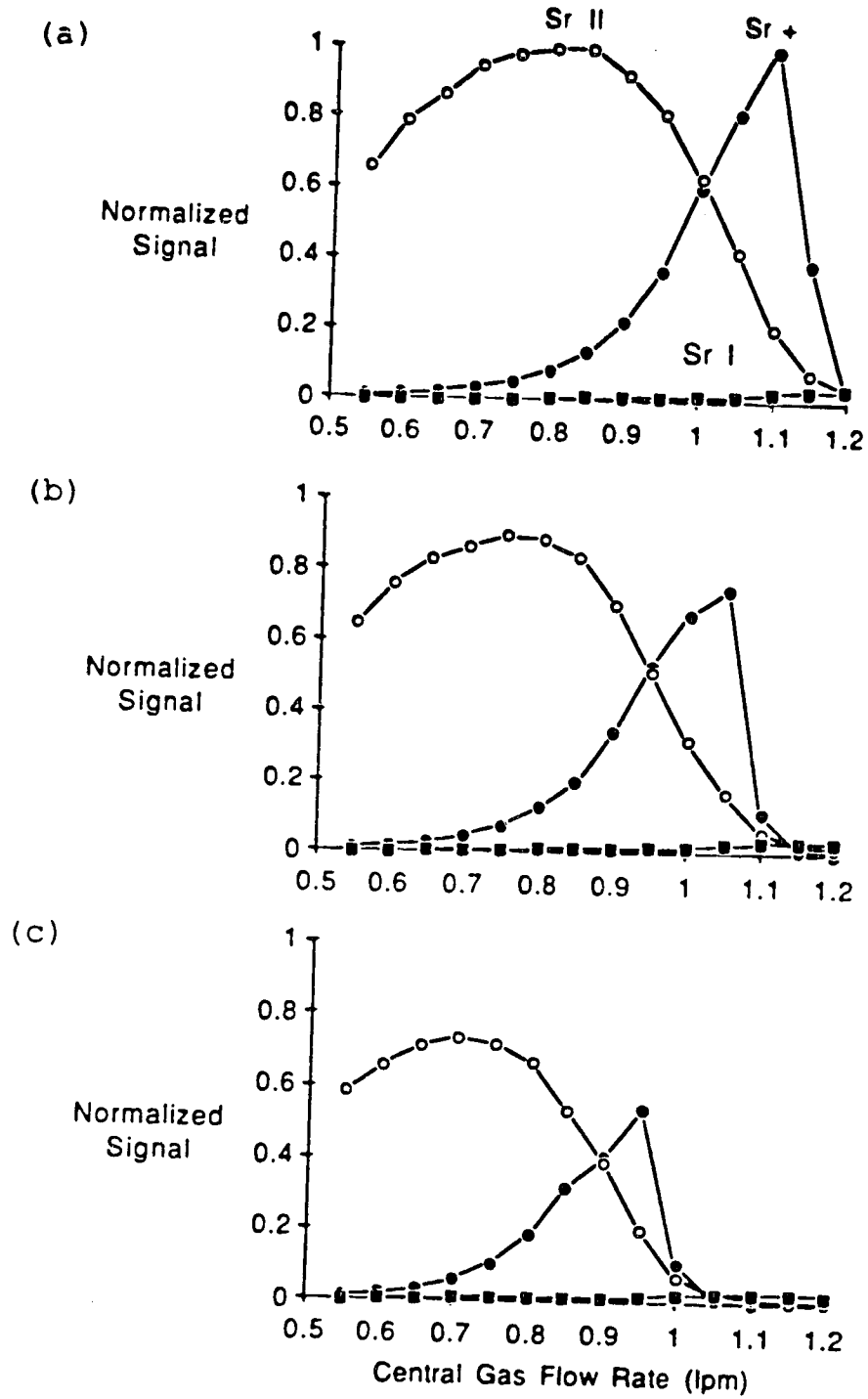


Figure 6.10 Sr II emission, Sr I emission, and Sr⁺ mass signals as function of central gas flow rate at a) 1.5, b) 1.3, c) 1.1 kW RF power.

Koirtiyohann et al. [10] have designated two regions in the plasma, the initial radiation zone (IRZ) and the normal analytical zone (NAZ). The IRZ is lower in the plasma i.e. closer to the load coil, and is the region where maximum atom emission occurs. The NAZ is higher in the plasma and is the region of where maximum ion emission occurs. If the central gas flow rate is increased the central channel of the ICP will expand and the IRZ will extend higher into the plasma. If power is increased, the central channel of the ICP contracts and the IRZ moves lower in the plasma. Therefore, at a fixed viewing position, as the flow rate increases, the plasma region changes from NAZ to IRZ and the ion emission decreases and atom emission increases. Between the NAZ and IRZ is the region for optimum Sr^+ mass signal. This remains between the NAZ and IRZ at all powers. The relatively narrow width of the peak in the Sr^+ mass signal flow rate plot indicates that this zone is smaller than either the NAZ or IRZ.

6.4 Effect of Plasma Parameters on Oxides Species

As discussed earlier, oxides of Ar, analyte elements, and matrix elements are present in the ICP-MS spectrum, and all forms of oxides are a potential spectral interference. The effect of plasma operating parameters on the optical and mass analyte signals and analyte-oxide signals were

investigated. Emission from La ion (La II) at 442.99 nm (Figure 6.11) and LaO at the 437.57 nm bandhead (Figure 6.12) was measured simultaneously with the PDA spectrometer. La ion (La^+) and LaO ion (LaO^+) signals were measured with the ICP-MS. The central gas flow rate plots for 1.1 kW are shown in Figure 6.13.

The optimum flow rate for La II emission occurred at 0.7 Lpm. The maximum LaO emission occurred at 1.1 Lpm. The La II emission profile was similar to the emission profile of Sr II, while the LaO emission profile was similar to the Sr I profile (Figure 6.10). The optimum flow rate for the La^+ signal was 0.9 Lpm, as in the case for Sr^+ (Figure 6.10). The maximum LaO^+ signal occurred a flow rate of 1.0 Lpm.

If the same description of the ICP is used as in the previous section, then the LaO emission occurs in the IRZ of the ICP. The LaO ion occurs between the IRZ and NAZ, similar to the La ion, but at a slightly different position. Spectral interferences from oxide species is not normally a problem in ICP-AES as the emission is spatially separated in the plasma. At central gas flow rates used in emission measurements there are little or no oxides present. In ICP-MS ions and oxides occur in the same spatial region of the plasma. If the signal due to the oxide in mass spectrometry is to be reduced, then the central gas flow rate must be reduced. As a result the ion signal will also be reduced.

As discussed in section 6.1, the optical channel can be used to correct for the spectral interference of oxides. One

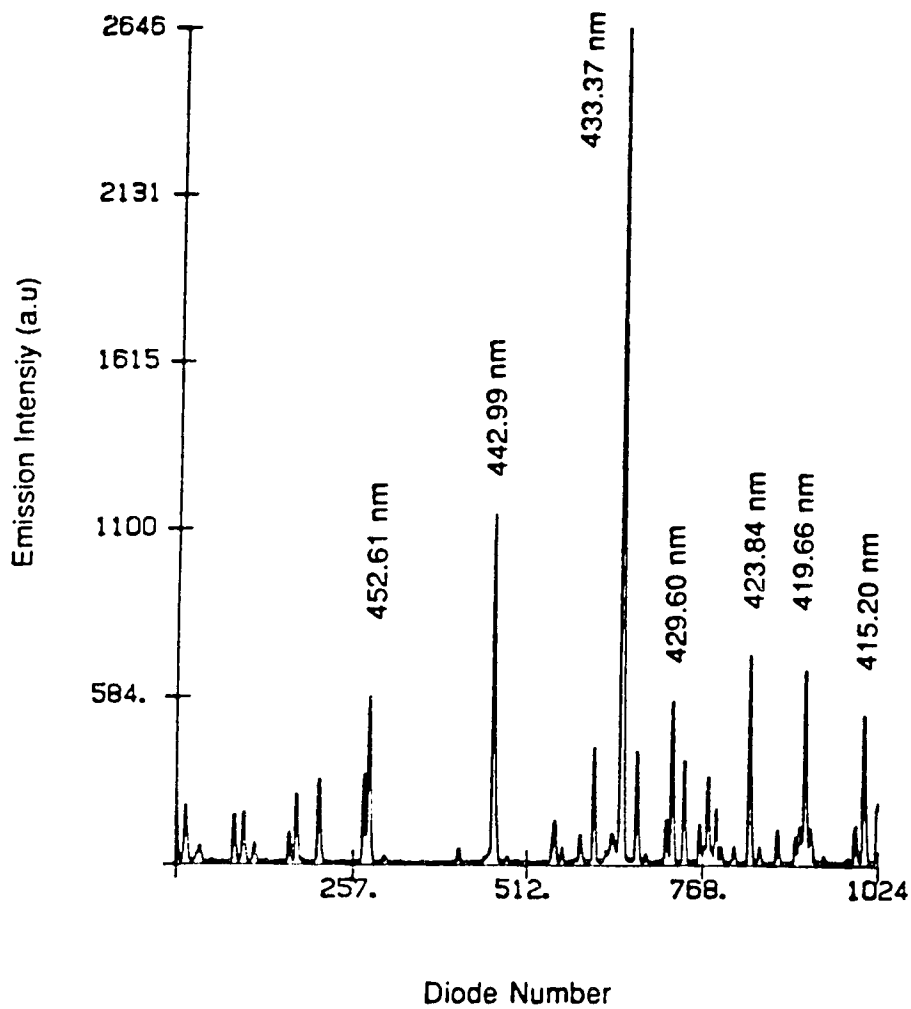


Figure 6.11 ICP-PDA La II emission spectrum, 0.7 Lpm central gas flow rate and 1.1 kW RF power.

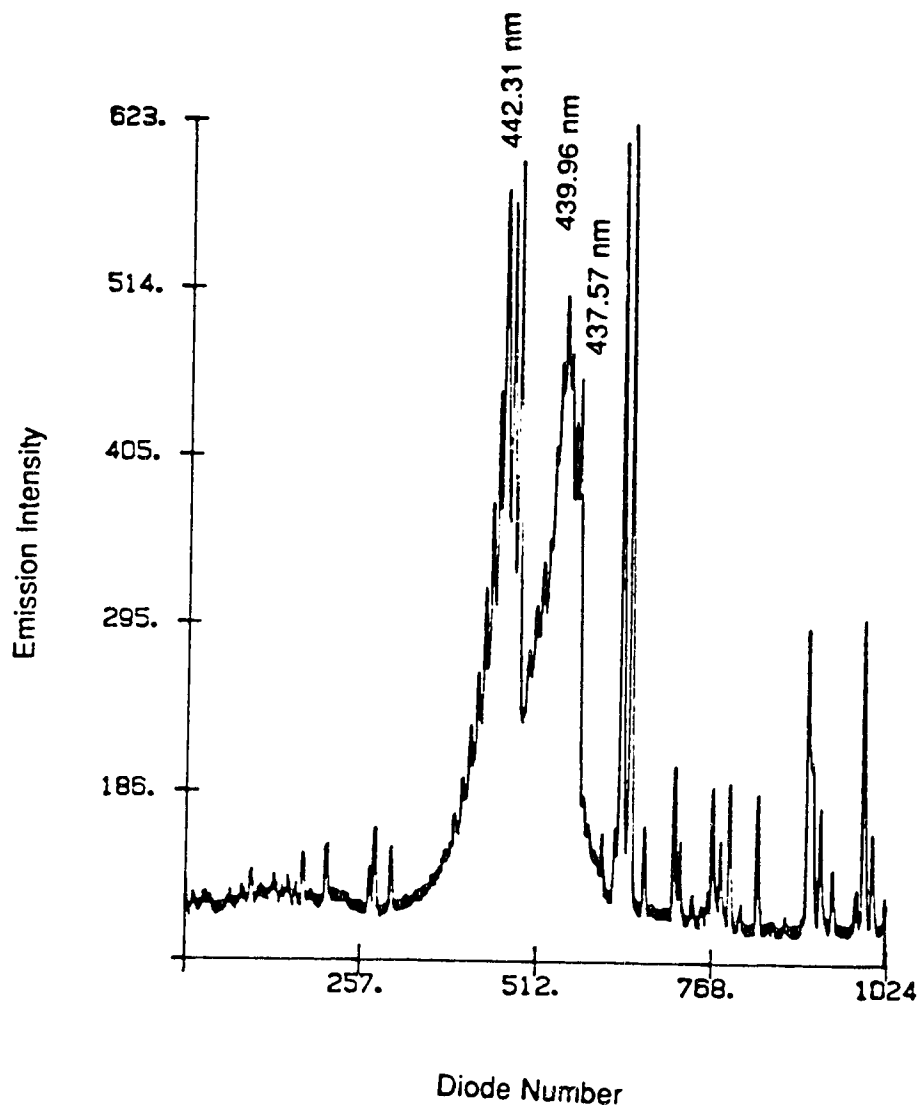


Figure 6.12 ICP-PDA LaO emission spectrum, 1.1 Lpm central gas flow rate and 1.1 kW RF power.

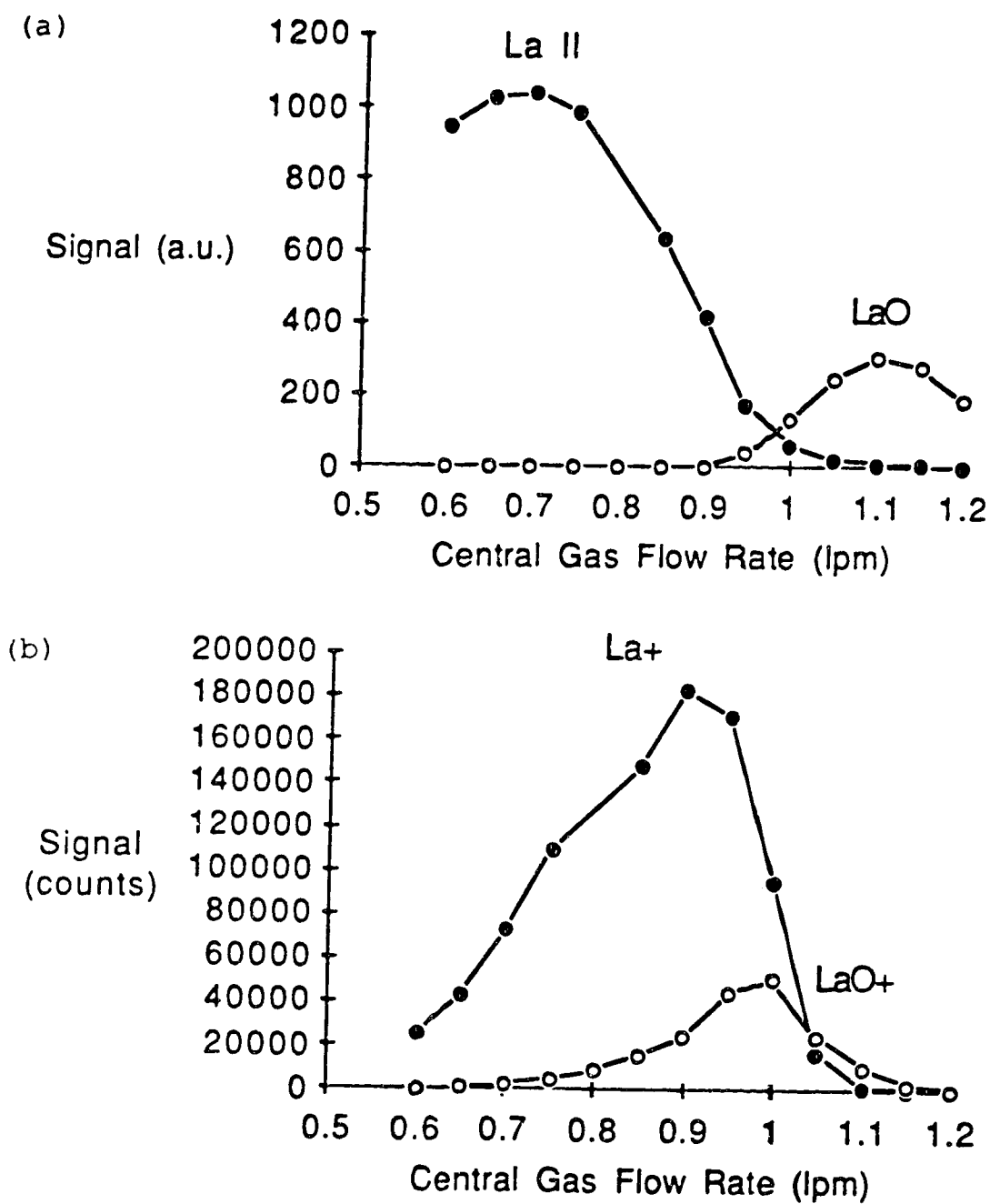


Figure 6.13 a) La II and LaO emission and b) La⁺ and LaO⁺ mass signals as a function of central gas flow rate.

example discussed was the interference of TiO on Zn at mass 64. If the contribution of TiO to the signal at mass 64 can be determined, then a correction can be applied to the total signal and the contribution from Zn at mass 64 can be determined. Ti II emission was measured with the PDA optical channel and mass 64 signal was measured with the mass spectrometer for Ti solutions over a range of concentrations. The plot of Ti II emission versus TiO^+ has a slope of 1.13 (± 0.03) indicating a linear relationship over the two orders of magnitude measured (Figure 6.14). This plot can now be used as a calibration plot for the correction of the TiO interference. To apply the correction, the optical channel measures the Ti II emission intensity while the mass spectrometer measures the signal at mass 64. Using the Ti II intensity, the number of TiO^+ counts can be read off of the plot in Figure 6.14. The number of TiO^+ counts is subtracted from the total counts at mass 64, leaving the counts due to Zn.

6.5 Matrix Effects

Matrix effects are signal intensity changes induced by the sample matrix. The discussion of matrix effects in this section will not include intensity changes due to a spectral overlap of a matrix element or matrix element oxide with an analyte. The effect of Na concentration on the intensity of

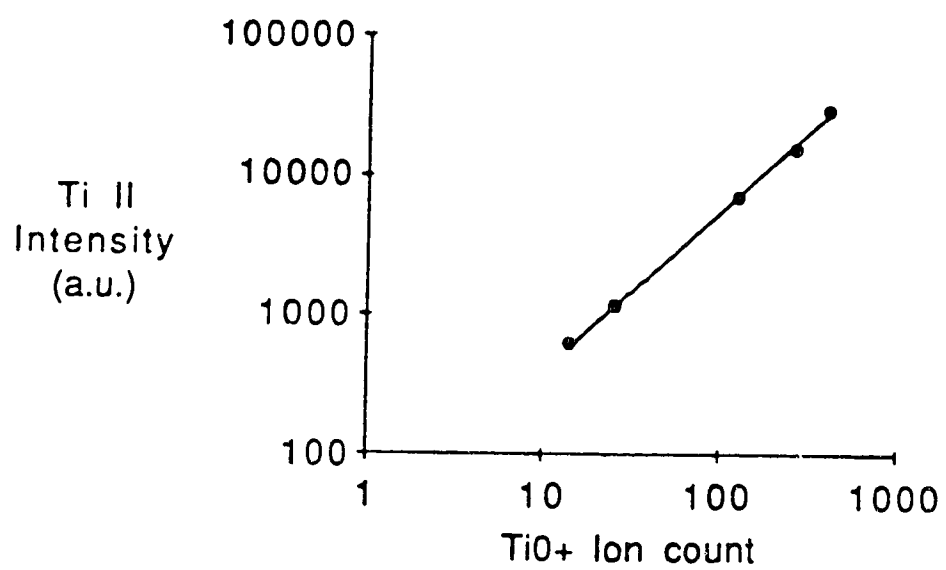


Figure 6.14 Ti II emission measured with the PDA spectrometer versus TiO^+ signal measured with the mass spectrometer.

optical and mass signals was investigated for Sc. Sc II emission was measured with the PDA spectrometer and simultaneously, Sc^+ was measured with the mass spectrometer, for a series of solutions each containing 1 $\mu\text{g}/\text{mL}$ Sc, and with Na concentrations ranging from 0 to 1000 $\mu\text{g}/\text{mL}$ (Figure 6.15). The RF power was 1.3 kW and the central gas flow rate was 1.1 Lpm.

The Sc II emission signal was enhanced by the presence of Na. An enhancement of 20% was observed at a Na concentration of 1000 $\mu\text{g}/\text{mL}$. On the other hand, the Sc^+ mass signal was suppressed by the presence of Na, with a suppression of 30% at a Na concentration of 1000 $\mu\text{g}/\text{mL}$.

The effect of central gas flow rate on the matrix effect was also studied. Optical and mass intensity measurements were made for two solutions, one containing 1 $\mu\text{g}/\text{mL}$ Sr and the second containing 1 $\mu\text{g}/\text{mL}$ Sr and 1000 $\mu\text{g}/\text{mL}$ Na, over a range of flow rates (Figure 6.16). At flow rates greater than 0.85 Lpm, an enhancement was observed for the Sr II emission signal. Over the flow rate range of 0.8 Lpm to 1 Lpm the Sr^+ mass signal was suppressed, but at higher flow rates an enhancement was observed. At flow rates less than 0.8 Lpm, there was little or no matrix effect for either the Sr II emission or Sr^+ mass signal.

Na is a relatively light element, the effect of a heavier element on the optical and mass signal was also studied. The central gas flow rate profiles for the optical and mass signals of two samples, one containing 1 $\mu\text{g}/\text{mL}$ Sr

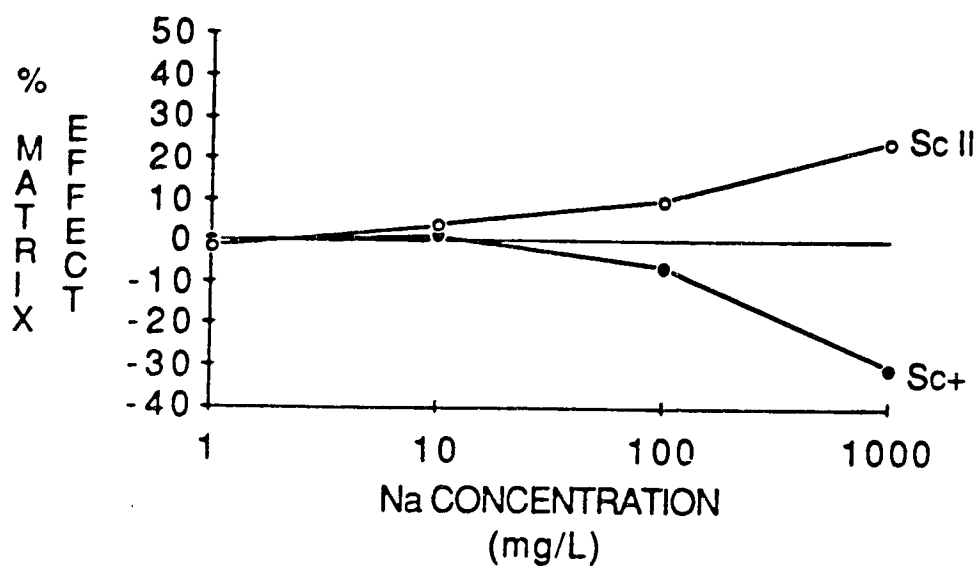


Figure 6.15 Effect of Na concentration on Sc II emission and Sr^+ ion signals.

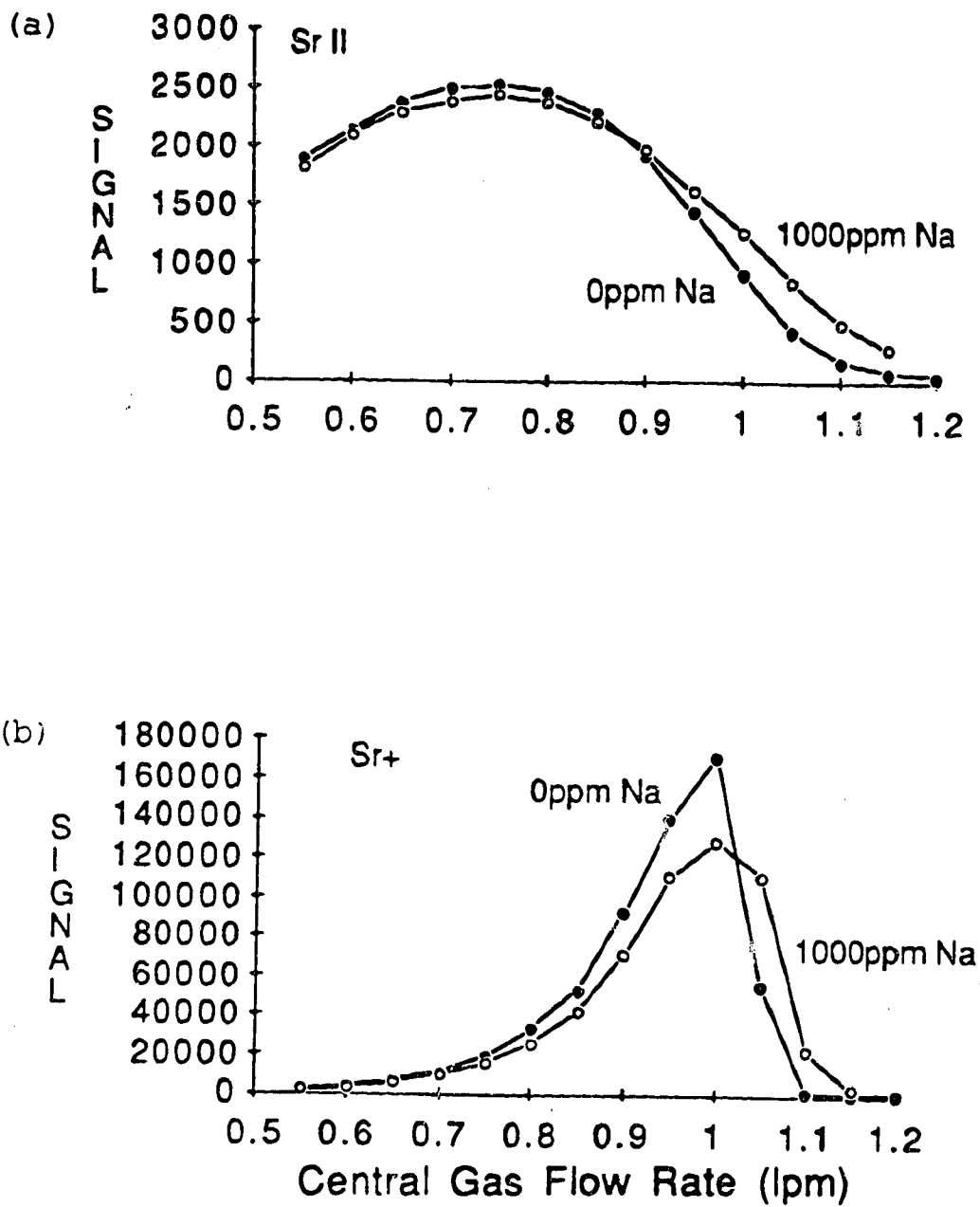


Figure 6.16 Effect of central gas flow rate on a) Sr II emission and b) Sr⁺ ion signals with and without 1000 $\mu\text{g}/\text{mL}$ Na.

and the second, 1 $\mu\text{g/mL}$ Sr and 1000 $\mu\text{g/mL}$ Tl are plotted in Figure 6.17. For the optical channel little or no matrix effect was observed at all flow rates, while at a flow rate of 1 Lpm a 70% suppression was observed for the mass signal.

A single matrix element may cause a suppression, enhancement, or no effect in optical emission spectroscopy, depending on the operating conditions and spatial observation zone used to make the measurement [11]. A similar statement can be made for matrix effects in the ICP-MS. Suppression of analyte signal however, is the most significant effect. Only at very high flow rates was an enhancement observed. The matrix effect is more serious for the mass spectrometer signal than for the optical signal. The matrix effect on the mass signal is dependent on the mass of the matrix element, and under identical operating conditions, the mass signal matrix effect will be a suppression while the optical signal matrix effect will be an enhancement. These results would indicate that the matrix effect on the mass signal and on the optical signal operate via two different mechanisms.

The matrix effect in the optical signal is thought to be from a shift in species distribution in the plasma, caused by the presence of a high concentration of a matrix element [11]. For the mass signal, the matrix effect is suspected to originate from a space-charge effect in the ion lens system in the mass spectrometer [7]. In the space-charge effect, a high density of matrix ions in the ion lenses will alter the field experienced by analyte ions as they travel through the

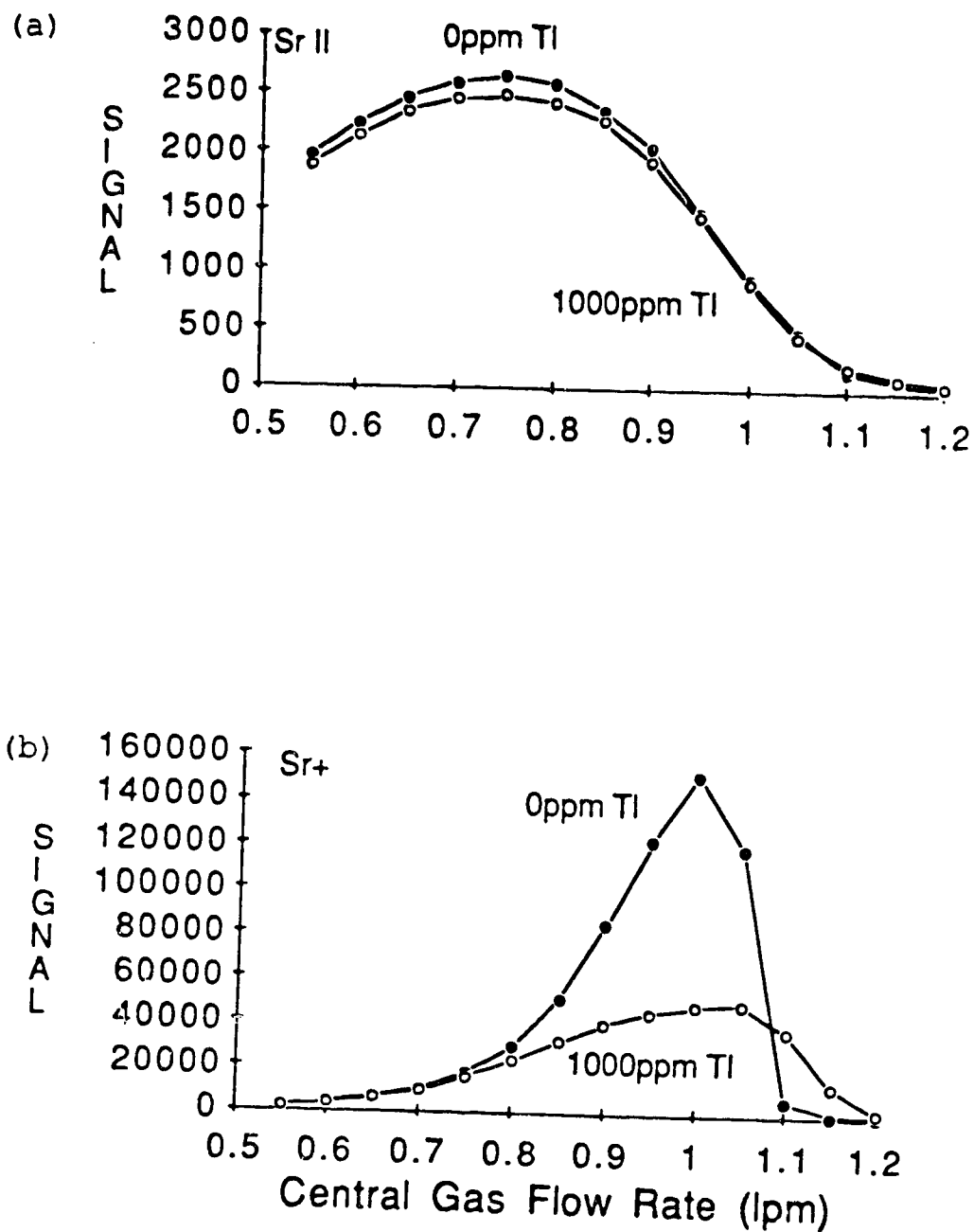


Figure 6.17 Effect of central gas flow rate on a) Sr II emission and b) Sr⁺ ion signals with and without 1000 $\mu\text{g/mL}$ Tl.

lenses, and thus the transmission characteristics of the lenses will be changed.

The simultaneous optical and mass data supports the theory of two separate mechanisms for the matrix effects, but caution must be used, as in this study we are comparing excited state ions (optical signal) with ground state ions (mass signal). The effect of a matrix element may be different for ground state and excited state ions in the plasma. To confirm this theory, fluorescence measurements of the ground state ions in the ICP-MS plasma are required.

6.6 Drift

A 1 $\mu\text{g/mL}$ Sr solution was continuously aspirated for 25 minutes and the Sr^+ mass signal, Sr II emission, and Sr I emission were measured at 5 minute intervals (Figure 6.18). The Sr^+ mass signal continually increased over the 25 minute period, increasing by 40%. The Sr II emission signal showed a small upward drift of about 10% in the first five minutes and remained almost constant for the next 20 minutes. The Sr I emission showed only small fluctuations and no definite drift in either direction. This result implies that the drift in mass and optical signals results from different sources.

From section 6.3 we know that the mass signal is more dependent on central gas flow rate than is the optical signal. Therefore it is possible that a drift in central gas flow rate would cause a more serious drift for the mass

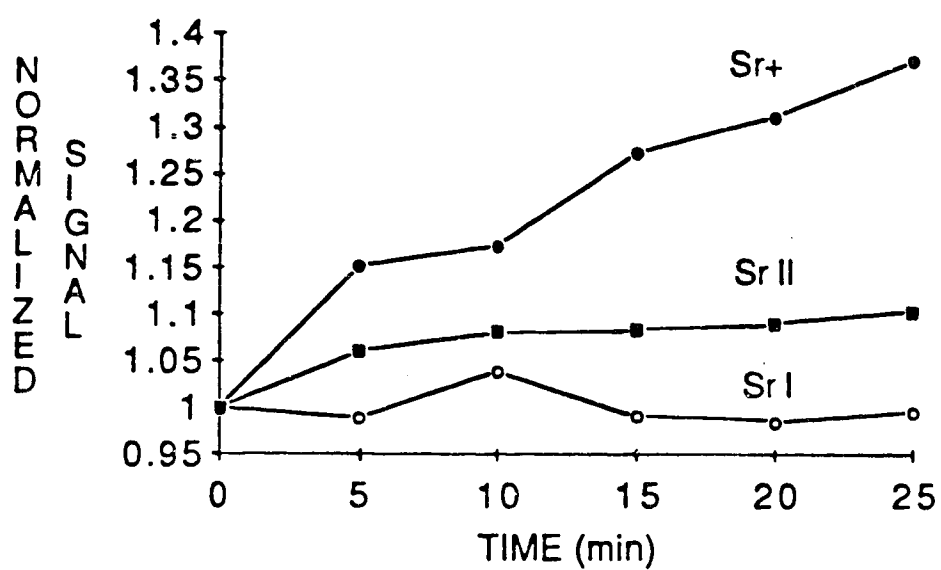


Figure 6.18 Drift of Sr II emission, Sr I emission, and Sr⁺ ion signals as a function of time.

signal than it would for the optical signal. For the drift experiment, the central gas flow rate was optimized for the mass signal, therefore an increase or decrease in flow rate would result in a downward, not upward drift, in mass signal. Therefore, it is suspected that drift in central gas flow rate is not the major source of drift in the ICP-MS signal.

It has been suggested that the source of drift in the mass spectrometer results from ions coating the ion optics in the mass spectrometer [12]. As ions coat the lenses, the fields in the mass spectrometer lens system gradually change, causing changes in the lens transmission characteristics. This effect would not change the emission signal. If the coating of the lenses with ions is responsible for the drift in ICP-MS, it is therefore, not possible to use the optical signal to correct the mass spectrometer signal.

6.7 Conclusions

There is not a combination of RF power, central gas flow rate, and observation zone that can be used to simultaneously measure optical emission and ion mass signal under optimum conditions. The sensitivity of one technique must be sacrificed for the other. The choice of operating conditions would depend upon the type of analysis desired. Factors such as detection limit, dynamic range, and matrix elements would have to be considered when deciding on plasma operating parameters. If the high sensitivity of the ICP-MS is desired,

then a higher central gas flow rate must be used, and as a result the emission signal will decrease. Conversely, if optimum sensitivity is required for the optical channel the central gas flow must be reduced, and a loss in the mass channel signal intensity will result. The selection of central gas flow rate will strongly depend on the requirements of the application.

The metal oxide species that are detected in the mass spectrometer also are present in the emission spectrum of the ICP. Emission from oxide species does not occur under normal operating conditions used for emission measurements. However, the oxides do exist under operating conditions used for mass measurements. The oxide signal can be reduced by decreasing the central gas flow rate, but at the expense of the ion signal. To reduce the metal oxide in the mass spectrum, two methods are being pursued. The most straight forward is to remove the source of the oxide in the plasma, water, by using a desolvation step after the spray chamber. The other method uses a N₂-Ar mixed gas ICP. The N₂ in the plasma is more energetic, and is able to dissociate the metal oxides [13].

Under normal operating conditions, the optical channel can be used to provide a correction for the oxide interference in the mass spectrometer.

Matrix effects are found to be more severe in the ICP-MS than in ICP-AES. Both techniques exhibit suppressions and enhancements to some degree, but not at the same operating conditions. It is possible that the matrix effects originate

in the plasma, but it is likely the mass spectrometer contributes, via a space-charge effect, to the overall matrix suppressions observed in ICP-MS. The extent of the plasma contribution to ICP-MS matrix effects would require ion ground state densities in the plasma. To obtain this information atomic fluorescence measurements are required.

Drift in the ICP-MS signal was observed to be more severe than in the ICP-AES signal. The ICP-MS has relatively poor medium to long term stability. As a result, internal standards are required for most quantitative analysis with the ICP-MS. An internal standard is an element or elements not naturally occurring in the sample, added to all samples and standards used in the analysis. The signal from the internal standard is measured and ratioed to the signal of the analyte elements to compensate for instrumental fluctuations. Using an internal standard increases sample preparation time, increases the complexity of the measurement, and reduces the sample throughput. If the source of drift can be located it may be possible to reduce or eliminate the error and eliminate the need for the internal standard. The nature and possible sources of the drift will be discussed in the next chapter.

References

1. R. S. Houk, V. A. Fassel, G. D. Flesch, H. J. Svec, A. L. Gray, and C. E. Taylor, *Anal. Chem.*, **52**, 2283, (1980)
2. D. F. Douglas, E. S. K. Quan, and R. G. Smith, *Spectrochim. Acta*, **38B**, (1983)
3. G. Horlick, S. H. Tan, M. A. Vaughan, and Y. Shao, "Inductively Coupled Plasma", in "Inductively Coupled Plasmas in Analytical Atomic Spectroscopy", A. Montaser and D. W. Golightly ed., VCH Publishers, Chapter 10, p. 361, (1987)
4. D. W. Koppenaal, *Anal. Chem.*, **60**, 113R, (1988)
5. S. H. Tan and G. Horlick, *Appl. Spectrosc.*, **40**, 445, (1986)
6. M. A. Vaughan and G. Horlick, *Appl. Spectrosc.*, **40**, 434, (1986)
7. S. H. Tan and G. Horlick, *J. Anal. Atom. Spectrom.*, **2**, 745, (1987)
8. M. A. Vaughan and G. Holick, *J. Anal. Atom. Spectrosc.*, in press, (1988)
9. M. A. Vaughan, G. Horlick, and S. H. Tan *J. Anal. Atom. Spectrom.*, **2**, 765, (1987)

10. S. R. Koirtyohann, J. S. Jones, C. P. Jester, and D. A. Yates, *Spectrochim. Acta*, **36**, 49, (1981)
11. M. W. Blades and G. Horlick, *Spectrochim. Acta*, **36B**, 861, (1981)
12. D. J. Douglas, *Can. J. Spectrosc.*, in press, (1988)
13. J. Lam, PhD. Thesis, Department of Chemistry, University of Alberta, Edmonton, (1988)

Chapter 7

Simultaneous Optical and Mass Noise Studies for the ICP

7.1 Introduction

The signal to noise ratio is the most common figure of merit used to describe noise in an analytical system. The signal to noise ratio provides only a quantitative measure of noise in a system. A complete analysis of noise requires both quantitative information over a range of signal intensities and qualitative information. Qualitative information is obtained in the form of noise power or noise amplitude as a function of frequency. To obtain a noise amplitude spectrum, a bandlimited signal measured as a function of time is recorded with a digital computer. The Fourier transform of the time domain signal is calculated to give the noise amplitude spectrum. The noise power or noise amplitude spectrum has been used to characterize emission noise in flames [1,2], ICPs [3-6], and neutron stars [7].

The emission noise in the ICP has been categorized as three types: 1) white noise, 2) $1/f$ noise, and 3) fixed frequency noise. White noise is noise made up of all

frequencies. In a noise amplitude spectrum, white noise appears as a straight line with a constant amplitude at all frequencies i.e. a flat line. The major source of white noise in the ICP is the photon shot noise.

For $1/f$ noise, or as it may also be also called, excess low frequency noise or non-fundamental noise, the noise amplitude increases as frequency decreases. The plot of noise amplitude versus frequency often has a $1/f$ form (where f is frequency). The gradual change in instrumental factors is the source of $1/f$ noise in the ICP. Factors such as line voltage fluctuations, changes in RF power, changes in Ar gas flow rate, detector voltage fluctuations, and changes in temperature all contribute to $1/f$ noise in the ICP. Drift of the nebulizer has been demonstrated to be a major source of $1/f$ noise in ICP-AES [4].

Fixed frequency noise is noise composed of one or more discrete frequencies. Fixed frequency noise appears as one or more peaks in the noise amplitude spectrum. The most common source of fixed frequency noise is the line voltage. Frequencies of 60, 120, 180, and 240 Hz all may appear in an ICP-AES noise amplitude spectrum, as a result of the line voltage frequency coupling with the RF power supply or the detector power supply. Another fixed frequency noise has been observed in the noise amplitude spectrum of ICP-AES, and it appears in the 100 to 300 Hz region [3-6]. The source of this fixed frequency noise is related to the plasma discharge but the exact nature of the noise is not clear. This fixed

frequency noise has been attributed to an asymmetric rotation of the plasma [4] and to an up-down fluctuation in the plasma [5].

The objective of the work in this chapter is to compare the noise amplitude spectra of ICP-AES and ICP-MS. In doing so, it is hoped that the nature of the noise in ICP-MS can be better understood and that the source of fixed frequency noise in the ICP can be isolated.

7.2 Instrumentation for Noise Amplitude Studies

Noise amplitude spectra were acquired over the range 0 to 500 Hz for both the optical and mass spectral signals. To prevent aliasing, the time domain signal must be sampled at twice the highest frequency in the noise amplitude spectrum, in this case the sampling frequency must be at least 1000 Hz. The PDA is capable of reading out a spectrum every 0.042 seconds, thus the highest sampling frequency available with a PDA detector is 24 Hz. Therefore, the fast response of a PMT is required for all optical noise amplitude measurements and a PMT was used for all optical measurements in this chapter.

The optical spectrometer was the PDA spectrometer with fiber optic input cable described in Chapter 5, with a folding mirror placed in front of the PDA and an IP28 PMT mounted behind the exit slit (Figure 7.1). The output from the PMT was amplified with a high speed current amplifier (Keithly, Model 427) and the amplified signal was low pass

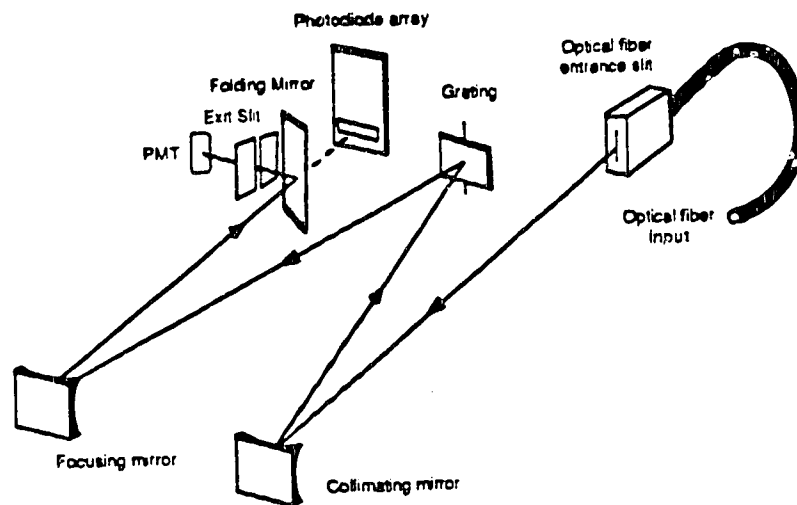


Figure 7.1 Schematic diagram of Czerny-Turner type monochromator with fiber optic input and PMT detector.

filtered (Krohn-Hite, Model 3343). The upper cut off frequency was 700 Hz with a -48 db/octave roll off. The filtered emission signal was digitized with channel C of the 16 channel ADC (Data Translation, DT2801-A). The digitization rate was 1400 Hz. A 1:1 image of the plasma was formed at the fiber optic input cable as described in Chapter 6.

The ICP-MS used in this study was the Sciex, Elan Model 250. The software of the Elan did not permit data to be acquired at high data rates and at equally spaced time intervals. Therefore, it was necessary to bypass the Elan data processing system.

The Elan measurement system employs an ion counting system, which was modified to provide a continuous analog output signal. When an ion reaches the channel electron multiplier (CEM) of the mass spectrometer, a small current pulse results. The current pulses from the CEM are amplified and converted to TTL compatible pulses. The digital pulses are then passed through a series of flip-flops (74S74) to divide the count rate by a factor of four (Figure 7.2). At this point (Pin 9, on Chip U18 on the Signal Processing Board Figure 7.3) the signal was extracted and fed into a frequency to voltage converter (F/V). The F/V was an AD650 Voltage-to-Frequency and Frequency-to-Voltage Converter, operated in the F/V mode (Figure 7.4) [8]. Resistor R_1 ($22k\Omega$) and capacitor C_{INT} ($0.01\mu F$) were selected to pass frequencies from 0 to approximately 1000 Hz. The analog output from the F/V was then low passed filtered, with a cutoff frequency of 700 Hz,

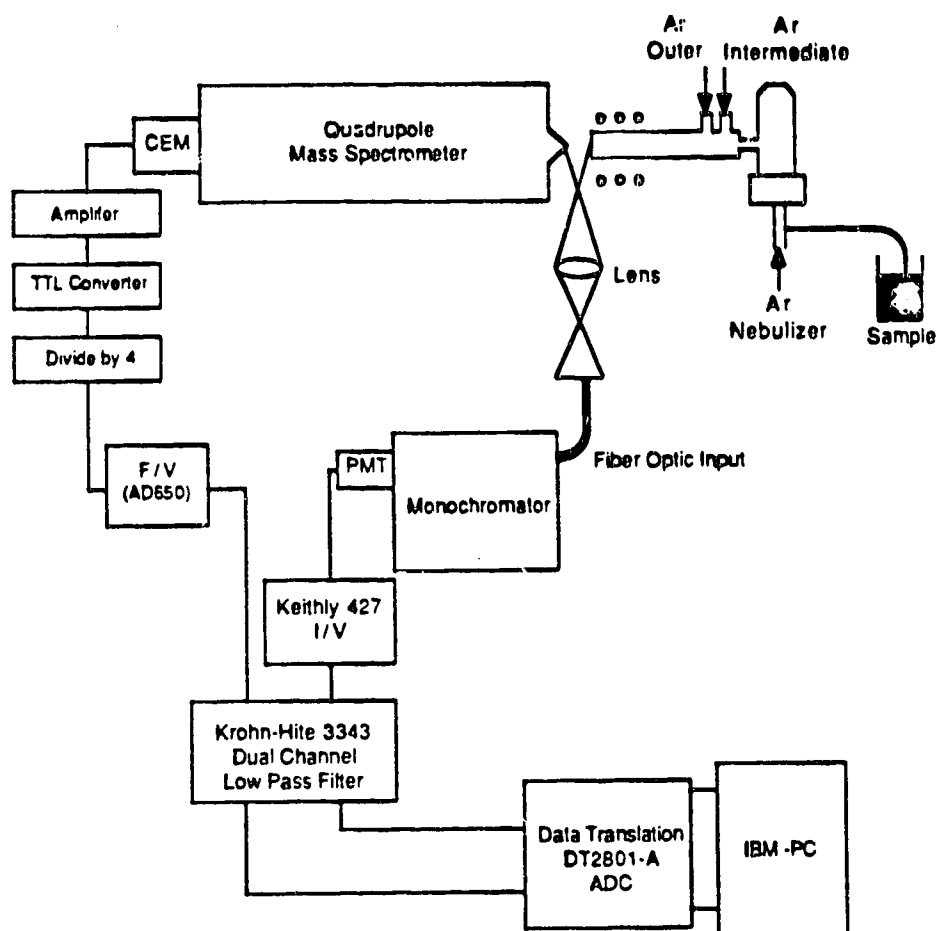


Figure 7.2 Schematic diagram of simultaneous optical and mass noise amplitude measurement system.

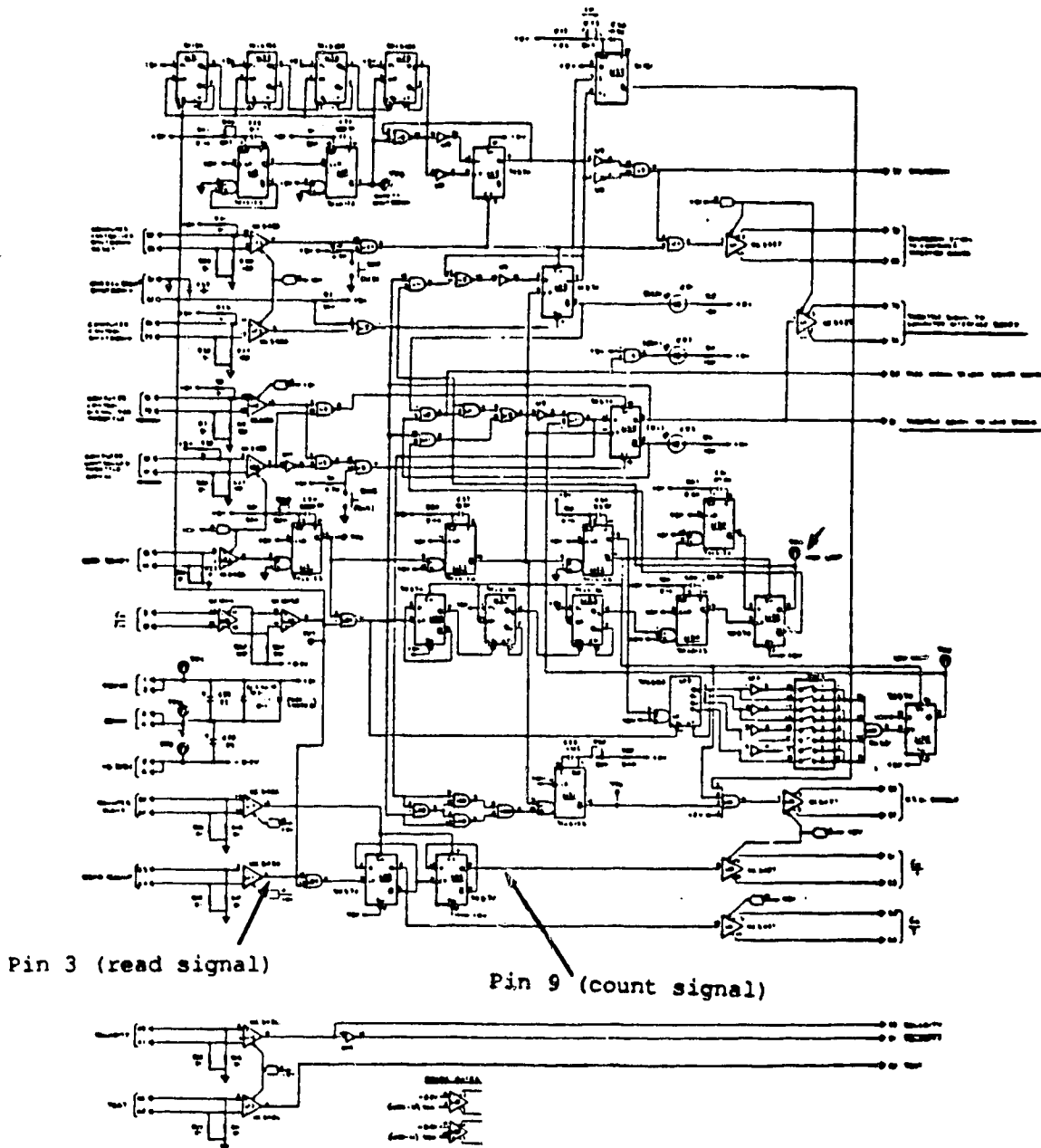


Figure 7.3 Diagram of portion of Elan signal processing board electronics.

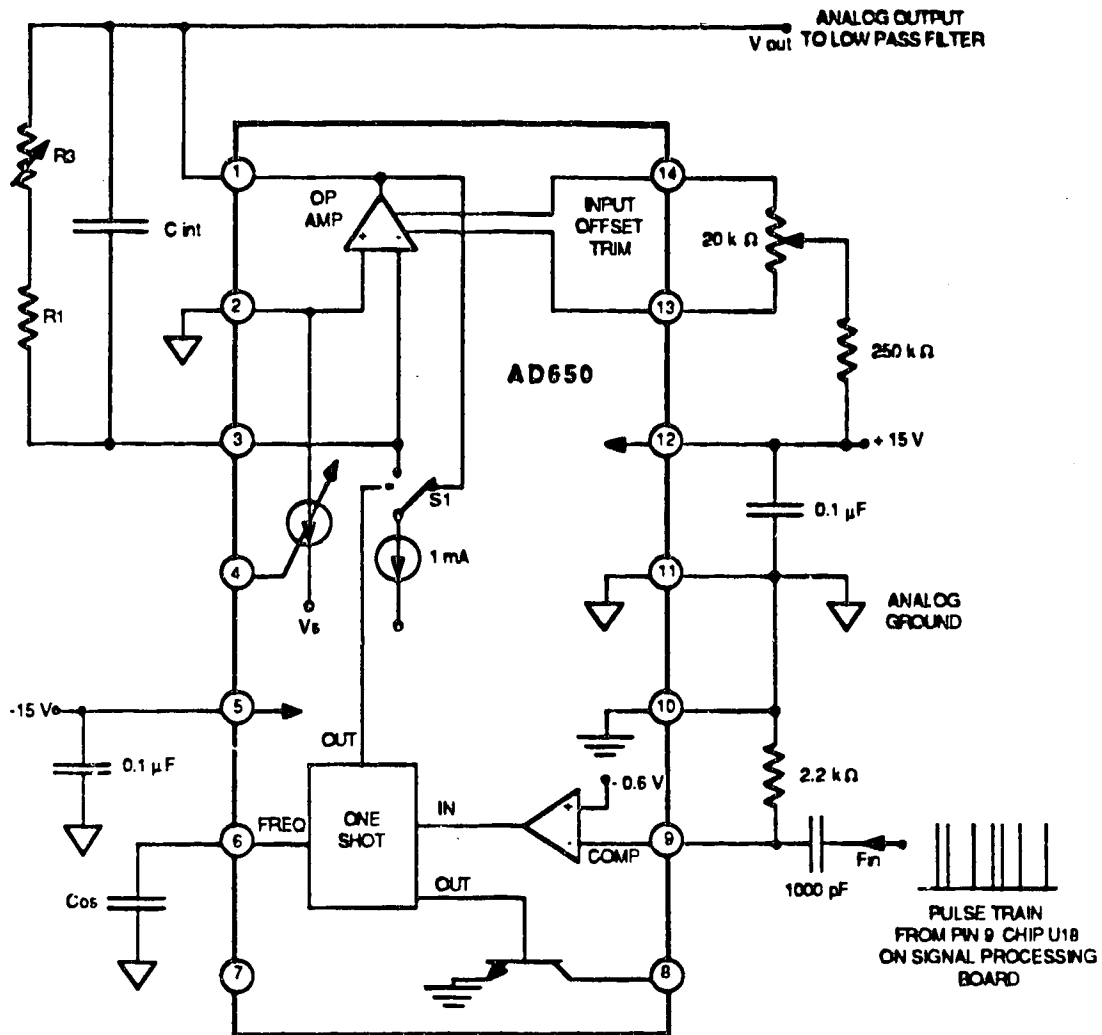


Figure 7.4 Diagram of Analog Devices AD650 configured in the frequency to voltage conversion mode.

with the second channel of the Krohn-Hite filter. The filtered ICP-MS analog signal was digitized with channel 1 of the ADC. To ensure that the new F/V output operated properly, an ICP-MS calibration curve for Sr was measured (Figure 7.5). The plot had a slope of 1.02 (+/-0.03). The maximum count rate that can be handled with the F/V system was 2×10^5 counts per second (2 $\mu\text{g/mL}$ Sr). The maximum count rate could be extended to higher count rates if required by adding a series of flip-flops before the input to the F/V.

Data acquisition was synchronized with the READ/COUNT signal from the Elan's Signal Processing Board. The READ/COUNT signal was extracted from Pin 3 on Chip U17 (Figure 7.3), and buffered with a single inverter (7406 Hex Inverter). This signal was connected to the external trigger port of the ADC to trigger the start of data acquisition.

Ideally, both optical and mass time domain signals should be acquired simultaneously, but the ADC was able to digitize only one channel at a time. Therefore, an alternating routine was set up, where first a point from the optical emission channel (ADC channel 0) was digitized, then a point from the mass spectral channel (ADC channel 1) was digitized. The data acquisition alternated between the two channels until 2048 points were acquired, 1024 points per channel. The overall digitization rate was 2800 Hz, 1400 Hz per channel.

The Elan was run with the MULTIPLE ELEMENTS program, in the TEST AND MAINTAINCE menu. The spectrometer was set up to

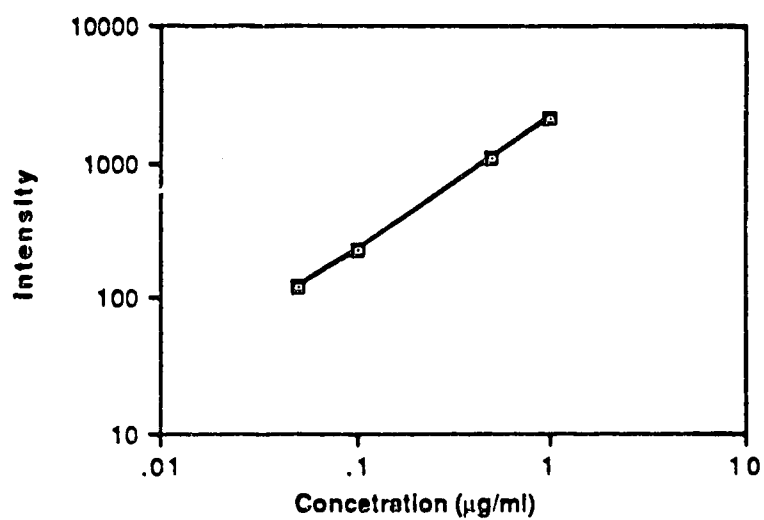


Figure 7.5 Analytical calibration curve for analog measurement of Sr^+ mass signal.

continuously measure a single element, with a single point per peak and with no background or isobaric corrections. The detector dwell time was 1.0 second, just slightly longer than the time required to digitize the 2048 data points at the 2800 Hz sampling rate. The Elan system was therefore only used to control the scanning of the quadrupole, all data acquisition and processing for both optical and mass systems were performed with an IBM pc.

The ASYST FFT routine was used to Fourier transform the time domain data from the optical and mass channels. Ten replicates of each Fourier transformed data set were averaged to give a single noise amplitude spectrum.

7.3 Results and Discussion

7.3.1 Noise Amplitude Spectra

The plasma operating parameters for the simultaneous optical and mass spectral noise measurements are listed in Table 7.1. Noise amplitude spectra obtained with these operating conditions are plotted in Figure 7.6. The three types of noise described in section 7.1 are apparent in both optical and mass spectral noise amplitude spectra.

The $1/f$ noise is clearly present in both noise spectra. The noise amplitude is low at 500 Hz and steadily increases as the frequency decreases. White noise is present in the spectrum, but is relatively small compared to the $1/f$

Table 7.1 Standard Plasma Operating Conditions

RF power	1.1 kW
Outer gas flow rate	12 Lpm
Inner gas flow rate	1.4 Lpm
Aerosol gas flow rate	0.95 Lpm
MS sampling distance	15 mm from load coil
Optical viewing zone	1 mm from sampler
Sample Sr	1 $\mu\text{g/mL}$

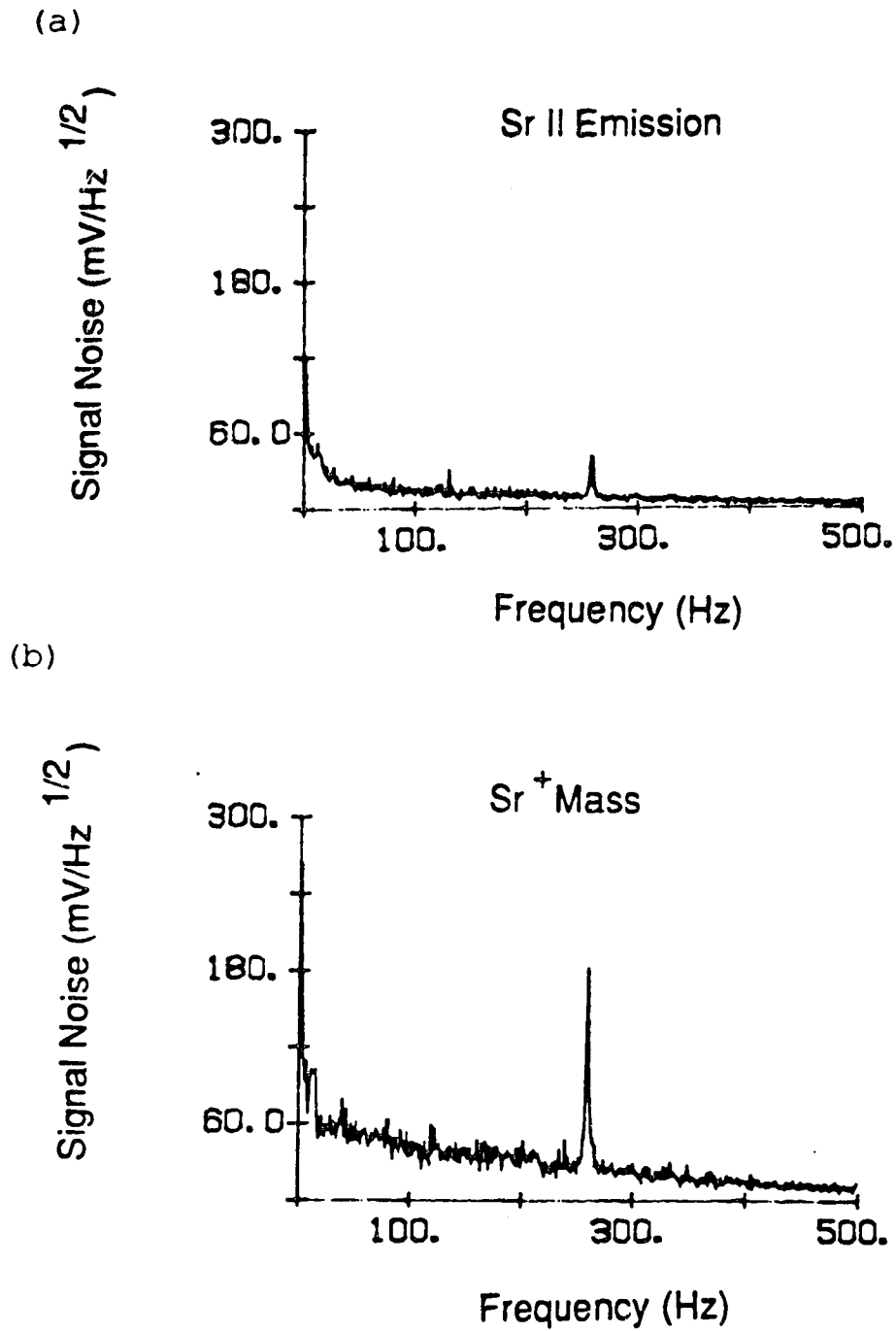


Figure 7.6 Noise amplitude spectra of a) Sr II emission and b) Sr⁺ mass signal.

component of the noise. There is a relatively small peak at 120 Hz in both optical and mass noise spectra. This fixed frequency noise is due to pick up of the line voltage frequency and is also relatively small compared to the $1/f$ component of the noise. There is a second large peak in both noise spectra, occurring about at 250 Hz. The frequency of this peak does not correspond to the line voltage frequency or any harmonics of the line frequency. The frequency of this peak is exactly the same in both the optical and mass noise spectra, indicating it is possibly plasma related.

The intensity of the noise feature at 250 Hz in the mass noise spectrum was approximately $150 \text{ mV/Hz}^{1/2}$ and the same noise feature in the optical noise spectrum was $34 \text{ mV/Hz}^{1/2}$. The net mass signal is approximately 2.06 V and the net optical signal is 1.50 V, therefore under these operating conditions the fixed frequency noise is relatively 3.2 times more intense in the mass signal. The next section will describe the effect of operating parameters on this fixed frequency noise feature and will attempt to describe its source.

7.3.2 Noise Feature in the ICP

The effect of plasma operating parameters on the noise feature was studied. The plasma operating parameters listed in Table 7.1 were used in this study and only one parameter was varied at a time.

The first parameter investigated was RF power. The RF power was increased from 0.8 to 1.4 kW in 0.1 kW increments and noise amplitude spectra were acquired for both the optical and mass signal channels at each power. The noise feature in the optical noise spectrum increased in frequency as the RF power was increased (Figure 7.7). The noise feature in the mass noise spectrum also increased in frequency with increasing RF power (Figure 7.8). The frequency of the noise feature in both the optical and mass noise spectra matched exactly at all RF powers and the increase in noise feature frequency of this feature with RF power (Figure 7.9) is consistent with previous optical noise spectral studies [4].

The outer gas flow rate was varied from 9 to 15 Lpm in 1 Lpm increments. At low outer gas flow rates (9-10 Lpm) the noise feature was not observed in either the optical or mass spectral noise amplitude spectra (Figures 7.10 and 7.11). At higher flow rates the noise feature appears and as the flow rate increased, the noise feature increased in frequency (Figure 7.12). This result is again consistent with previous optical noise studies [4].

The effect of the intermediate gas flow rate and central (nebulizer) gas flow rate were also studied. No change in the frequency of the noise feature was observed for changes in either of these two gas flow rates.

The sampling distance, the distance from load coil to the mass spectrometer sampling cone, was varied from 9 to 23 mm in 2 mm increments. The optical observation zone was

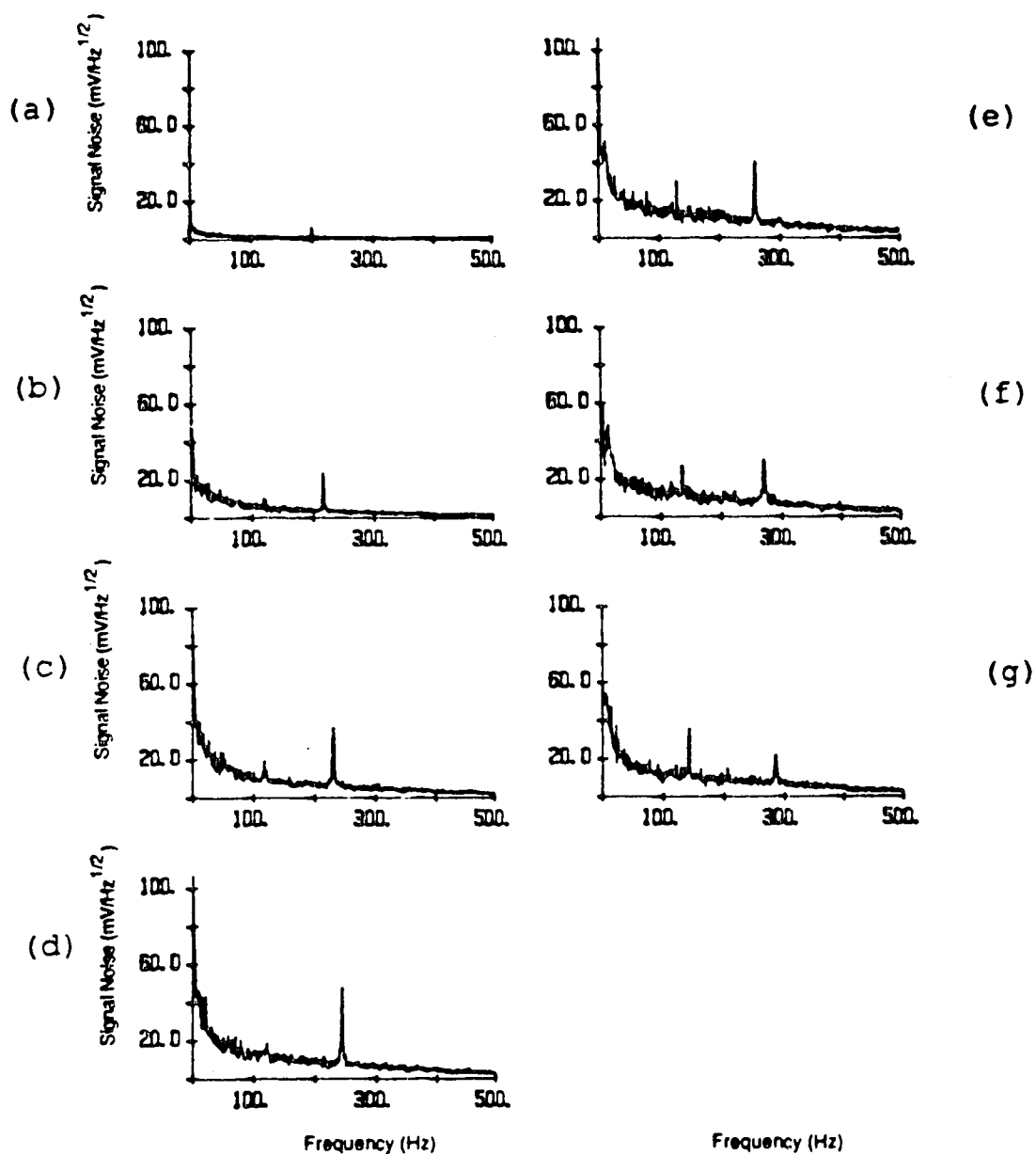


Figure 7.7 Noise amplitude spectra of Sr II emission measured at RF powers of a) 0.8, b) 0.9, c) 1.0, d) 1.1, e) 1.2, f) 1.3, and g) 1.4 kW.

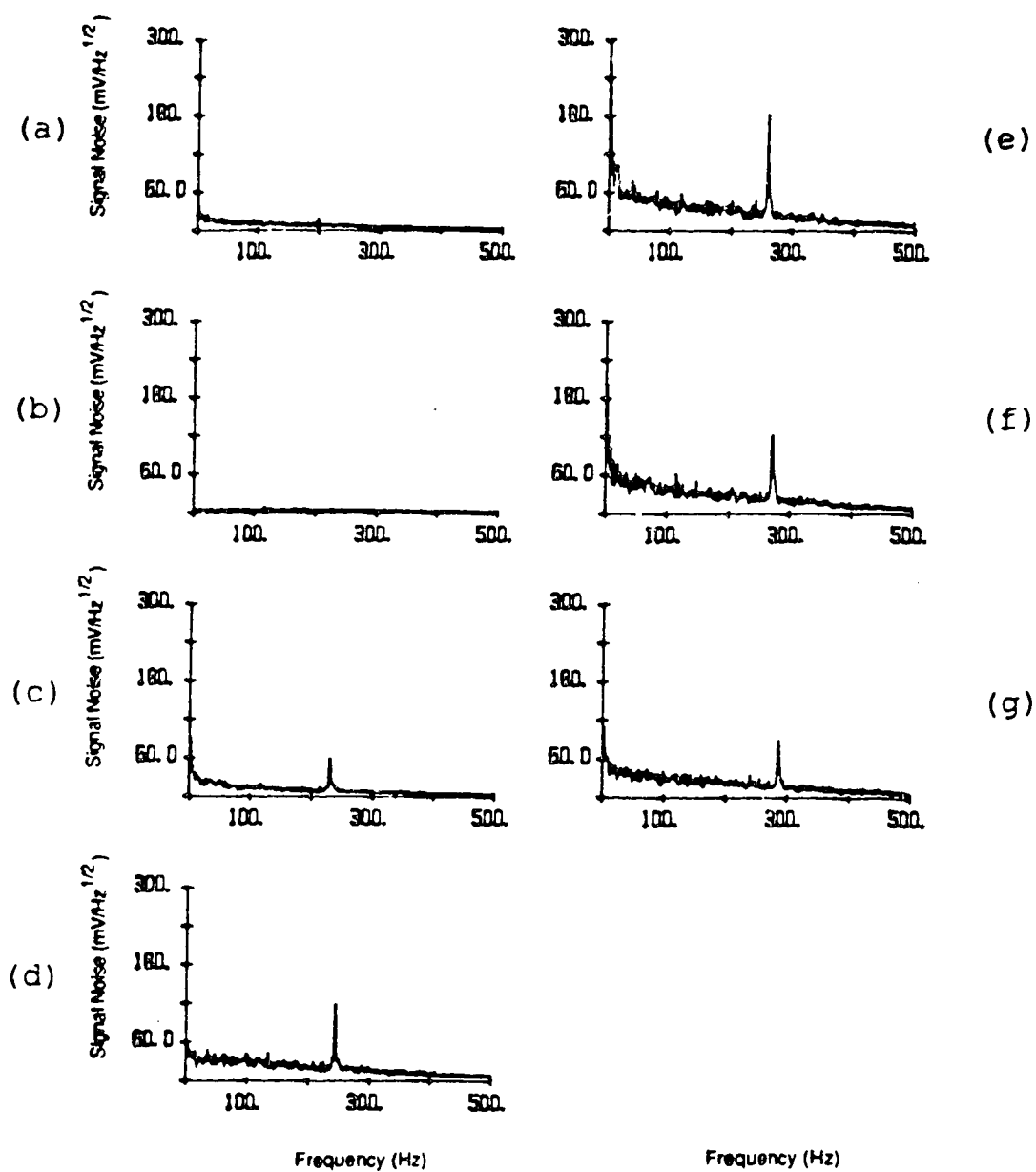


Figure 7.8 Noise amplitude spectra of Sr^+ mass signal measured at RF powers of a) 0.8, b) 0.9, c) 1.0, d) 1.1, e) 1.2, f) 1.3, and g) 1.4 kW.

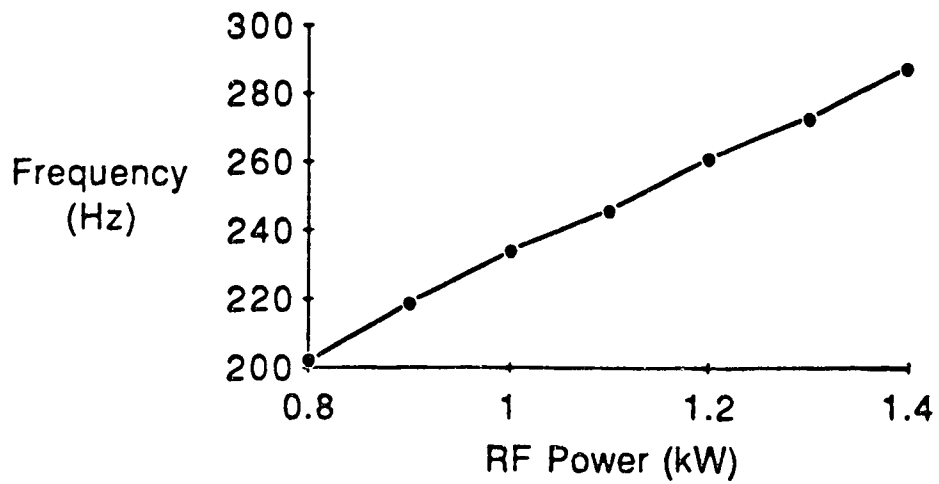


Figure 7.9 Frequency of noise feature in optical and mass signal as a function of RF power.

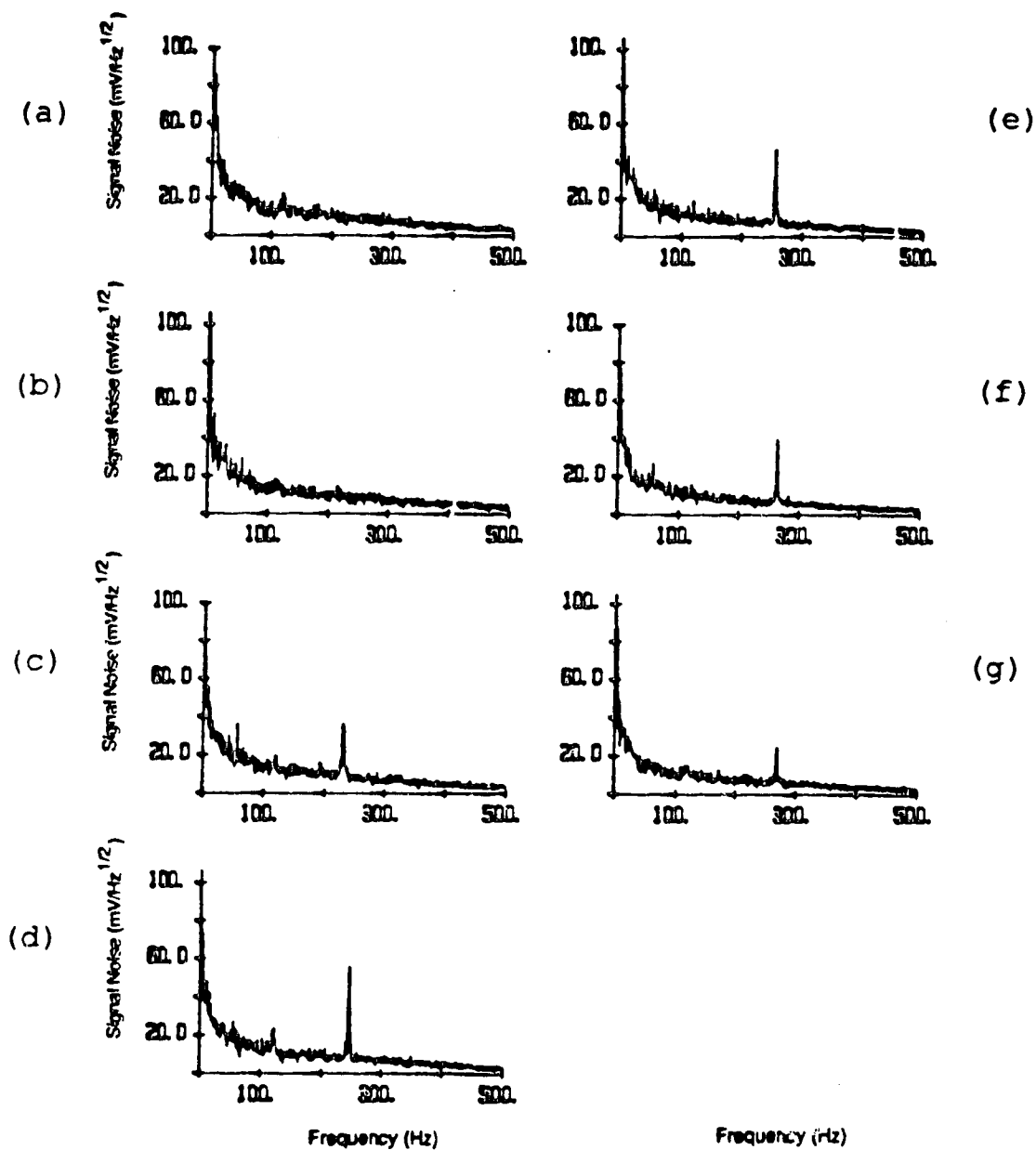


Figure 7.10 Noise amplitude spectra of Sr II emission measured at outer gas flow rates of a) 9, b) 10, c) 11, d) 12, e) 13, f) 14, and g) 15 Lpm.

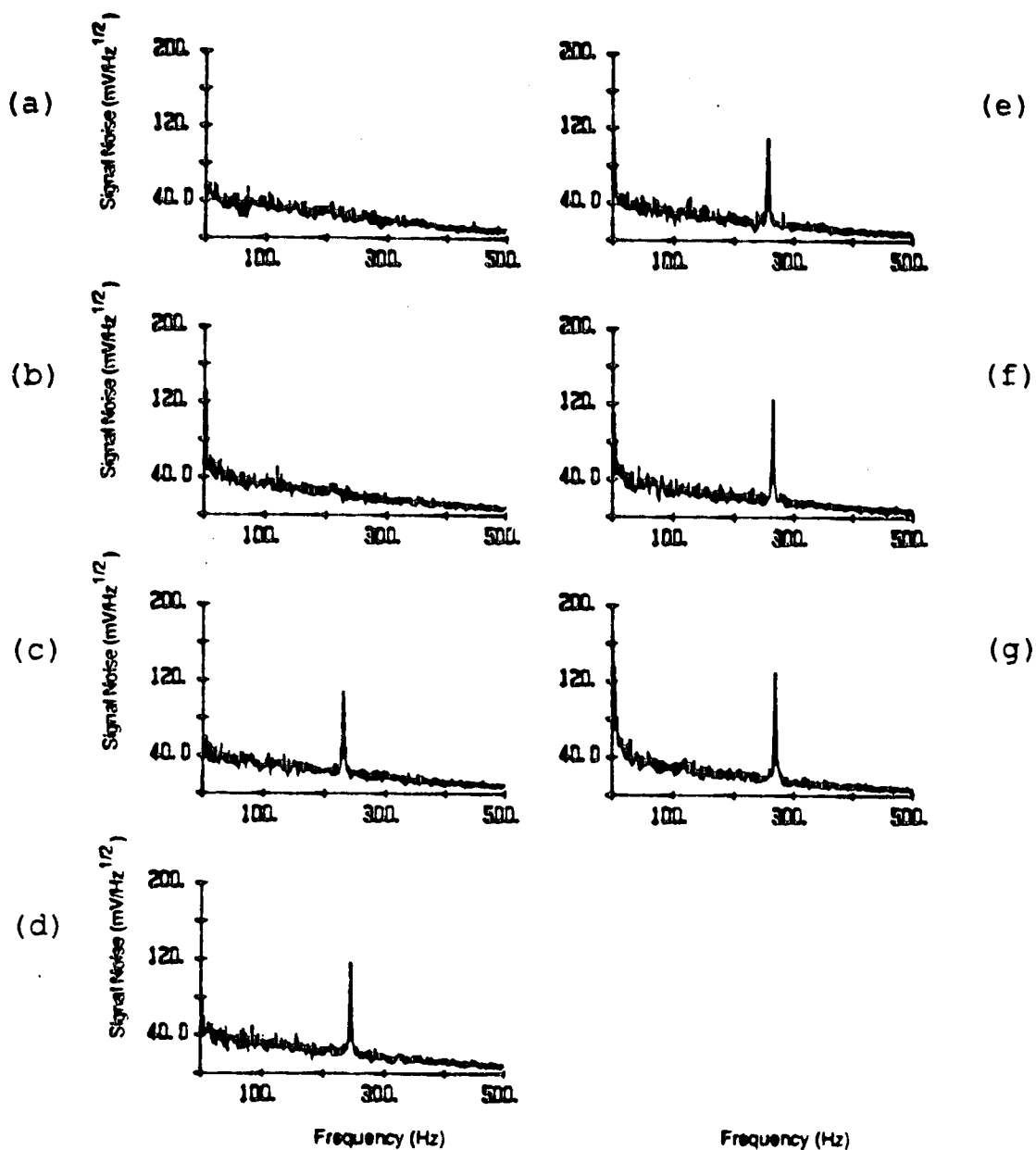


Figure 7.11 Noise amplitude spectra of Sr^+ mass signal measured at outer gas flow rates of a) 9, b) 10, c) 11, d) 12, e) 13, f) 14, and g) 15 Lpm.

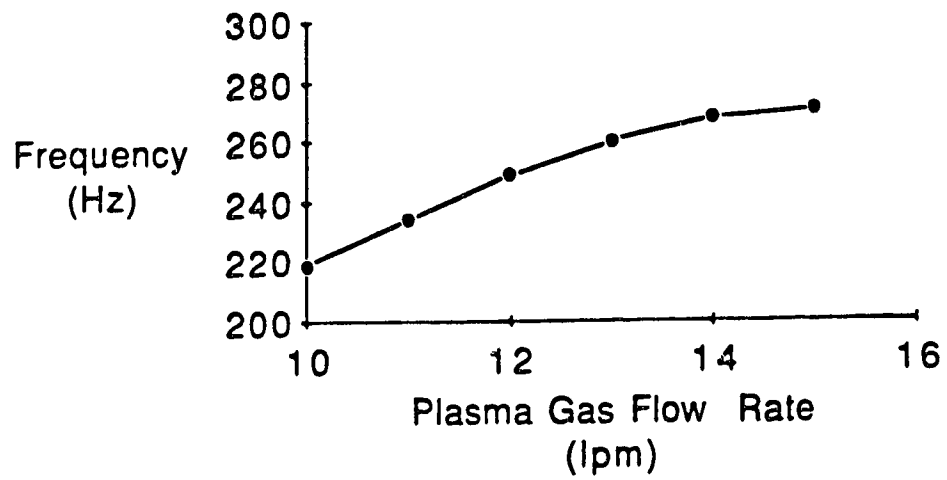


Figure 7.12 Frequency of noise feature in optical and mass signal as a function of outer gas flow rate.

maintained at 1 mm in front of the sampling cone for this series of measurements. The frequency of the noise feature in the optical noise amplitude spectrum decreased as the sampler to load coil distance increased (Figure 7.13). The noise feature in the mass noise spectrum followed the same trend as the optical channel (Figure 7.14), with the noise feature ranging from 260 Hz at 13 mm to 200 Hz at a 23 mm sampling distance (Figure 7.15). At closer sampling distances (9 and 11 mm), the net signal was weak for both optical and mass channels and for this reason a significant noise feature was not observed. Changing the observation zone for both the optical and mass channels caused the frequency of the noise feature to change. This result could mean one of two things: 1) the frequency of the noise feature varied with spatial position in plasma or 2) moving the plasma toward the sampling cone caused the frequency of the noise feature to change. To clarify this point, the sampler to load coil distance was held fixed and the optical observation zone was varied from 1 to 8 mm from the sampler, in 1 mm increments. The frequency of the noise feature did not change as the optical observation zone was moved from the sampler toward the load coil (Figure 7.16). This result indicates that it is moving the plasma relative to the sampler that causes the change in frequency.

The response of the noise feature to plasma operating conditions clearly indicates that the noise feature is plasma related and is the same effect reported in the literature for

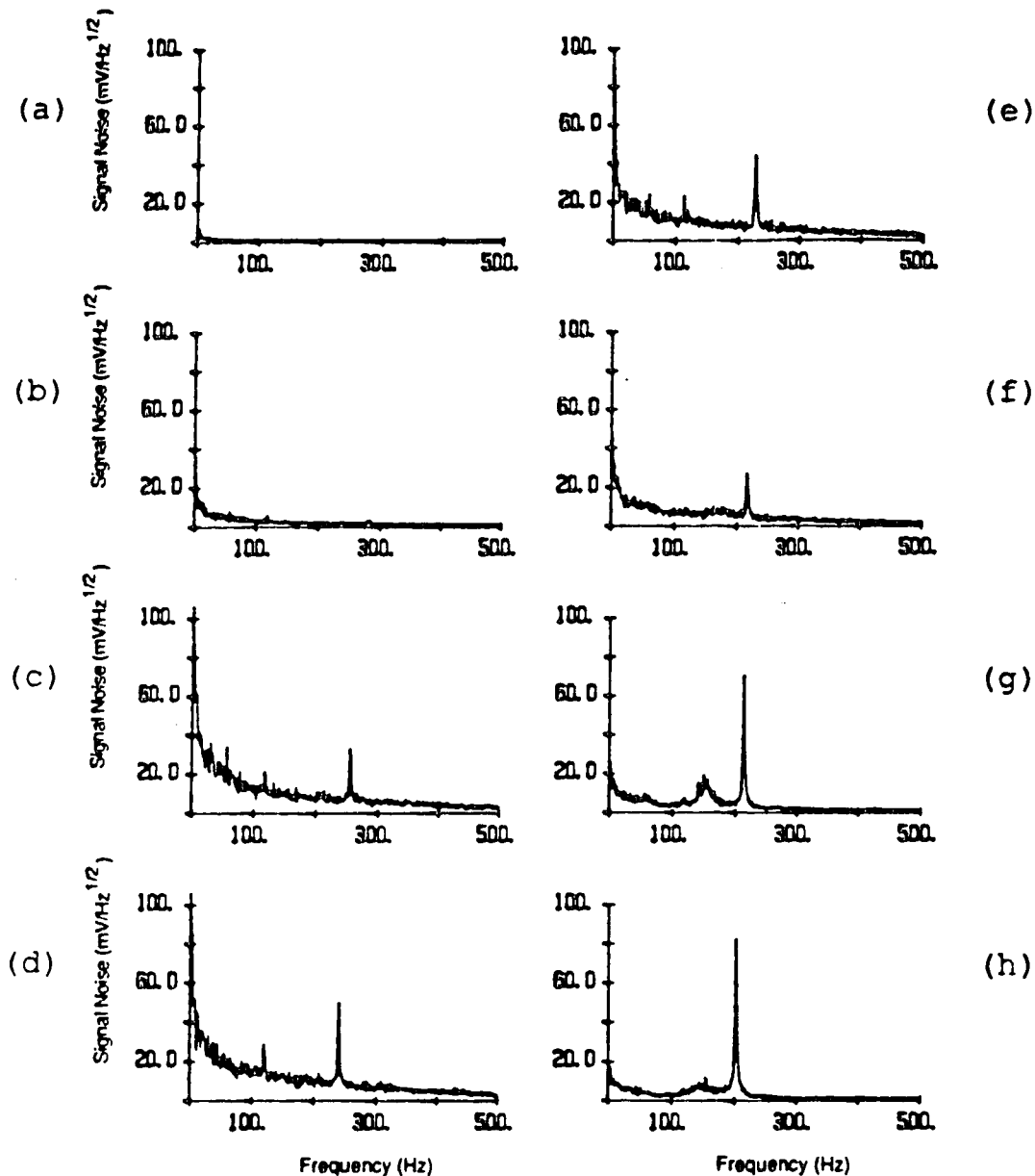


Figure 7.13 Noise amplitude spectra of Sr II emission measured at spatial positions of a) 9, b) 11, c) 13, d) 15, e) 17, f) 19, g) 21, and h) 23 mm from the load coil.

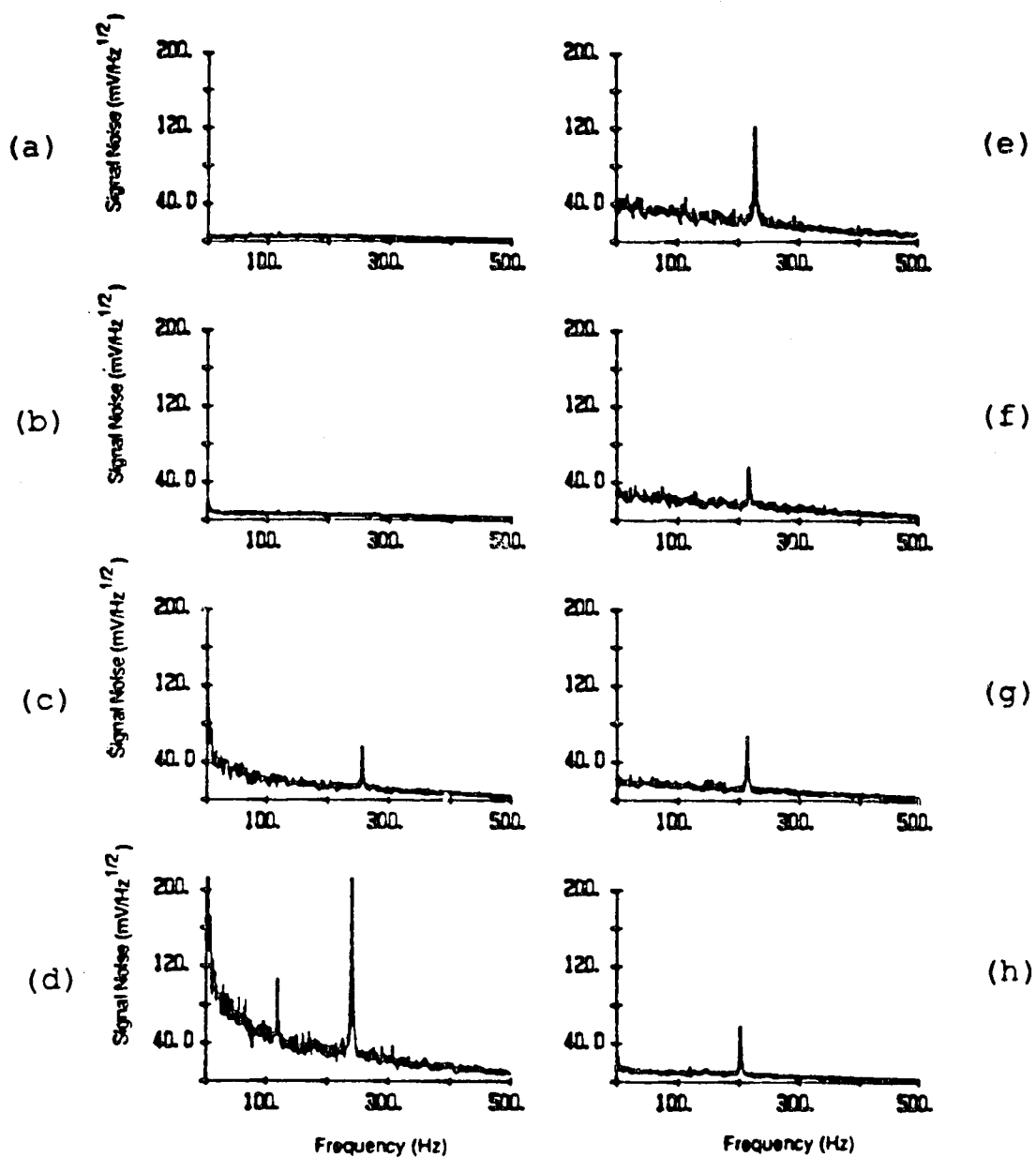


Figure 7.14 Noise amplitude spectra of Sr^+ mass signal measured at spatial positions of a) 9, b) 11, c) 13, d) 15, e) 17, f) 19, g) 21, and h) 23 mm from the load coil.

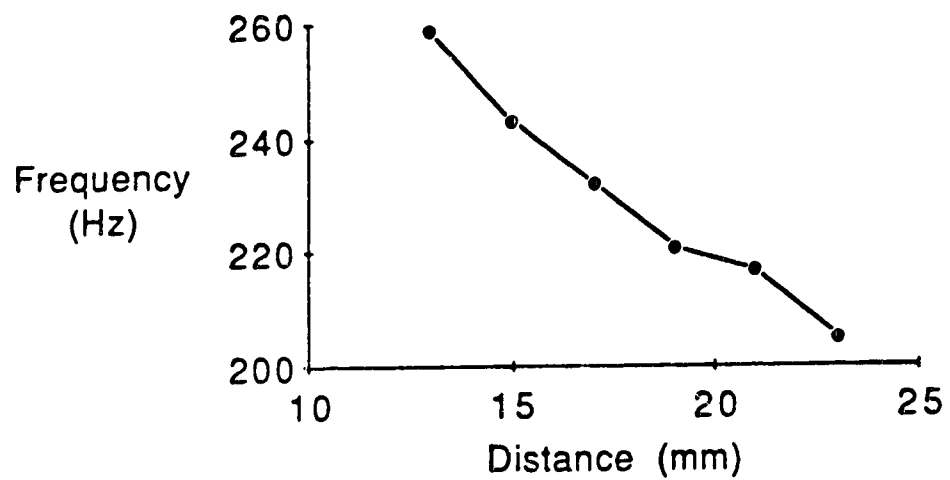


Figure 7.15 Frequency of noise feature in optical and mass signal as a function of sampling cone to load coil distance.

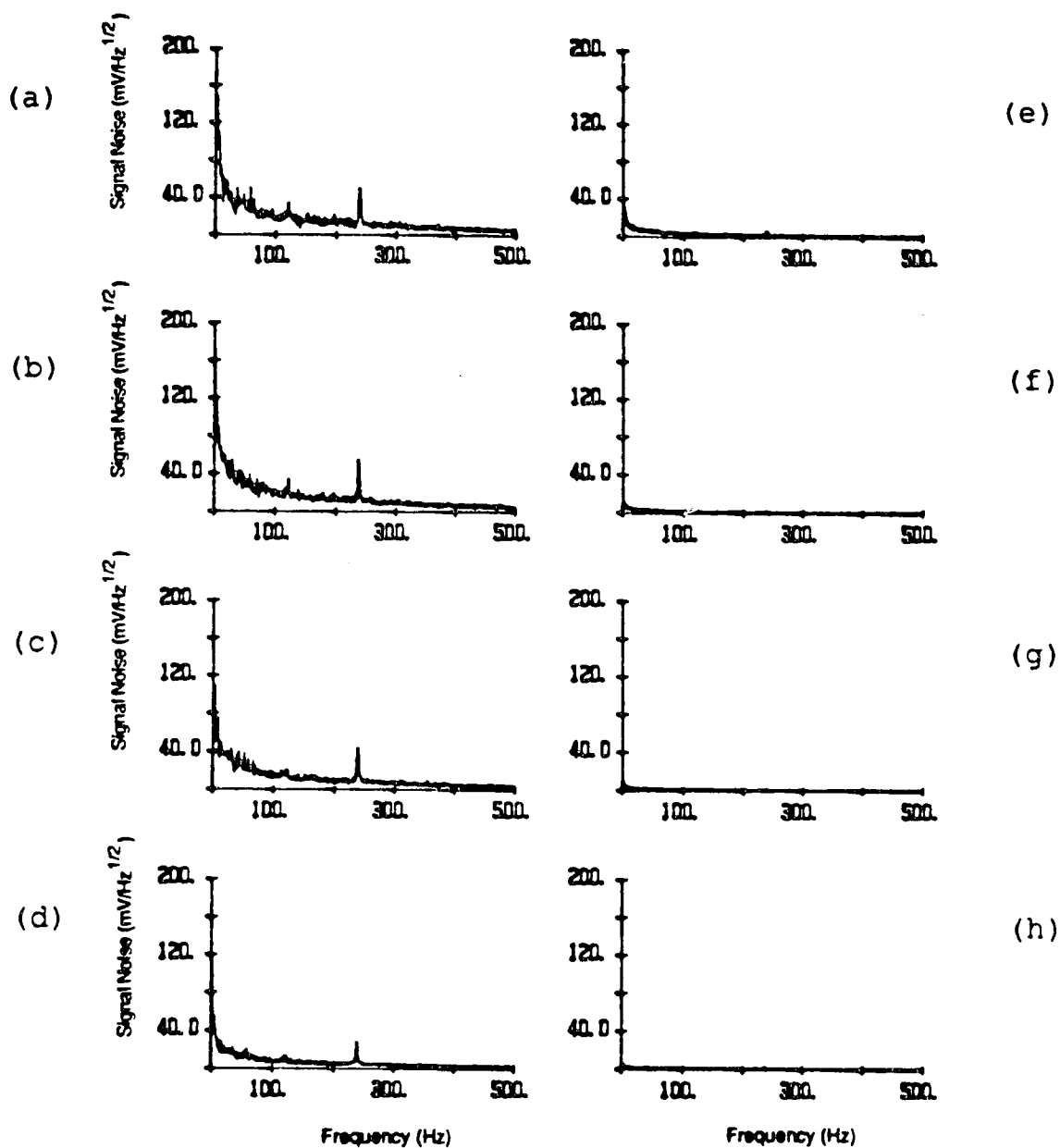


Figure 7.16 Noise amplitude spectra of Sr II emission measured at optical observation zones of a) 1, b) 2, c) 3, d) 4, e) 5, f) 6, g) 7, and h) 8 mm from the sampling cone.

ICP-AES [3-6]. If the noise feature is due to asymmetric plasma rotation as has been suggested [4], it would not be expected to affect the mass spectrometer signal, as the mass spectrometer samples the plasma end on, and along that axis, rotation would not be observed. Viewing a conventional ICP emission source end on, the noise feature is still present (Figure 7.17), therefore, plasma rotation is probably not the source of this noise.

RF power, by increasing the gas temperature, affects the gas velocity, as does the outer gas flow, while the intermediate gas and the central (nebulizer) gas are at low flow rates and do not contribute significantly to the total gas velocity. The position of the mass spectrometer sampling cone also affects the frequency of the noise feature. It therefore can be said that the plasma fluctuation is a result of the interaction of the Ar gas flow with the surroundings as it leaves the torch. The hot Ar gas creates a turbulence as it mixes with the surrounding air. This conclusion can be confirmed by optical noise amplitude measurements with a long torch. The long torch is a conventional ICP torch with an outer quartz tube that extends 22 mm above load coil. Emission was viewed through the outer tube at spatial locations 15 to 21 mm above the load coil (Figure 7.18). For noise amplitude spectra at these positions no fixed frequency noise feature was observed. Only at viewing positions above the extended torch (23 and 25 mm) is the noise feature apparent.

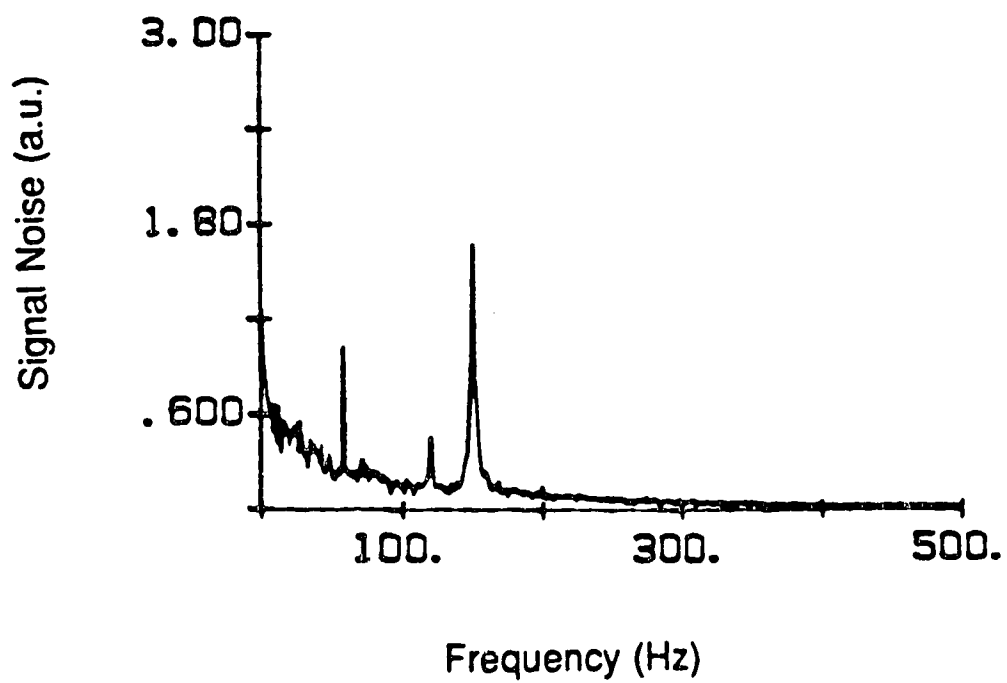


Figure 7.17 Noise amplitude spectrum of Sr II emission viewed end on from above the plasma.

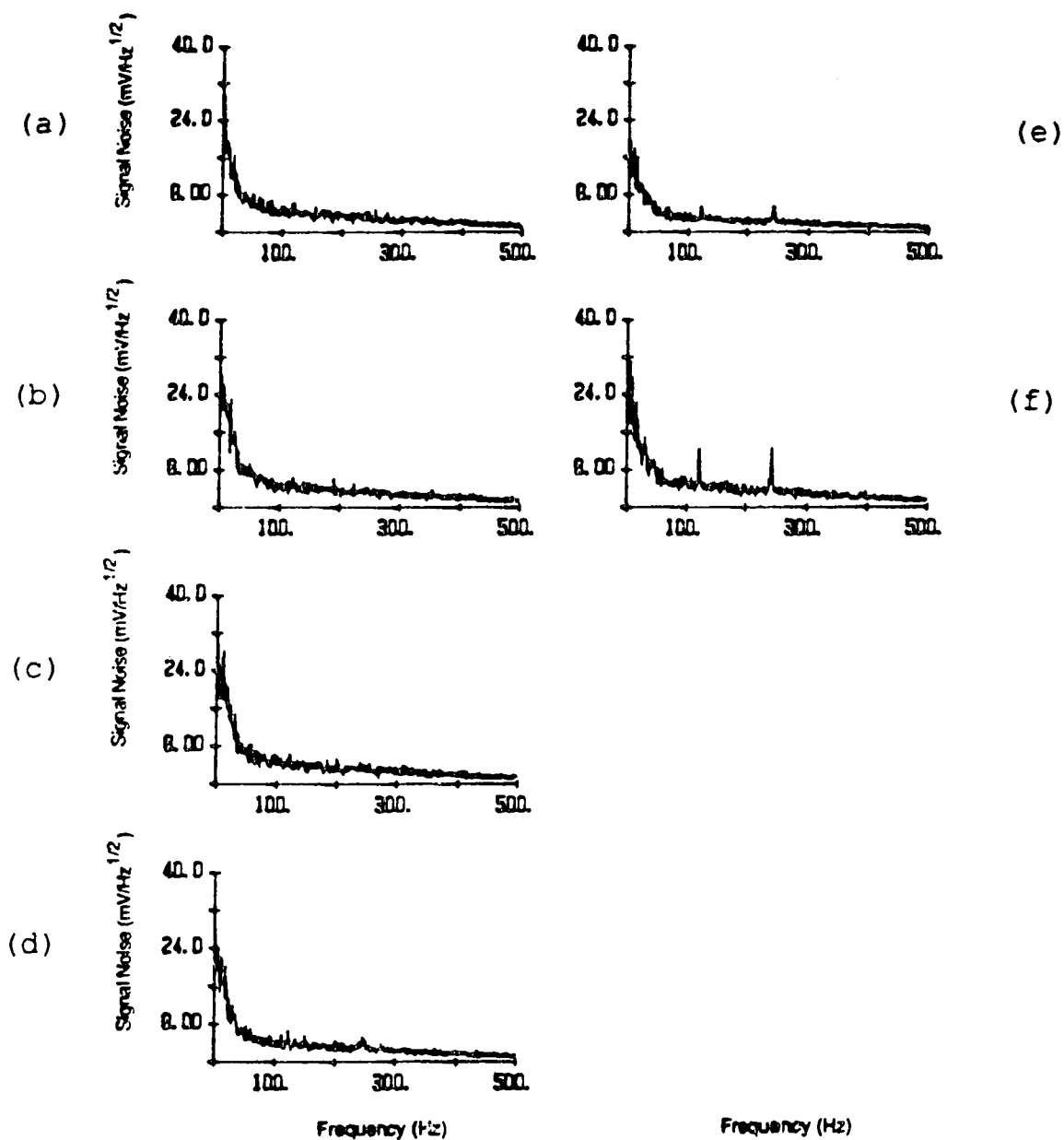


Figure 7.18 Noise amplitude spectrum of Sr II emission using a long torch with optical observation zones a) 15, b) 17, c) 19, d) 21, e) 23, and f) 25 mm above the load coil.

In ICP-AES integration times of 10 to 30 seconds are typical. Over this time period, the fixed frequency noise is averaged out and does not contribute significantly to the net noise on the signal. As measurement times decrease, as in the case of rapid peak hopping in multi-element mass spectrometry, the presence of the fixed frequency noise could become significant to the total noise.

The intensity of the noise feature can be reduced in optical measurement by the use of a long torch. However, by viewing through the side of the torch, signal intensities are attenuated by approximately a factor of two. A long torch would not decrease the noise feature in the mass spectral signal. Decreasing the outer gas flow rate will decrease the noise feature without significantly affecting the net signal, but low outer gas flow rates result in more air entrainment in the plasma and an increase in molecular nitrogen species will result in the optical and mass spectra. Therefore, it is important that mass spectrometer dwell times are sufficiently long, so as to average out the noise feature.

7.3.3 1/f Noise

Both the optical and the mass signal channels have significant 1/f noise components, as evident by the noise spectra in Figure 7.6. The nature of 1/f components of the noise in the two channels appears to be different in form.

The optical noise amplitude spectrum has the typical $1/f$ character, where the noise amplitude remains relatively low over the frequency range 100 to 500 Hz and increases rapidly at frequencies less than 100 Hz. The mass spectral $1/f$ noise is much higher at higher frequencies (300 Hz), than the optical $1/f$ noise and it does not increase rapidly until it reaches frequencies less than 25 Hz. This difference implies that the limiting $1/f$ noise, in the two techniques, are from different sources.

The differences in the $1/f$ character of the two systems are more evident as the intensity of the signal is changed. Noise amplitude spectra were obtained at a series of Sr concentrations, ranging from 0.004 $\mu\text{g/mL}$ to 1.00 $\mu\text{g/mL}$. For Sr emission (Figure 7.19), the $1/f$ character of the optical noise remains constant as concentration changes, i.e. the shape of the curve remains constant, only the intensity changes. This result implies that limiting source of drift remains constant over that concentration range. The $1/f$ character of mass spectral noise (Figure 7.20) changes with concentration. At lower concentrations the noise in the 0 to 50 Hz region is relatively less than at the higher frequencies. As the concentration increases the noise in the 0 to 50 Hz region increases more rapidly than the noise at higher frequencies. The change in shape of the noise amplitude spectrum with concentration suggests that more than one source contributes to the low frequency noise and each

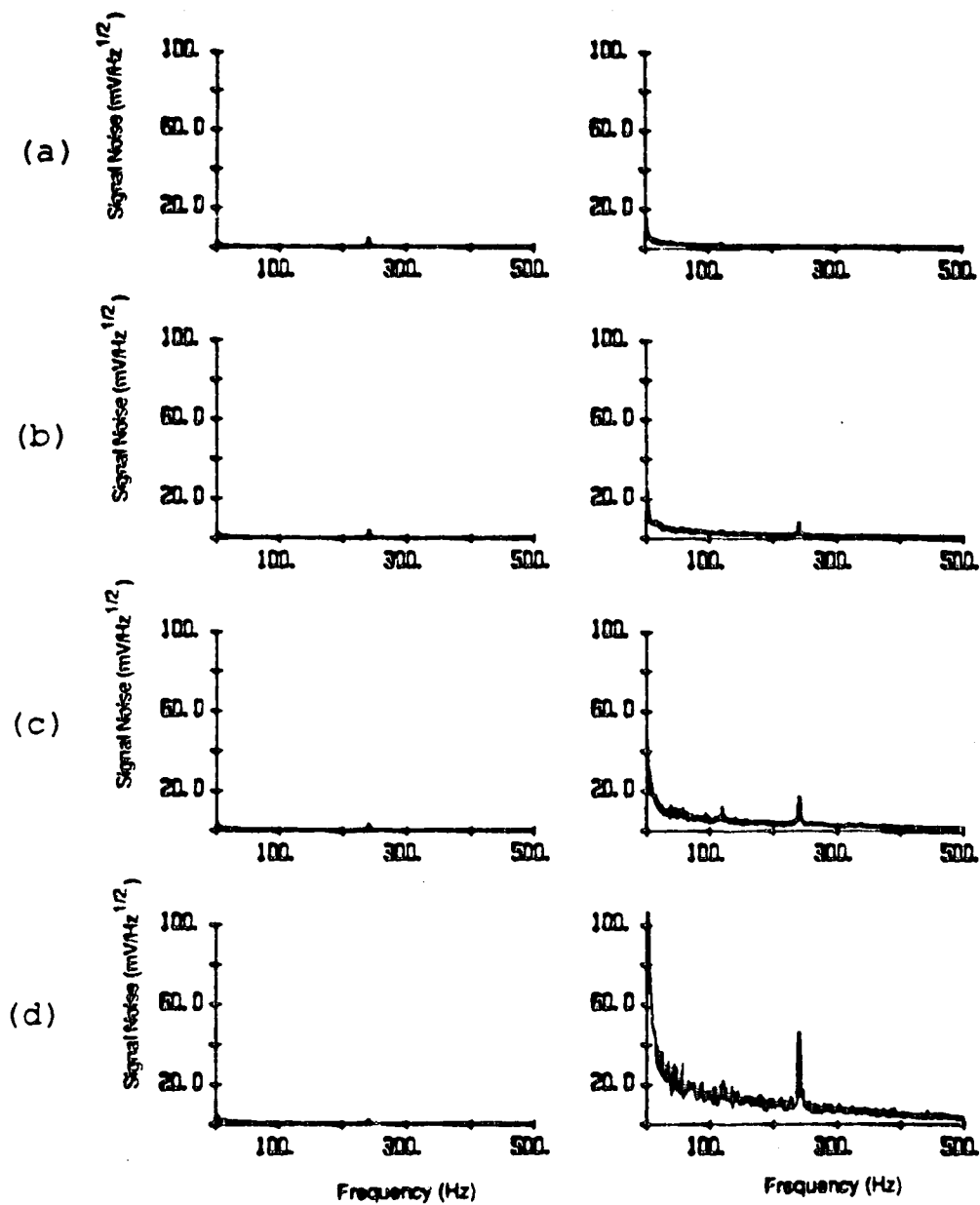


Figure 7.19 Noise amplitude spectra of Sr II emission measured at concentrations of a) 0.004, b) 0.01, c) 0.02, d) 0.04, e) 0.1, f) 0.2, g) 0.4, and h) 1.00 $\mu\text{g/mL}$.

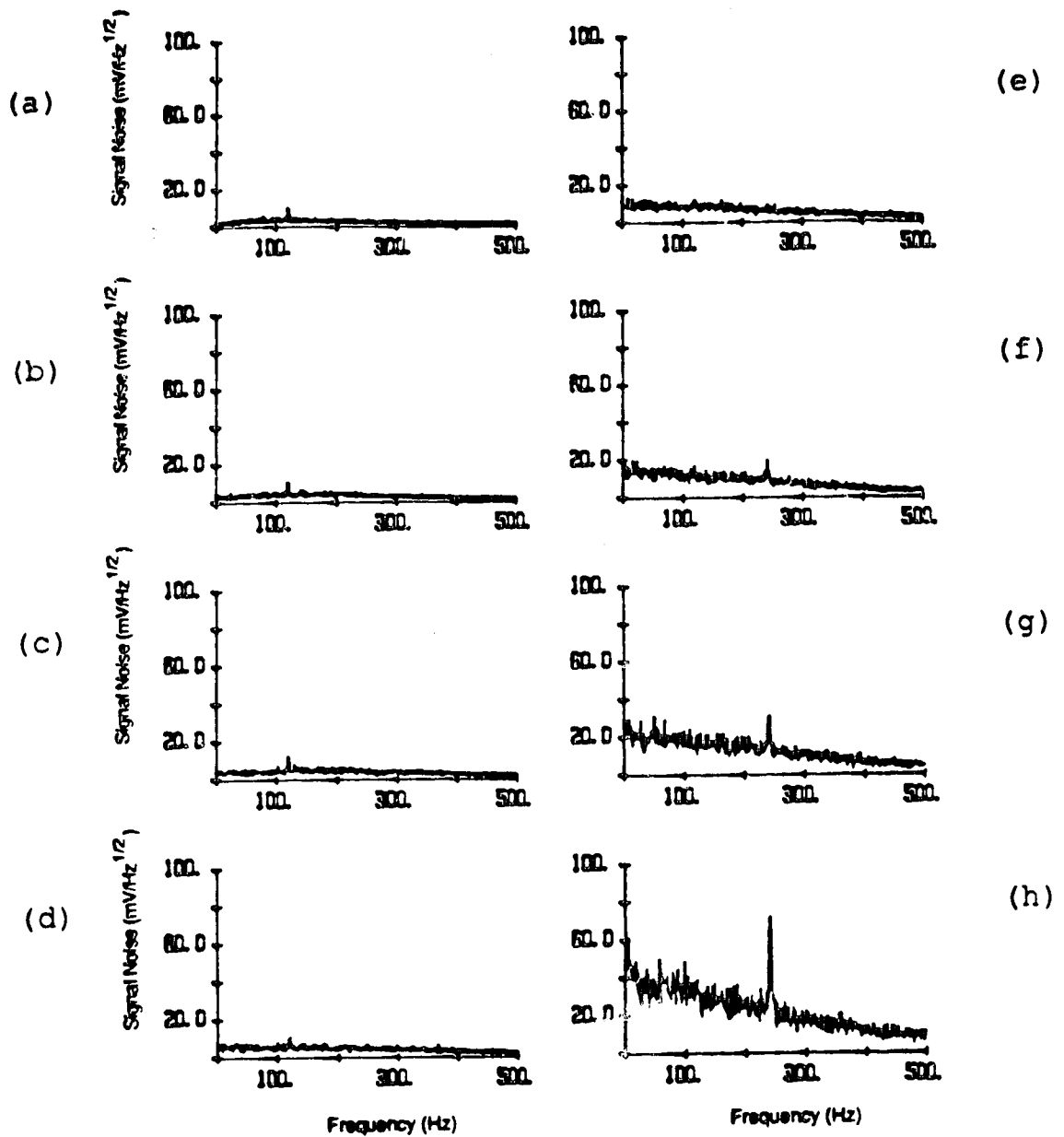


Figure 7.20 Noise amplitude spectra of Sr^+ mass signal measured at concentrations of a) 0.004, b) 0.01, c) 0.02, d) 0.04, e) 0.1, f) 0.2, g) 0.4, and h) 1.00 $\mu\text{g/mL}$.

source has a different functional dependence on signal intensity.

The $1/f$ noise in optical emission has been related to the stability of the nebulizer [4]. Drift in the mass spectrometer has been attributed to ions coating the lenses and changing the transmission characteristics of the lenses [9]. This effect combined with nebulizer drift may account for the shape of the mass spectral noise amplitude spectrum.

7.4 Conclusions

The fixed frequency noise feature that has been observed in ICP-AES, exists in the ICP-MS signal as well, and is relatively more intense in ICP-MS. This fixed frequency noise feature is a result of plasma fluctuations and is probably not due to a rotation of an asymmetric plasma, but is due to an up and down oscillation. The oscillation is caused by the hot Ar gas interacting with the surrounding air. To prevent this noise from affecting the signal, low outer gas flow rates or measurement times of at least 0.5 seconds should be used.

The medium term drift in ICP-MS is more severe than in ICP-AES, as evident from Section 6.3.3. The noise amplitude spectra suggest that the source of drift is also different for the two techniques. Drift in the ICP-MS appears to result from at least two sources, one the slow drift of the nebulizer, an ICP effect, and the second, the coating of the

lenses with ions, a mass spectrometer effect. The combination of the two effects makes it necessary that an internal standard be use for ICP-MS analysis and until changes are made to the ICP-MS lens system internal standards will be required.

References

1. C. Th. J. Alkemade, H. P. Hooymayers, P. L. Lijnse, and T. J. M. J. Uienberger, *Spectrochim. Acta*, **27B**, 149, (1972)
2. G. M. Heiftje and R. I. Bystroff, *Spectrochim. Acta*, **30B**, 187, (1975)
3. G. L. Walden, J. N. Bower, S. Nikdel, D. L. Bolton, and J. D. Winefordner, *Spectrochim. Acta*, **35B**, 535, (1980)
4. R. M. Belchamber and G. Horlick, *Spectrochim. Acta*, **37B**, 17, (1982)
5. N. Furuta, Winter Conference on Plasma Spectroscopy, San Diego, Ca., paper no. Th1, (1988)
6. R. K. Winge, D. E. Eckels, E. L. DeKalb, and V. A. Fassel, *J. Anal. Atom. Spectrosc.*, **3**, 849, (1988)
7. M. van der Klis, *Scientific American*, **259**, 50, (1988)
8. Analog Devices, *Integrated Circuits Data Book Vol.1*, (1984)
9. D. J. Douglas, *Can. J. Spectrosc.*, in press, (1988)

Chapter 8

Future Developments

8.1 Advances in Image Sensor Technology

Developments in image sensor technology are currently occurring in three basic areas; 1) improvements in semiconductor device fabrication techniques, 2) improvements to supporting devices for the PDA, and 3) development of solid state image sensors other than the PDA.

Improvements in fabrication techniques for semiconductor devices have enabled the production of large pieces of pure silicon, free of defects. As a result, devices 50 mm in length or greater can be produced at a reasonable cost. Currently, E.G. & G. Reticon has available a 2048 pixel PDA. Each pixel is on 25 μm centers, therefore the total light sensitive area is 51 mm in length. Reticon also manufactures a 4096 pixel PDA with pixels on 15 μm centers and a total light sensitive area 61 mm in length. Larger PDAs can increase the wavelength covered by a PDA spectrometer in one spectral window, without decreasing the spectral resolution.

Better doping techniques, such as plasma coupled deposition, are able to produce uniform p-type and n-type

regions, and result in reduced sensitivity variations across the length of the PDA. New fabrication methods may also improve the quality of circuitry on the PDA chip, and thus reduce the pixel switching noise, the fundamental limiting noise of the PDA.

A reduction in on chip circuitry size has been realized in recent years. As a result more components can be included on the PDA chip. Reticon has taken advantage of this fact and included a 10 line to 1024 line multiplexer on the PDA chip. The multiplexer enables random access of each of the 1024 individual pixels, i.e. the PDA pixels can be readout in any order and each pixel can have a different integration time. With the random access PDA the multiple integration time technique discussed in Chapter 3 can be implemented in the readout step and not as a post processing technique.

The second area where PDA noise and sensitivity may improve will be in supporting circuitry used to operate the PDA. A factor of 10 times reduction in readout noise may be realized if the amplifier noise (from analog amplifiers on the PDA driver/amplifier board) could be reduced. PDA camera systems report significantly lower noise levels than the PDA systems described in Chapter 2. PDA cameras incorporate a PDA sensor into package, with all interface, amplification, and digitization electronics included as a unit. PDA cameras use high quality electronic subsystems which give superior performance but at a higher cost.

PDA sensitivity is improved a factor of 10 to 100 times with an image intensifier. An image intensifier is a series of small tubes a few microns in diameter, placed directly in front of the entire surface of the PDA. The inside of the tubes are coated with a photo-emissive material and a potential gradient is applied along the length of the tube. Photons enter at one end of the tube and eject an electron from the photo-emissive material. The electron current is amplified as it passes through the tube. At the other end of the tube the electrons strike a phosphor screen placed in front of the PDA. Image intensifiers are expensive, often costing more than the PDA, and typically degrade resolution by a factor of 2. If the method of coupling the image intensifier to the PDA can be improved so that no resolution is lost, then for low light level applications, image intensifiers may become standard additions to PDA sensors.

The PDA is not the only image sensor available. Another class of image sensors called charge transfer devices (CTD) have recently been used in spectroscopic applications. CTDs include the charge coupled device (CCD) and the charge injection device (CID). Both types of sensors are constructed using metal oxide-semiconductor (MOS) technology. CCDs and CIDs are available in a two dimensional array format. This format may be useful in an echelle spectrometer or to obtain spatially resolved data. CCDs and CIDs use silicon as the photosensitive material and therefore have the same quantum efficiency as the PDA. CCDs and CIDs have a lower readout

noise than the PDA and the CID has the potential for a nondestructive readout, which could further enhance the S/N performance of the device.

CTDs are subject to blooming, and the MOS gates on the surface of the sensor reduce the number of photons reaching the photosensitive silicon below. Unlike PDAs, there are gaps between the pixels of some CTDs, which could cause aliasing of a spectral line in some cases. Currently there is no CTD sensor commercially available, which combines all possible advantages of CTDs into to a single device.

8.2 Other Advances Affecting PDAs

There are two other areas which will strongly affect the application of PDAs in spectroscopy. One is the rapid increase in the availability and the computing power of microcomputers used in the laboratory. The microcomputer used in this work was an IBM pc with 640 kBytes random access memory (RAM). Newer microcomputers are available with 2 MBytes RAM and computing speed which is approximately doubled. With the increased capabilities, larger PDAs can be used, and the time required for data processing is reduced, making such procedures as zero filling more practical to use on routine basis.

As well as new microcomputers, supporting hardware is also improving. The ADC used in this work had a maximum conversion rate of 27.5 kHz. Currently, ADC with 100 kHz

maximum conversion rate are readily available for use with microcomputer systems. Faster conversion rates would allow for shorter minimum PDA integration times, thus increasing the multiple integration time dynamic range.

The second area which will strongly affect the advancement of the PDA as a detector for ICP-AES is new spectrometer designs. The Leco Plasma Array Spectrometer was briefly described in Chapter 1. It is the first commercially available ICP instrument to use a PDA as the detector and is unique with its three grating system and PDA camera configuration. The spectrometer is capable of simultaneous multi-line and background measurements with high spectral resolution, wide wavelength coverage, and flexible line selection. It combines the advantages of the scanning monochromator with those of the direct reading polychromator. If the Plasma Array Spectrometer is to be wide accepted, the sensitivity of the instrument must also match the sensitivity of PMT based spectrometers. The relatively low throughput of the instrument requires integration times of 100 seconds or more to approach the sensitivity of PMT spectrometers. The time lost with long integration times can be recovered if the multi-line capabilities of the spectrometer are fully utilized. Therefore the success of the instrument may depend on the development of efficient masks for specific multi-elemental analysis applications. Since this instrument is the first commercial ICP using a PDA, the general acceptance of the PDA as a detector for routine ICP-AES applications may

depend strongly on the success to the Plasma Array
Spectrometer.